



# Displaced Shapes of Infilled RC Frames for Displacement-Based Design and Assessment

A Dissertation Submitted in Partial Fulfilment of the Requirements  
for the Master Degree in

Earthquake Engineering & Engineering Seismology

By

Onur Deniz Akan

Supervisors: Asst. Prof. Dr. Ricardo Monteiro, Dr. Gerard J. O'Reilly

March, 2019

Istituto Universitario di Studi Superiori di Pavia

The dissertation entitled “Displaced Shapes of Infilled RC Frames for Displacement-Based Design and Assessment”, by Onur Deniz Akan, has been approved in partial fulfilment of the requirements for the Master Degree in Earthquake Engineering & Engineering Seismology.

**Asst. Prof. Dr. Ricardo Monteiro** \_\_\_\_\_

**Dr. Gerard J. O'Reilly** \_\_\_\_\_

## **ABSTRACT**

Within a performance-based design and assessment framework, defining the complete performance of a structure subject to ground motion shaking is of utmost importance. Seismic assessment of structures is often performed using their force-displacement capacity – or pushover – curve, computed via non-linear static analysis. With today's computing power and the available structural analysis programs, conducting a pushover analysis is fairly automatic and the results are often taken for granted. However, the reliability of the results of these analyses depends on the detail of the model and its ability to capture salient failure mechanisms. Simplified analysis methods offer effective means of identifying structural deficiencies and provide analysts with a sound understanding of key structural characteristics, such as the strength hierarchy, status of each storey in terms of limit states and the progression of the inelastic mechanism, in addition to providing a method with which to check the feasibility of computational results. Building upon the efficiency of past research related to simplified pushover analysis of reinforced concrete (RC) bare frames, this work describes an extension to infilled RC frames. Despite the significant in-plane contribution of masonry infill panels to the lateral strength and stiffness of a structure, they are often considered as non-structural elements and disregarded, provided that predefined global drift limits are satisfied. The proposed methodology captures the in-plane effect of infill walls on the system response over the complete lateral deformation capacity of the structure. Individual storey responses are obtained by first decoupling the flexural resistance of the RC frame and the axial resistance of the infill (modelled via an equivalent diagonal truss) and RC columns, assuming both systems work in parallel. Then, the displaced shape of the structure is calculated for a given base shear, which can be repeated to result in a complete characterisation of the structural response. The procedure is tested using various infilled RC case study frames and it is shown that the proposed approach is capable of performing simplified pushover analysis for infilled frame structures with a high degree of fidelity.

*Keywords:* pushover; RC frames; infills; displacement-based assessment

## **ACKNOWLEDGEMENTS**

First of all, I would like to express my sincere gratitude for my advisors Professor Ricardo Monteiro and Professor O'Reilly and thank them for their detailed reviews, efforts, time, help, continuous support, understanding, trust and encouragement. This work would not be possible without their guidance. Moreover, I would like to thank MEEES Programme for giving me this opportunity, not only to become a significantly more knowledgeable and capable person in an academic sense but to discover many aspects of my personality and my limits that were unknown to me before.

This section would be missing without the beautiful people that I have had the chance to meet during my time in MEEES. I would like to thank all my friends Saroj, Subash, Thuva, Nic, Luke, Jose, Nevena, Andres, Diana, Pungky, Lovely and especially Lana for their unconditional friendship, support and company. They were able to teach me that there exists a totally unknown and unexpected side of friendships that I have not aware of before.

Finally, I would like to thank my dear parents and my family who continuously believed in me and supported me psychologically as well as financially while I was away from home for the first time. Thank you...

Onur Deniz Akan  
Pavia, 2019

## TABLE OF CONTENTS

.....	Page
ABSTRACT .....	i
ACKNOWLEDGEMENTS.....	ii
TABLE OF CONTENTS.....	iii
LIST OF FIGURES .....	v
LIST OF TABLES.....	viii
1 Introduction .....	1
1.1 General.....	1
1.2 Objective.....	5
1.3 Outline of the Thesis.....	6
2 Literature Review .....	7
2.1 Assessment of Existing Structures.....	7
2.1.1 A Displacement-Based Approach.....	7
2.1.2 Displacement-Based Assessment.....	8
2.1.3 Masonry Infill Consideration .....	11
2.2 Behaviour and Numerical Modelling of Infilled RC Frame Members .....	13
2.2.1 Modelling of RC Frame Members.....	13
2.2.2 Masonry Infill-RC Frame Interaction .....	15
2.2.3 Modelling of Masonry Infill Panels.....	16
3 Methodology.....	23
3.1 Theoretical Background.....	23
3.1.1 One-Bay-One-Storey Infilled Frame .....	25
3.1.2 Multi-Bay-One-Storey infilled frame .....	27
3.1.3 One-Bay-Multi-Storey Infilled Frame .....	28
3.1.4 Multi-Bay-Multi-Storey Infilled Frame .....	29

3.2 Proposed Method to Consider Infill Contribution within a Simplified Pushover Analysis Framework.....	33
3.2.1 Geometry & Material Definitions.....	34
3.2.2 Flexural Frame System Capacity.....	35
3.2.3 Truss Infill System Capacity.....	37
3.2.4 Combined System Capacity.....	41
3.2.5 Proposed Method .....	42
3.2.6 Application within Displacement-Based Assessment Framework .....	46
3.3 Summary .....	47
4 Validation of the Simplified Analysis Approach.....	49
4.1 Description and Modelling of the Case Study Structures .....	49
4.2 Influence of Frame-Infill Interaction on the Global Inelastic Mechanism.....	51
4.3 Application of the Proposed Simplified Assessment Procedure on a 6-Storey Case Study Structure.....	56
4.4 Comparison of the Proposed Methodology with Other Available Approaches.....	60
4.5 Summary .....	61
5 Conclusion .....	63
5.1 Summary .....	63
5.2 Future Work .....	64
5.2.1 Column and Beam-Column Joint Shear Failure .....	64
5.2.2 Out-of-Plane and In-Plane Infill Interaction and Infills with Openings.....	64
5.2.3 Towards a Probabilistic Displacement-Based Approach.....	65
5.2.4 Displacement-Based Design of Infilled Frames .....	66
6 REFERENCES .....	67
A. APPENDIX A.....	73
A.1. Modelling and the Simplified Analysis of the Case Study Structure: Galli-6-Storey-Medium-Single .....	73
A.1.1.Geometry & Material Definitions.....	73
A.1.2.Flexural Frame System Capacity .....	76
A.1.3.Truss Infill System Capacity.....	85
A.1.4.Combined System Capacities.....	91
B. APPENDIX B .....	93
B.1. Method of Virtual Work .....	93

## LIST OF FIGURES

.....	Page
Figure 1.1. Performance level matrix proposed in the Vision 2000 report (SEAOC, 1995) (Taken from O'Reilly [2016]) .....	2
Figure 1.2. Pushover performance levels (after R.O. Hamburger) .....	3
Figure 1.3. Displacement-based assessment (as described by Priestley [1997]) .....	4
Figure 2.1. Displacement-based design Process (Courtesy of G.J. O'Reilly).....	7
Figure 2.2. Determining the force-deformation response of MDOF Structures according to Priestley <i>et al.</i> [2007] (Taken from Sullivan <i>et al.</i> 2018) .....	9
Figure 2.3. Algorithm for iteratively computing the displaced shape as proposed by Sullivan <i>et</i> <i>al.</i> [2018] (Taken from Sullivan <i>et al.</i> 2018) .....	10
Figure 2.4. Method B for taking account of infill contribution in structural response as desctried by Saborio-Romano [2016] (Taken from Saborio-Romano 2016).....	12
Figure 2.5. Suggested method of modelling damping ratios for infill panels in MIMA (adopted form Cardone and Flora, 2017).....	13
Figure 2.6. Proposed element model by O'Reilly and Sullivan [2017] (adopted from O'Reilly and Sullivan 2017). .....	14
Figure 2.7. (a) Moment-Curvature relationship proposed by O'Reilly and Sullivan [2017] and (b) shear response backbone curve defined in Zimos <i>et al.</i> [2015] (adopted from O'Reilly and Sullivan 2017) .....	15
Figure 2.8. Truss analogy for large infilled frames (adopted from Crisafulli 1997) .....	16
Figure 2.9. (a) Strut models considered in the sensitivity study by Crisafulli <i>et al</i> [2000] (b) resulting bending moments of the frame associated with each model presents by Crisafulli <i>et al.</i> [2000] (adopted from Crisafulli <i>et al.</i> 2000).....	17

Figure 2.10. Modes of failure of the infill panel given by Crisafulli [1997] (Taken from Crisafulli 1997) .....	18
Figure 2.11. Trilinear backbone response of the equivalent strut as cited by O'Reilly [2016] (Taken from O'Reilly 2016) .....	18
Figure 2.12. Failure modes of the infill panel given by Decanini <i>et al.</i> [2004] (Taken from O'Reilly 2016) .....	20
Figure 2.13. Masonry infill typologies given by Hak <i>et al.</i> [2012] (Taken from Hak <i>et al.</i> 2012) .....	21
Figure 3.1. (a) Two springs connected in parallel to a mass (b) Superposition of the flexural and the axial stiffness of the system .....	24
Figure 3.2. Steep initial stiffness portion due to the contribution of the reverse strut through gravity load unloading (Pushover curve of a 6-storey infilled frame). ....	25
Figure 3.3. (a) Resultant forces on a one-bay-one-storey truss setup due to applied lateral load P (b) Virtual case set for the horizontal displacement (c) Internal work done in the structure due to 1kN external force.....	26
Figure 3.4. Summed individual stiffnesses assuming that bays are connected with a rigid beam (a) Individual stiffnesses of bays (b) Total stiffness of the multi-bay frame.....	27
Figure 3.5. (a) Real Case: One-bay-two-storey representative truss structure (b) Virtual Case I: System set for computing the 2 <sup>nd</sup> storey displacement (c) Virtual Case II: System set for estimating 1 <sup>st</sup> floor displacement (d) Isolated internal work done by the 2 <sup>nd</sup> storey due to 1kN external force.....	28
Figure 3.6. (a) Real multi-bay-multi-storey frame (b) Virtual Case 1 to compute the 2nd floor displacement (c) Virtual case 2 to compute 1st floor displacement .....	30
Figure 3.7. (a) V.C. I.a: Node 03 is released in the vertical y direction. (b) V.C. II.a: Node 03 is released in the vertical y direction. (c - d) V.C. I-II.b: An external force is applied to node 03 to counter the computed displacement.....	31
Figure 3.8. (a) Infilled frame structure (b) Single strut model representation (c) Simplified MDOF structure representation of the strut model with the estimated storey system stiffnesses $K_{sys,i}$ (d) Final SDOF sub-structure with an applied horizontal force and a resulting displacement .....	33
Figure 3.9. Flow pattern of the external forces through an internal beam-column joint of a multi-bay-multi-storey infilled frame structure. (Observing the joint between 1 <sup>st</sup> and 2 <sup>nd</sup> bay of the i-th storey. Total number of bays is $\geq 3$ ).....	39

Figure 3.10. Approximate procedure to estimate the upper storey stiffness (Illustrated for a multi-storey-three-bay infilled frame) .....	40
Figure 3.11. Flowchart of the proposed simplified analysis procedure.....	43
Figure 4.1. The set of 2D bare frame structures adopted from Galli [2007] by O'Reilly [2016] .....	50
Figure 4.2. Illustration of the infill typologies and distributions for the 6-storey frame, for example.....	50
Figure 4.3. Geo-mean response spectra of the 30 events taken from INNOSEIS high seismicity record set. The geometric mean of each station's two component pairs is plotted. ....	53
Figure 4.4. Single component mean spectra of the reduced record set, where 10 selected events are seen to faithful represent the original mean and the standard deviation of the INNOSEIS database.....	54
Figure 4.5. Inter-storey Drift Ratio (IDR) Profile of each structure obtained through incremental dynamic analysis (IDA) [axes: Y - IDR (%)   X - $Sa(T)$ (g)] .....	55
Figure 4.6. Comparison of the force-displacement response computed via the simplified method with the SPO analyses.....	57
Figure 4.7. Comparison of the displacement profile obtained through the simplified method with the SPO analyses at various roof displacements.....	58
Figure 4.8. Evolution of the computed lateral storey force profile through subsequent limit states.....	59
Figure 4.9. Comparison of the force-displacement behaviour obtained with different approaches at limit state 1 ( $\Delta_{\text{roof}} = 0.02\text{m}$ ).....	60
Figure 4.10. Comparison of the displaced shapes obtained by utilising different approaches at limit state 1 ( $\Delta_{\text{roof}} = 0.02\text{m}$ ).....	61
 Figure A.1. Section Distribution of Galli_6st_WeakSingle vs Assigned Member and Component Numbering.....	73
Figure A.2. Element flexural strengths (kNm) (at joint centrelines) .....	76

## LIST OF TABLES

.....	Page
Table 2.1. Coefficients suggested by Bertoldi <i>et al.</i> [1993] .....	19
Table 2.2. Experimental median drift and dispersion corresponding to each limit state (Sassun <i>et al.</i> 2016) .....	21
Table 2.3. Mechanical properties of the masonry (Hak <i>et al.</i> 2012) .....	21
Table 3.1. List of Required Mechanical and Geometrical Properties.....	34
Table 3.2. An example model table of behaviour hierarchy for the first storey .....	42
Table 4.1. Modal analysis output of the bare frame .....	52
Table 4.2. Percent mass participation of each mode for different infill typologies.....	52
Table 4.3. Final set of selected 10 records for IDA .....	54
Table 4.4. Observed vs. proposed storey stiffness for the 6-storey weak infill structure considering limit state 1.....	62
Table 4.5. Observed vs proposed combined storey stiffness for the 6-storey weak infill structure. .....	62
Table A.1. Distribution of Masses on Galli_6st_MediumSingle.....	74
Table A.2. Mechanical Properties of the Weak/Medium/Strong Infill Typologies (Hak <i>et al.</i> 2012) .....	74
Table A.3. Frame Section Properties of Galli_6st_MediumSingle .....	75
Table A.4. Beam section moment-curvature results done in OpenSees .....	77
Table A.5. Beam section moment-curvature results done in OpenSees (cont.) .....	78
Table A.6. Column section moment-curvature results done in OpenSees .....	79
Table A.7. Column section moment-curvature results done in OpenSees (cont.) .....	80
Table A.8. Yield moment capacities obtained through joint equilibrium.....	81

Table A.9. Capping moment capacities obtained through joint equilibrium.....	81
Table A.10. Ultimate moment capacities obtained through joint equilibrium .....	82
Table A.11. Residual moment capacities obtained through joint equilibrium .....	82
Table A.12. Frame element moment-rotation capacities .....	83
Table A.13. Storey Flexural Backbone Curves .....	84
Table A.14. Infill-strut geometry computations. ....	85
Table A. 15. Strut model calculations for the medium infill typology.....	86
Table A.16. Strut element force-drift values for different critical points .....	87
Table A. 17. Strut element force-drift values for different critical points (cont.).....	88
Table A. 18. Unit horizontal displacements due to the axial stiffness of each member.....	88
Table A.19. Computed horizontal axial storey stiffnesses .....	89
Table A.20. Infill storey backbone. Shear resistance vs drift values.....	89
Table A. 21. Infill storey stiffness values. ....	90
Table A.22. Table of behaviour hierarchy for all storeys .....	91

*This page is intentionally left blank...*

# 1 Introduction

## 1.1 General

On the morning of January 17<sup>th</sup>, 1994 a part of the Oak Ridge Fault (aka Pico Thrust) ruptured, resulting in a Mw 6.7 earthquake causing 57 deaths, injuring more than 8,700 and inducing great losses in the order of tens of billion dollars - an iconic event which would be later called the Northridge earthquake (USGS 2013; SCEDC 2013). Due the proximity of the epicentre to Los Angeles, it was a major disaster with unacceptable consequences that pushed the civil engineering community in search for maturity, endurance and resilience for many years to come. Among other events with similar magnitude (such as Kobe 1995, Kocaeli 1999), the Northridge earthquake has become more famous for the lessons it taught and the improvements it triggered in the field of earthquake engineering. In the aftermath of 1994, a significant conceptual change in earthquake-resistant design and in the understanding of its potential economic impacts were initiated mainly with the Vision 2000 report (SEAOC 1995), ATC-40 [1996] and later with the series of FEMA reports FEMA 273 [1997], FEMA 356 [2000] and FEMA P-58 [2012]. Noticing the shortcomings of designing for the prevention of collapse in high intensity, low probability earthquakes which lead to unacceptable damage and high economic losses, the engineering community moved towards a performance-based earthquake engineering (PBEE) framework that focused on achieving a desired level of “system performance” under a given “earthquake design level” (Günay and Mosalam, 2013).

Under the early PBEE framework, the hazard intensity levels and the performance of the system were quantified with rigorous methods and the designer was able to “adjust” the properties of the structure in order to stay within a previously agreed performance state boundary. An example of such a design strategy was first given in the Vision 2000 report [1995]. The main idea was to commence with a design objective and limit the system response (forces, displacements etc.) within boundaries of performance levels given typically described via the performance matrix shown in Figure 1.1, thus maintaining complete control over the behaviour spectrum of the designed system. By applying this methodology in practice, engineers expected to ensure a minimum performance of a city/town during an expected seismic event like Northridge by, in a way, “programming” their structures to act in a certain way under earthquake shaking. Such an extensive check of the structural response requires detailed analysis of the system often with complex and computationally demanding numerical simulations. However, as the computational technology and resources became more and more

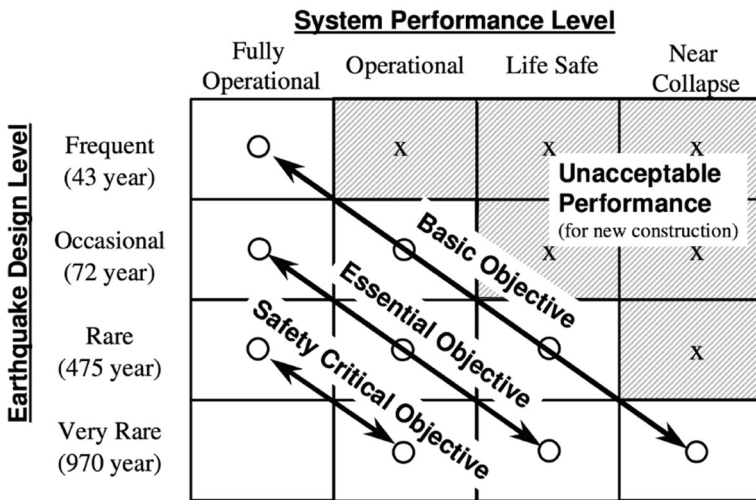


**Figure 1.1. Performance level matrix proposed in the Vision 2000 report (SEAOC, 1995) (Taken from O'Reilly [2016])**

available to the public, applying these kinds of analyses has become the norm of design in seismic codes.

The response capacity of the system was computed by either creating and analysing non-linear models (via time-history and/or pushover analysis, for example) or by approximating the non-linear behaviour with simplified methods. The superiority of a well-established non-linear time history analysis was widely accepted by the structural engineering community in representing the complete response and overall capacity of a structure with respect to the other methods. However, due to the somewhat tedious preparation process, extensive knowledge and detailed decisions (record selection, material behaviour, damping etc.) necessary prior to the analysis, opting for the comparatively easier pushover analysis that requires relatively fewer decisions is often preferred by practitioners. By simply pushing the structure with a monotonically increasing lateral force vector along the structure height and recording the base shear and the roof or inter-storey displacements, the response capacity of the system can be obtained and plotted. Upon characterising the system response, the concepts of PBEE can be applied as illustrated in Figure 1.2. Once the capacity of the system has been determined, the assessment process can be completed by comparing the capacity with the demand from the design earthquake by employing one of the several assessment methods or non-linear static procedures (NSPs) like the capacity spectrum (Freeman, 1978; ATC-40), N2 (Fajfar 2000; Eurocode 8) or displacement coefficient (FEMA 365, 2000) methods. The engine of most NSPs is based on the idea of reducing the non-linear multi-degree-of-freedom (MDOF) behaviour to an equivalent single-degree-of-freedom (SDOF) system in addition to quantifying an equivalent viscous damping. The displacement demand is then computed by matching the capacity curve with the inelastic acceleration-displacement response spectra (Monteiro *et al.* 2014). These assessment procedures are adopted by many modern seismic design codes and rehabilitation guidelines for the assessment of newly designed or existing buildings. However, even though the “early” PBEE methodology was a leap forward in late 1990s and even in 2000s, it was terminally missing a probabilistic aspect, characteristic to earthquakes (Günay and Mosalam, 2012).

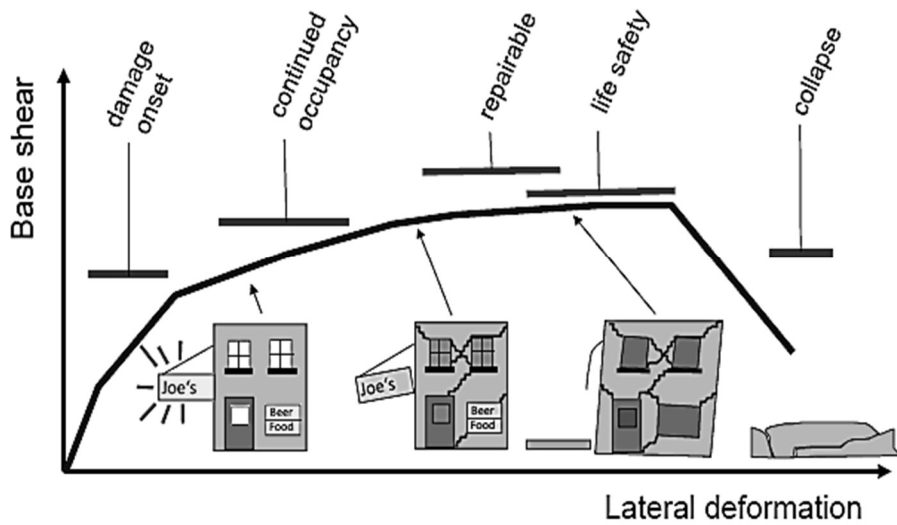


**Figure 1.2. Pushover performance levels (after R.O. Hamburger)**

Engineering problems have always been complex and often chaotic in the sense that they include various independent and interdependent parameters. In most cases, a certain problem is handled either by conducting detailed analyses or making simplifications. In any case, the obtained solution is an idealised construction of the reality and represents only one of the possible outcomes amongst all the scenarios in a broad solution space. Hence, defining the uncertainties in a problem is a crucial step to set the boundaries of the solution space and, further, defining the likelihood of each possible outcome. Thus, by having an expected value and its associated dispersion, the assessment process could be taken to a higher dimension, providing an enhanced understanding of the complete possible response capability of the system. As the locomotive of this breakthrough approach, the Pacific Earthquake Engineering Research (PEER) Centre, initiated a next-generation PBEE methodology that utilises all sources of identified uncertainties (hazard, record-to-record variability, structural response, modelling uncertainty etc.) in the construction of a problem. Each part was combined via the integral given in Equation 1.1. This approach was termed the PEER PBEE framework (Cornell and Krawinkler. 2000).

$$\lambda(DV) = \iiint G\langle DV | DM \rangle \, dG\langle DM | EDP \rangle \, dG\langle EDP | IM \rangle \, d\lambda(IM) \quad 1.1$$

The PEER PBEE framework drastically changed the understanding of structural assessment and introduced a loss-based (Deaths, Dollars and Downtime) estimation approach which has been mainly adopted in the FEMA P-58 (ATC 2012) guidelines, for example.

In parallel with the developments within the PBEE community and drawing attention to the shortfalls of the current force-based approaches and the stronger correlation between the structural damage and the earthquake-induced displacements (Moehle 1992; Priestley 1993, 2003; Priestley *et al.* 2007), a displacement-based design strategy was introduced to control the expected structural deformations during non-linear response. Later, building upon a capacity-based assessment procedure (Priestley and Calvi 1991) (later termed as force-based in Priestley

1997), the guidelines of a novel displacement-based assessment (DBA) approach were described by Priestley [1997] and revisited more recently by Priestley *et al.* [2007]. By following a defined procedure, obtaining the force-displacement, or pushover, curve of the structure under consideration was possible without rigorous computational analysis. This information could then be used for comparing the structural capacity with the seismic displacement demand. A flowchart of the early displacement-based assessment procedure is shown in Figure 1.3. DBA was revamped again by Sullivan and Calvi [2011] and further considerations were made regarding the application of the method and possible ways of probabilistically incorporating uncertainties in the overall assessment process. Finally, a further extension was presented by Welch *et al.* (2012) to bridge PEER's loss-assessment framework with the DBA methodology and an attempt to incorporate record-to-record variability together with loss estimation in a simplified analysis context was performed by Cardone and Flora [2017].

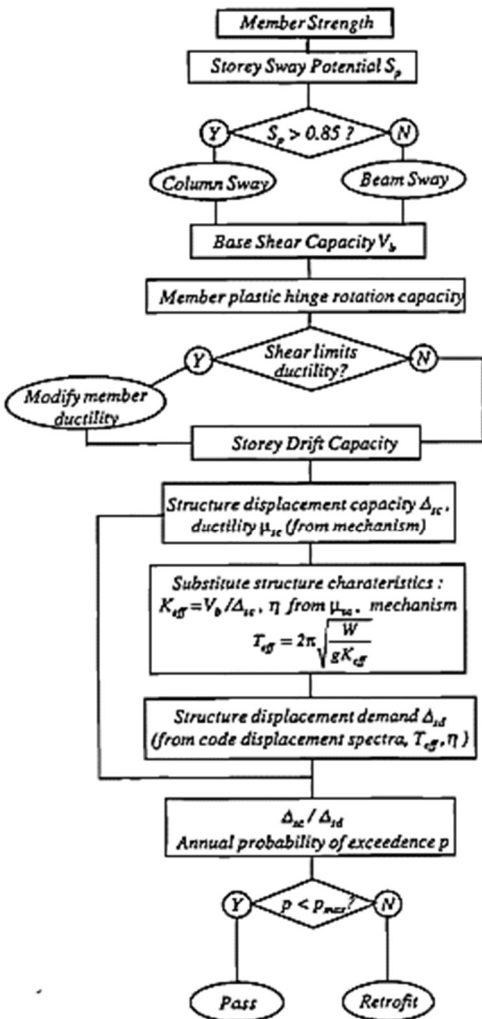


**Figure 1.3. Displacement-based assessment (as described by Priestley [1997])**

## 1.2 Objective

The PEER PBEE framework is one of the most powerful tools in modern seismic assessment. By far, it is the most extensive and reliable analysis methodology available in the literature for practitioners and academics. The PBEE framework relies on detailed and comprehensive analysis (often more than one) of a structure in order to extract the mean load-deformation response of the system and its associated dispersion. Requiring a lot less effort and being straightforward, a well-built pushover model can be quite efficient in characterising the building performance and is generally preferred as the first method of analysis by practitioners. Considering the computational capacity of today's computers, conducting a non-linear static analysis is a fairly automatic procedure and a structural model can be prepared with relatively little effort by the aid of the analysis software and built-in tools. This apparent automation often compromises the reliability of the results, sometimes even pushing the analyst to trust the output without questioning how realistic they actually may be.

Simplified analysis methods offer effective means of identifying structural deficiencies and provide analysts with a sound understanding of key structural characteristics, such as the strength hierarchy, status of each storey in terms of limit states and the progression of the inelastic mechanism, in addition to providing a method with which to check the feasibility of computational results. As recently shown by Sullivan *et al.* [2018], an efficient and precise pushover analysis of moment resisting frame buildings is possible in a simplified manner by adopting DBA principles. The output force-displacement plot can be used to estimate the loss distributions associated with the structure. However, there is a need to develop a methodology to extend the current procedure in order to account for masonry infills present together with the frame members in the computation of the lateral force-displacement capacity and include identification of the infill limit states to the overall assessment procedure. Following the aforementioned need, the main goal of this study is to outline a simplified nonlinear static analysis procedure that is able to capture the effects of masonry infill panels on the structural response of the frame structure. For the sake of simplicity, this study will not consider shear-flexure interaction for the capacity calculations of the frame members or effects of shear or joint failure in the boundary columns and beam-column joints which is also a phenomenon in infilled frames. However, the shear capacity of the columns may be computed with empirical equations such as the UCSD shear model introduced in Priestley *et al.* [1994] as a parallel process. Also, only the in-plane contribution of the infills without openings on the structural response is considered, ignoring the out-of-plane and its combined effect of the infill panel. This might be included by making use of recently developed macro-models for the combined response of the infill panels such as Di Trapani *et al.* [2018]. The aforementioned aspects are noted as future topics to be revisited. Finally, the developed methodology will be validated through comparing the force-displacement curves of several existing (pre-1970s) structures that are obtained through non-linear static analysis with the ones computed with the proposed simplified pushover methodology.

### 1.3 Outline of the Thesis

The outline and the structure of the thesis is as follows:

Chapter 1 provides the background for the main study in this thesis and to define the position of DBA amongst the current trends in the structural engineering community. For this reason, various related improvements in the field of assessment are mentioned together with a short history and the underlying ideology of the displacement-based procedures and the observed migration towards a PEER PBEE integrated assessment procedure is stated. Finally, the objective of this work is fully defined.

Chapter 2 is a review of the current state of research and knowledge on displacement-based design and assessment for frame structures. The behaviour of infilled frames and the associated damage states, numerical modelling and relevant modelling strategies available for infill panels are described.

In Chapter 3, the problem definition and assumptions made to handle the problem are given in detail. The theory of the proposed simplified analysis method is described and formulated. Later, based on the deduced formulas, a practical procedure is introduced to estimate the storey stiffness of an arbitrary infilled frame. Finally, a simplified method of nonlinear static analysis is proposed.

In Chapter 4, the description of the case study structures is given and the environment of numerical analysis together with the non-linear modelling of these frames is described. Following, in order to validate the results obtained through the simplified procedure in the next step, a series of linear and nonlinear dynamic analysis are done to case study frames to fully assess their behaviour. Next, the 6-storey case study frame is analysed with the proposed method and the obtained results are compared with the ones that were obtained through IDA and pushover analyses. Finally, the performance of the proposed method is compared with the other simplified methods available in the literature.

In Chapter 5, the proposed procedure is summarised and critically evaluated. Finally, several topics to be addressed in the future that are deemed beyond the scope of this thesis are outlined, in addition to possible applications for which this work can be developed.

Finally, in Chapter 6, the references that are cited throughout this thesis are given.

## 2 Literature Review

### 2.1 Assessment of Existing Structures

#### 2.1.1 A Displacement-Based Approach

At the beginning of the 20<sup>th</sup> century, Moehle [1992] and Priestley [1993] proposed a displacement-based design strategy, presenting evidence that the earthquake-induced displacements are better linked with structural damage than seismic forces. In addition, a force-based design approach leads engineers to significant errors in estimating the lateral structural stiffness and its inelastic capacity due to a series of misguided core assumptions (such as modal combinations, equal displacements etc.) according to Priestley [1993; 2003]. As a remedy to these problems, Priestley [1993; 2003] introduced a displacement-based design procedure instead of a traditional force-based procedure to design and detail new structures. With the described displacement-based procedure, a target displacement profile is chosen, and the structural stiffness computed based on the corresponding period defined through the design displacement spectrum. The expected displaced shape is conditioned on the structural type as well as whether or not the capacity design requirements have been met (Priestley, 1993; 2003; Priestley *et al.* 2007; Sullivan *et al.* 2012). The MDOF structure is then converted to a SDOF substitute-structure (Shibata & Sözen, 1987) and the inelastic displacement demand is computed with an analogous equivalent viscous damping (Gülgan & Sözen, 1974). A short summary of the displacement-base design procedure can be seen in Figure 2.1

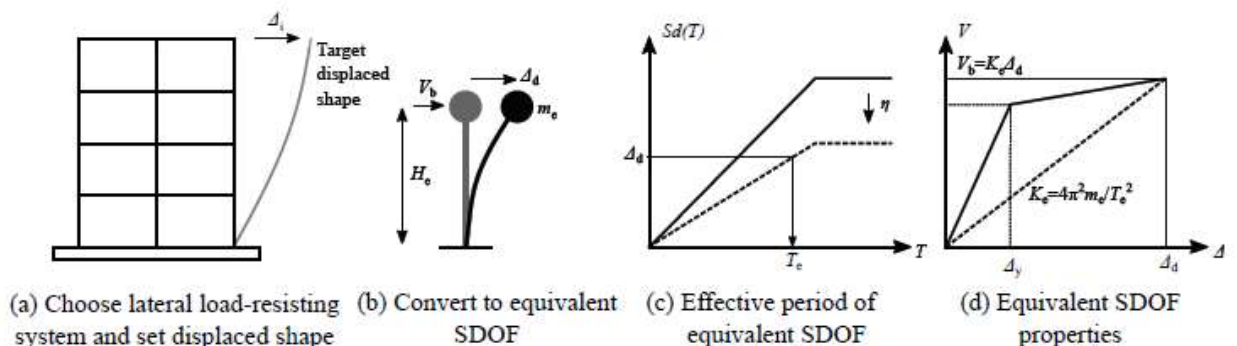


Figure 2.1. Displacement-based design Process (Courtesy of G.J. O'Reilly)

### 2.1.2 Displacement-Based Assessment

The displacement-based seismic assessment methodology was first introduced by Priestley [1997], (and revisited in Priestley *et al.* 2007) as an amendment to the standard force-based assessment procedure which comprises a simple check of force demand and capacity and misses several critical aspects of an assessment method such as the estimation of displacements, structural ductility or the inelastic mechanism (Priestley *et al.* 2007). Also, Priestley *et al.* [2007], critically discuss the downside of using Incremental Dynamic Analysis (Vamvatsikos & Cornell 2002) results, such as the introduced bias due to scaling of the records, as a basis of assessment and the comparative advantages of using of a displacement-based approach. Priestley *et al.* [2007] proposed two alternative approaches to conduct DBA: the first as a pass/fail assessment of the code compliance of the structure in terms of displacements; whereas in the second methodology, the objective was to determine the risk of the system. As one of the outputs of this thesis, one possible use of the obtained force-displacement response of the infilled structure would be to employ it in one or both of these procedures in order to complete the assessment procedure.

The framework to compute the complete force-displacement response of bare frame structures was described in Priestley *et al.* [2007]. After the yield mechanism is identified (column-sway or beam-sway) with the help of the sway potential index described in Equation 2.1,  $S_i$ , for the beam-sway, the characteristic displaced shape is obtained with two empirical shape functions proposed by Priestley [1997] (also advocated in Priestley *et al.* 2007) and verified by Pettinga and Priestley [2005]. The ***sway potential index*** of a storey is given by:

$$S_i = \frac{\sum_j (M_{bl} + M_{br})}{\sum_j (M_{ca} + M_{cb})} \quad 2.1$$

where  $M_{bl}$  and  $M_{br}$  are the flexural strengths of the right and left beams connecting to the joint and  $M_{ca}$  and  $M_{cb}$  are the flexural strengths of the above and below columns connecting to the joint. According to Priestley [1997], obtaining an  $S_i$  lower than 1.0 indicates a beam-sway mechanism while a column-sway type of failure is associated with a value higher than 1.0. However, Priestley [1997] also suggests assuming a column-sway mechanism when  $S_i$  is greater than 0.85. Finally, the ***displaced shape function*** to be employed is given by Equations 2.2 and 2.3 (as rearranged in Sullivan *et al.* 2012):

$$\text{for } n \leq 4: \quad \Delta_i = \theta_c h_i \quad 2.2$$

$$\text{for } n > 4: \quad \Delta_i = \theta_c h_i \left( \frac{4H_n - h_i}{4H_n - h_1} \right) \quad 2.3$$

where  $n$  is the number of storeys,  $\theta_c$  is the critical storey drift,  $h_1$  is the height of the first storey,  $h_i$  is the height of the  $i^{\text{th}}$  storey and  $H_n$  is the total height of the structure. The overall procedure can be seen in Figure 2.2.

Utilising DBA principles, Cardone and Flora [2017] proposed an assessment scheme called multiple inelastic mechanisms analysis (MIMA) method to estimate the force-displacement response of RC frame structures and then employ the results in a PEER PBEE-based assessment

framework, addressing the uncertainties coming from record-to-record variability. This was done by using the displacement response spectrum obtained through the conditioned mean spectrum (CMS) (Baker 2011) associated with the site in which the displacement capacity of the corresponding sub-structure was compared with the mean displacement demand given by the CMS. Furthermore, an application of the proposed methodology was illustrated by Cardone and Flora [2017] with an example pre-1970s RC frame structure which is designed only for gravity loads.

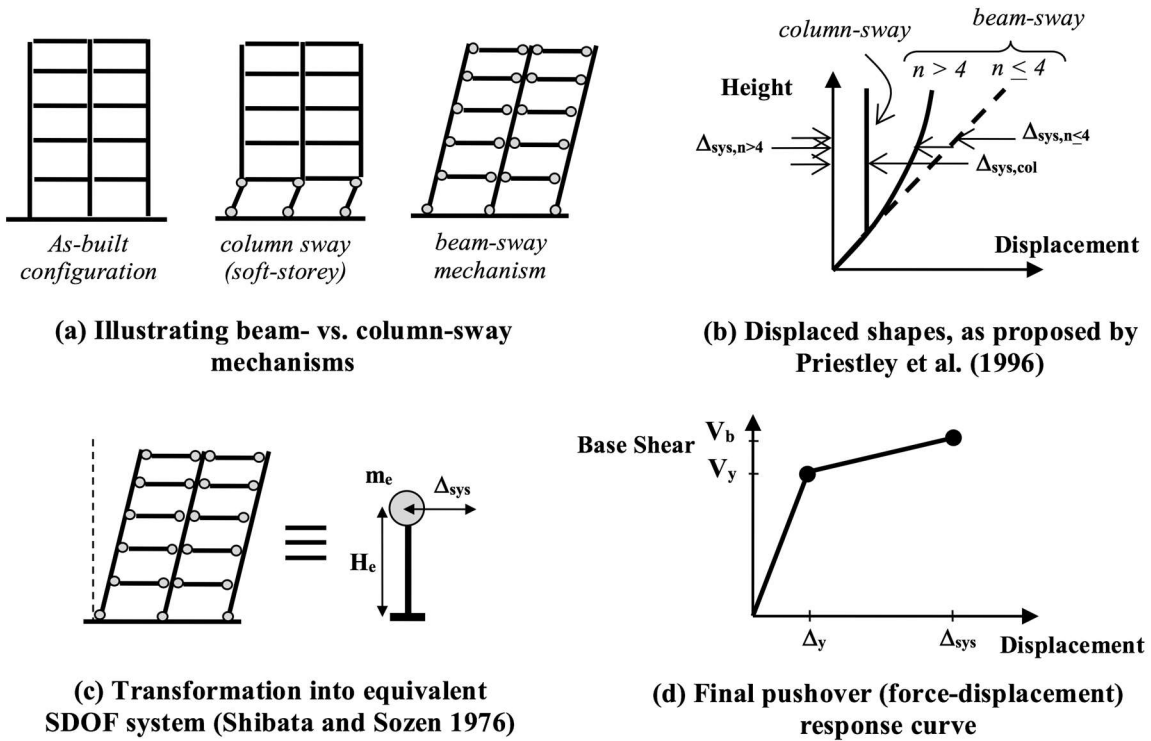


**Figure 2.2. Determining the force-deformation response of MDOF Structures according to Priestley *et al.* [2007]** (Taken from Sullivan *et al.* 2018)

Aligned with the developments in the original DBA procedure, the New Zealand Society of Earthquake Engineering (NZSEE), introduced the Simple Lateral Mechanism Analysis (SLaMA) procedure for the assessment of the frame structures in “The Seismic Assessment of Existing Buildings: Technical Guidelines for Engineering Assessments” [2017] (Gentile *et al.* 2019a). As reported by Gentile *et al.* [2019a], the SLaMA procedure is emphasised in the NZSEE guideline in order to provide greater understanding of the “deformability” of the structure to the analyst, prior to other numerical analysis-based assessment techniques. Gentile *et al.* [2019a] provided improvements and refinements to the SLaMA strategy in order to compute the displaced shape of the assessed structure using the shape equations proposed by Priestley *et al.* [2007].

Recently, Sullivan *et al.* [2018], revisited and updated the force-deformation analysis procedure proposed by Priestley *et al.* [2007] for RC frame structures by proposing refinements and an extended mechanical basis for the computation of the expected displaced shape. According to Sullivan *et al.* [2018], the employment of empirical expressions (2.2 - 2.3) yields significant

errors in the prediction of the displaced-shape and this was demonstrated for a 6-storey frame where the displaced shape was computed with an error as high as 34%, when compared to the pushover analysis. Hence, building upon Priestley *et al.* [2007], Sullivan *et al.* [2018] proposed an iterative procedure to compute the structure-specific displaced shape and backbone pushover curve. As an adjustment, the ground storey yield drift was suggested to be computed with a new formula dependent on the contraflexure height where the boundary condition is assumed as a cantilever. Furthermore, in order to better identify the strength hierarchy of the structure under assessment, a sway-demand index,  $S_{Di}$ , as introduced by Sullivan and Calvi [2011], was incorporated in the analysis procedure. The flowchart of the algorithm constructed by Sullivan *et al.* [2018] can be seen at the Figure 2.3 and the **sway demand index** proposed by Sullivan and Calvi [2011] is described in Equation 2.4.

$$S_{Di} = \frac{V_i}{V_{R,i}} \quad 2.4$$

where  $V_i$  is the storey shear demand and the  $V_{R,i}$  is the storey shear capacity at level i.

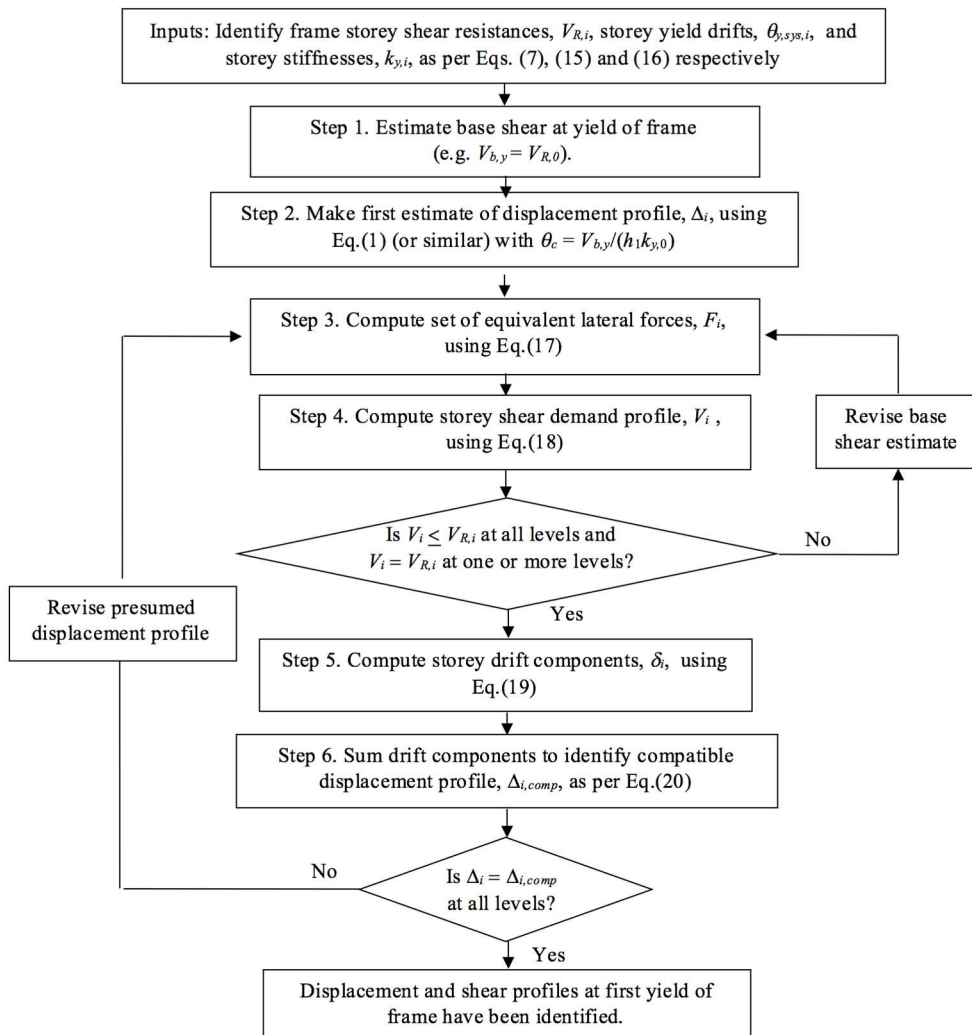


**Figure 2.3. Algorithm for iteratively computing the displaced shape as proposed by Sullivan *et al.* [2018]**  
(Taken from Sullivan *et al.* 2018)

Further details about the methodology and the full suite of formulas employed by Sullivan *et al.* [2018] will be covered in more detail in Chapter 3.

### 2.1.3 Masonry Infill Consideration

The majority of the developments for the DBA of frame structures have been done considering only bare frames, ignoring the presence of masonry infill panels often found inside the frame system. Per contra, the in-plane contribution of the infills to the structural has been shown to be significant and ought to be included in both design and assessment.

The issue of masonry infilled frames was addressed by Priestley *et al.* [2007] within a displacement-based context. According to Priestley *et al.* [2007], the DDBD of an infilled frame is done by targeting the damage-control limit state ( $\sim 0.02$  radians drift for the design earthquake), assuming that the infill contribution was negligible for small drifts. To characterise the load-deformation capacity for DBA, Priestley *et al.* [2007] did not describe any specifications in order to account for the infill contribution which eventually leads to overestimation of the displaced shape and hinders the capability of the overall procedure in predicting the infill panel damage states.

In an attempt to remedy this, Landi *et al.* [2016] suggested the use of calibrated ductility-damping (equivalent viscous damping) expressions for the DBA of infilled frames based on the results of numerous nonlinear time-history (NLTH) analyses done on three different types of single-storey infilled and bare frames. In addition, the displaced shape of the infilled frame was computed by scaling the shape functions given by Equations 2.2 – 2.3 with the mean value of the infilled to bare frame displacement ratios obtained for all storeys that were obtained through pushover analysis.

In the same year, Saborio-Romano [2016], proposed two different methodologies to account for infills in the computation of the force-deformation behaviour. The first formulation, “Method A,” assumed that the global mechanism of the frame was not affected by the presence of the infills. Hence, the contribution of the infill panels was considered as increased base shear, included in the overturning moment (OTM) resistance and the displacement behaviour was thought to be following the experimentally calibrated backbone curve given by Sassun *et al.* [2016]. On the other hand, in “Method B”, the displaced shape prediction was based on the individual stiffnesses of the infill wall and the bare frame. The storey system (infilled frame) yield drift was calculated by adding the two couple moments due to infills at levels  $i-1$ ,  $i$  and  $i+1$  storeys in addition to the frame top and bottom moment capacities. An illustration of the procedure can be seen in Figure 2.4. The storey yield drift was computed by the Equation 2.5.

$$\theta_{y,sys,i} = \frac{\sum M_i \theta_{y,i} + \sum M_{i-1} \theta_{y,i-1} + \sum M_{i,m} \theta_{y,i,m} + \sum M_{i-1,m} \theta_{y,i-1,m} + \sum M_{i+1,m} \theta_{y,i+1,m}}{\sum M_i + \sum M_{i-1} + \sum M_{i,m} + \sum M_{i-1,m} + \sum M_{i+1,m}} \quad 2.5$$

where  $M_i$ ,  $M_{i-1}$ ,  $\theta_{y,i}$ ,  $\theta_{y,i-1}$  and  $M_i$ ,  $M_{i-1}$ ,  $M_{i+1}$ ,  $\theta_{y,i}$ ,  $\theta_{y,i-1}$ ,  $\theta_{y,i+1}$  are the moment capacities and the yield drifts of the frame and infill elements distributed around the  $i$ -th storey. Finally, the moment capacities of the infill elements were computed with the following expressions:

$$\sum M_{i,m} = \sum V_{y,i,m} h_{s,i} \quad \sum M_{i-1,m} \sum V_{y,i-1,m} \frac{h_{s,i-1}}{2} \quad \sum M_{i+1,m} \sum V_{y,i+1,m} \frac{h_{s,i+1}}{2} \quad 2.6$$

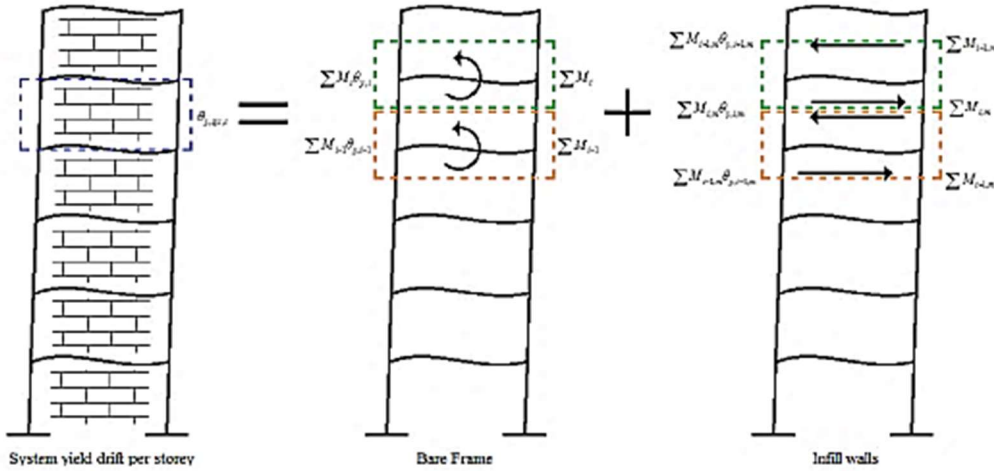


**Figure 2.4. Method B for taking account of infill contribution in structural response as described by Saborio-Romano [2016] (Taken from Saborio-Romano 2016)**

Then, the equivalent viscous damping was computed first with the damping expressions given by Landi and Benedetti [2013] in addition to a second hybrid methodology in which the damping was assumed to be 5% throughout the initial structural stiffness until the exceedance of the 1<sup>st</sup> damage state of the infill walls, after which the expression of Landi and Benedetti [2013] was used.

The MIMA method (Cardone and Flora, 2017) proposed a coefficient-based approach to account for the effects of infills and stairs. The displaced shape of the infilled frame was obtained by first computing the bare frame yield profile and scaling it with a reduction factor ( $\alpha$ ) which was iteratively updated until the sub-structure displacement meets with the one obtained through the displacement response spectra. Furthermore, Cardone and Flora [2017] suggested employing an equivalent viscous damping based on the strength characteristics of the infill panels and is shown in Figure 2.5.

Recently, Gentile *et al.* [2019b] proposed and extension of the SLaMA methodology for infilled RC frames. In the SLaMA infilled methodology, the bare frame and the infill force-displacement curves were separately computed (decoupled). The combined storey response was then obtained by the superposition of the two results. The in-plane infill contribution was taken into account with the horizontal axial force capacity of the infill, modelled as a diagonal strut. Since the failure modes of the infill could be differentiated, the strut model developed by Bertoldi *et al.* [1993] was employed in the introduction of the procedure.

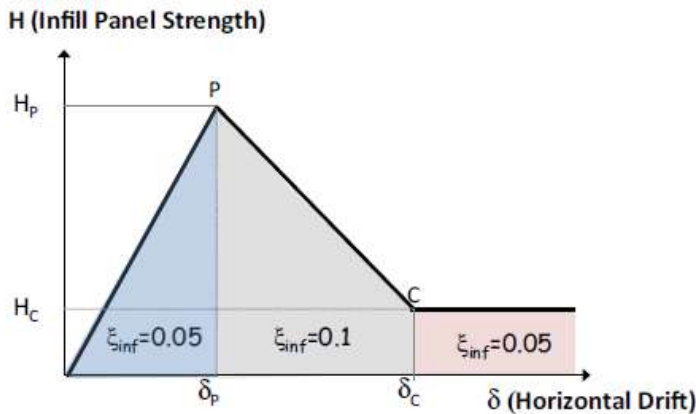


**Figure 2.5. Suggested method of modelling damping ratios for infill panels in MIMA (adopted from Cardone and Flora, 2017)**

## 2.2 Behaviour and Numerical Modelling of Infilled RC Frame Members

### 2.2.1 Modelling of RC Frame Members

In a PBEE framework, seismic assessment of structures may be done either by quantifying and validating the performance of a newly designed structure or characterising the vulnerability of an existing structure in order to aid decision making. For example, the results obtained can be used in making possible retrofit considerations and by repeating the analysis, the effect of the chosen improvement on the expected monetary loss can be studied. From an assessment point of view, the development of modern seismic regulations is a relatively recent step taken in some countries while it is currently under process in many others. Hence, when the current existing building stock in seismic-prone countries around the world is considered, it is often possible to encounter those without seismic code compliant buildings or even with structures that were not designed for any earthquake loading considerations.

Italian RC frame structures designed prior to the introduction of the first modern seismic design in the 1970s are a representative sub-group in this regard, with their design and detailing of the lateral load resisting system done according to the Royal Decree [Regio Decreto, 1939]. According to this, allowable stress philosophy was adopted in design, smooth bars were used and there was no regulation on the amount of transverse reinforcement to be used neither throughout the length of the RC elements nor in the beam-column joint regions. (O'Reilly and Sullivan 2017). In order to emphasise the lack of seismic design provisions in these frame structures, O'Reilly and Sullivan [2017] defined them as gravity load designed (GLD) frames. Moreover, these types of frames are most likely to be found with masonry infills and subjected to infill-frame interaction.

Referring to the field observation or experimental results of various authors, the overall behaviour of the GLD frames are reported by O'Reilly and Sullivan [2017]. The main issue identified regarding the performance of the GLD frames was their susceptibility to column and/or joint shear failure due to insufficient transverse reinforcement ratios. This problem was emphasised even more in cases with masonry infills or mezzanine floors which may lead to increased shear forces at the boundary columns and joints or cause short column failures. In

addition, these frames were lacking any capacity design requirements thus, increasing the likelihood of observing soft-storey mechanisms. Pampanin *et al.* [2002] identified, in terms of joint failure, a “concrete wedge” yielding mechanism that was observed due to beam-column joints consisting of insufficient transverse reinforcement. In a similar study, Calvi *et al.* [2002] reported the effect of this phenomenon on the global mechanism as a spreading of increased deformation in the beam-column joint to both adjacent storeys. Finally, Melo *et al.* [2015] pointed out that a different type of plastic hinging at the end regions of the columns was observed as a result of using plain bars. The effect of plain bars on the hinge region was seen to concentrate fewer but wider cracks instead of many small distributed cracks leading to a lower energy dissipation capacity and a pinched hysteretic behaviour. However, Di Ludovico *et al.* [2014] showed that the use of plain bars could lead up to 40% of increase in the deformation capacity of the RC frame members due to the increased plastic rotation at the column hinge zone.

Considering the aforementioned properties of GLD frames, O'Reilly and Sullivan [2017] proposed a modelling strategy based on an experimental database of 23 GLD test specimens. This database of beam-column members was gathered by picking test cases representing the behaviour of pre-1970 Italian frames with plain bars and poor seismic detailing. O'Reilly and Sullivan [2017] then proposed a lumped plasticity element with flexural hinges and uncoupled shear hinges in OpenSees (McKenna *et al.* 2010) to model these GLD frame members. An illustration of the element model can be seen at Figure 2.6.

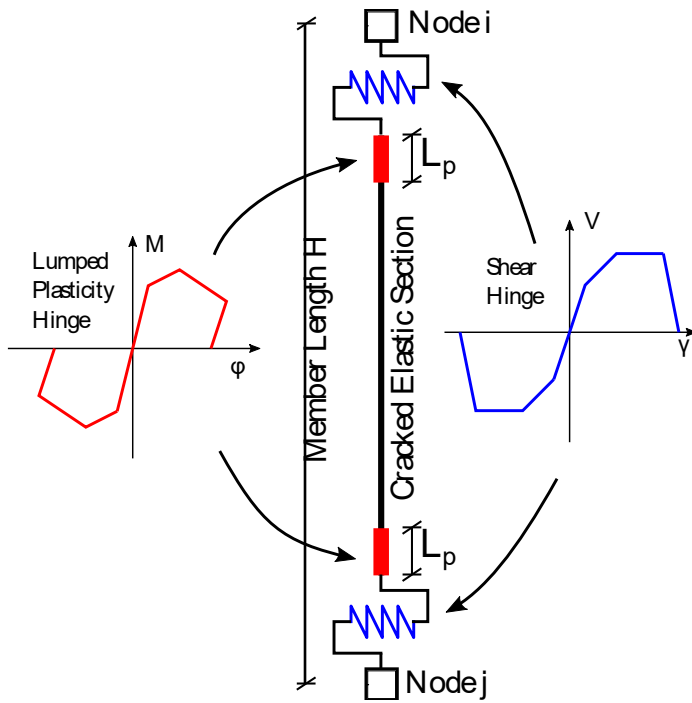


**Figure 2.6. Proposed element model by O'Reilly and Sullivan [2017] (adopted from O'Reilly and Sullivan 2017).**

The hysteretic response of the flexural hinges was constructed in line with the approach adopted by Haselton *et al.* [2008], where a moment-curvature relationship and plastic hinge length were calibrated with the data available in the database of pre-1970 frame members. For the shear

hinges, a shear force-deformation backbone curve was defined using the work developed by Zimos *et al.* [2015]. The flexure and shear backbone curves employed by O'Reilly and Sullivan [2017] can be seen at Figure 2.7. In OpenSees, the backbone curves are computed for each member by applying a moment-curvature analysis while assembling the model. Finally, no axial-flexure-shear interaction is considered during the analysis.

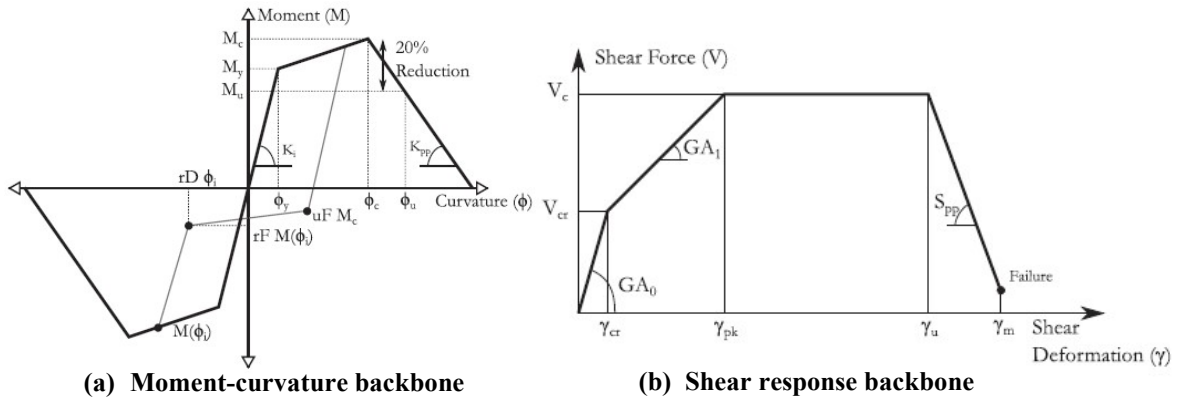


**Figure 2.7. (a) Moment-Curvature relationship proposed by O'Reilly and Sullivan [2017] and (b) shear response backbone curve defined in Zimos *et al.* [2015] (adopted from O'Reilly and Sullivan 2017)**

O'Reilly and Sullivan [2017] also proposed an external and an internal joint modelling strategy to model the under-reinforced (transverse) joints of GLD frames by using the so called “scissors model” setup where connecting beams and columns were linked with rigid elements and a rotational spring to capture their shear deformations. More detailed information on the modelling decisions and backbone curves can be found in O'Reilly [2016].

### 2.2.2 Masonry Infill-RC Frame Interaction

Often considered non-structural elements, infills have typically been ignored by many codes and practitioners while computing the force-displacement capacity of the structure. During design, seismic codes (EC 8) allows engineers to design the frame without considering the infill-frame interaction, provided that a previously determined drift limit is satisfied by the system under the design ground motion. However, it has been shown by many studies that infill-frame interaction significantly alters the response of the surrounding frame (Panagiotakos and Fardis 1996; Crisafulli 1997; Calvi *et al* 2004; Fenerci *et al.* 2016). According to Fenerci *et al.* [2016], the ductility capacity of the system was significantly affected by the shear damage on the boundary columns due to the large shear forces transferred by the infill panels. The global stiffness of the structure was increased due to the contact between the infill wall and the frame and the diagonal strut action provided by the infills. As the lateral force increases, this contact partially separates along the tension diagonal of the wall. Considering multi-storey infilled RC frames subjected to horizontal loads, Crisafulli [1997] proposed an equivalent truss mechanism in which the lateral force applied at a higher storey is transferred by the diagonal strut and the boundary column to the below storey while applying tension to the first boundary column and compression to the strut and the secondary column. The force flow diagram given by Crisafulli [1997] can be seen in Figure 2.8. For multi-bay frames, Crisafulli [1997] noted that the truss mechanism for multi-storey configuration is also reasonably applicable to multi-bays as well,

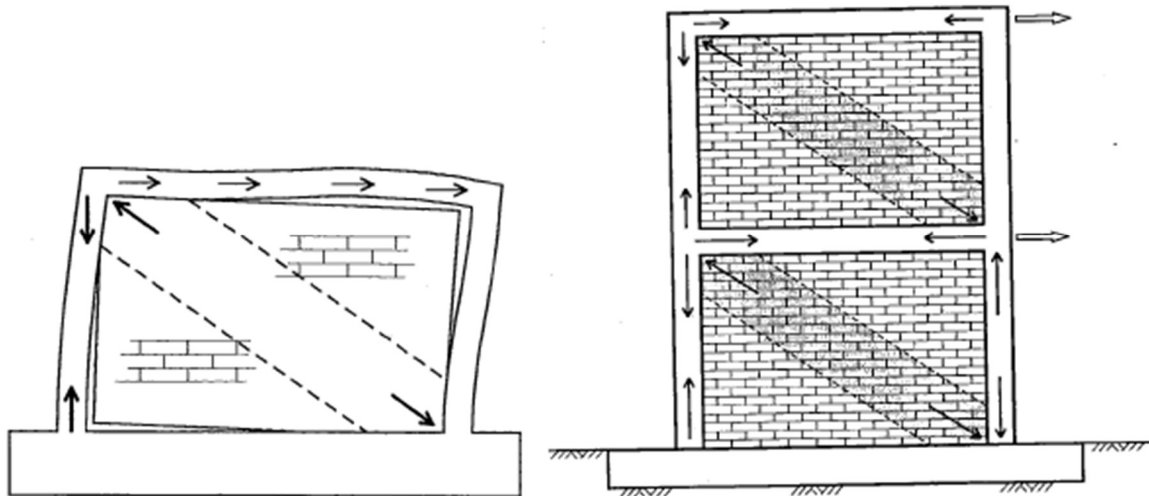


**Figure 2.8. Truss analogy for large infilled frames (adopted from Crisafulli 1997)**

despite the complex behaviour of the setup due to the mid-column, as noted by Kwan *et al.* [1990].

### 2.2.3 Modelling of Masonry Infill Panels

In line with the scope of this thesis, the infill panel contribution to the overall structural response should be taken into account first in the numerical model and second, in the proposed design and assessment methodology. The modelling strategy should be capable of accurately transferring the strut horizontal force components to the lower storeys, represent the presence of infills on the global displacement profile, accurately model the shear transferred to the boundary columns and finally, it should be straight-forward enough to be incorporated into a simplified procedure. There is rich literature on modelling approaches for infill panels from various backgrounds and with different objectives in mind. To start with, modelling strategies are famously divided into two classes: micro and macro-models.

Micro models are created by considering the infill panel as a wall element consisting of smaller member either modelled as real sized bricks or representative elements. These modelling strategies are capable of representing the mechanical behaviour of the wall and the infill-frame interaction with relative accuracy. Micro-models are often used by researchers to simulate experiments or the complex phenomena such as crack propagation or failure of the system. However, these methods are computationally expensive and unsuitable for simplified analysis problems related to seismic design and assessment. Extensive information and review on the micro-modelling of infill walls was reported by Crisafulli [1997] and Asteris *et al.* [2013].

Macro models, on the other hand, reduce the infill wall system to an equivalent strut member or set of struts to represent the contribution of the infills. These types of models are more focused on the structural behaviour of the system rather than specific mechanics of the masonry infill wall. Later, the state of the infills can be indirectly obtained by relating the system forces and displacements to a backbone response for the infill panel. By nature, macro models are

more suitable to a simplified analysis context and compatible with the existing approaches that has been used to compute element capacities in the DBA procedure.

Crisafulli *et al.* [2000] presented an extensive review of the strut modelling approaches available in the literature. It referred the strut model as an interpretation of the diagonal compression zone of the masonry wall as a result of the horizontal loading. Furthermore, the single strut model was extended to a double and triple strut model to represent the infill column and infill-beam interaction in an efficient manner. Crisafulli *et al* [2000] also conducted a sensitivity analysis where the performance of the single strut analogy was compared with the double, triple strut model and FEM analysis. The typology of the models that were studied and the resulting bending moment diagrams can be seen in Figure 2.9. According to Crisafulli *et al.* [2000], single strut models underestimate the bending moments mainly due to the truss mechanism resisting the lateral forces, while a double strut analogy overestimates the frame moments. The best approximation was obtained with a triple strut approach where, still, some slight differences in the bending moments are seen at the column ends. Crisafulli *et al.* [2000] concludes by stating that, although the single strut model is relatively simple, it yielded adequate prediction of the infilled frame's stiffness.

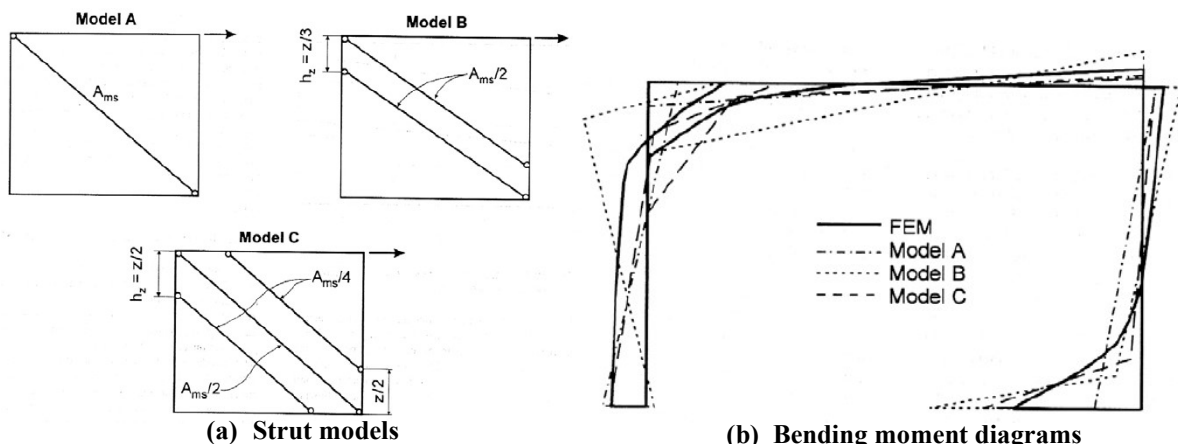


**Figure 2.9. (a) Strut models considered in the sensitivity study by Crisafulli *et al* [2000] (b) resulting bending moments of the frame associated with each model presents by Crisafulli *et al.* [2000] (adopted from Crisafulli *et al.* 2000)**

Finally, an axial backbone curve to represent the masonry behaviour should be adopted. In the past, numerous proposals were made by Bertoldi *et al.* [1993], Panagiotakos and Fardis [1994], Crisafulli [1997] and Decanini *et al.* [2004] to define the parameters of the backbone response. These particular models have been drawn attention due to their capability in identifying the failure modes of the infill setup. Crisafulli [1997] described the classical failure modes of the infill panel as: cracking along mortar joints; diagonal tension; failure of the compression strut; and corner crushing. An illustration of the possible failure modes was given by Crisafulli [1997] and is shown in Figure 2.10.

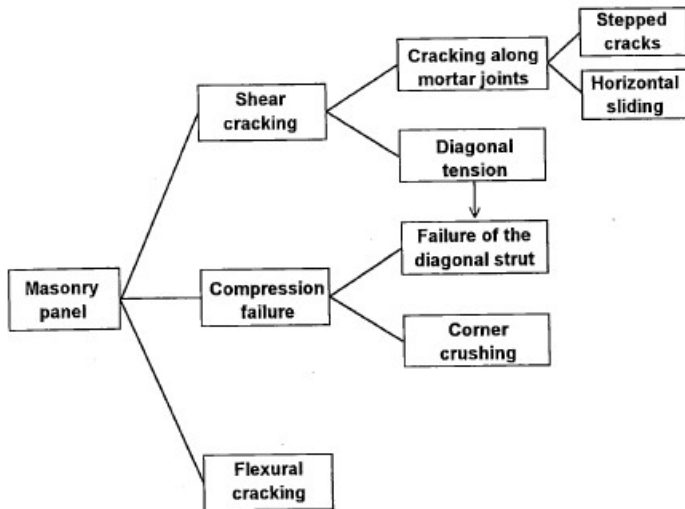


**Figure 2.10.** Modes of failure of the infill panel given by Crisafulli [1997] (Taken from Crisafulli 1997)

Hak *et al.* [2012], Sassun *et al.* [2016] and O'Reilly [2016] utilised a hybrid modelling approach for the hysteretic backbone of the strut. The characteristics of the backbone curve can be seen in Figure 2.11.

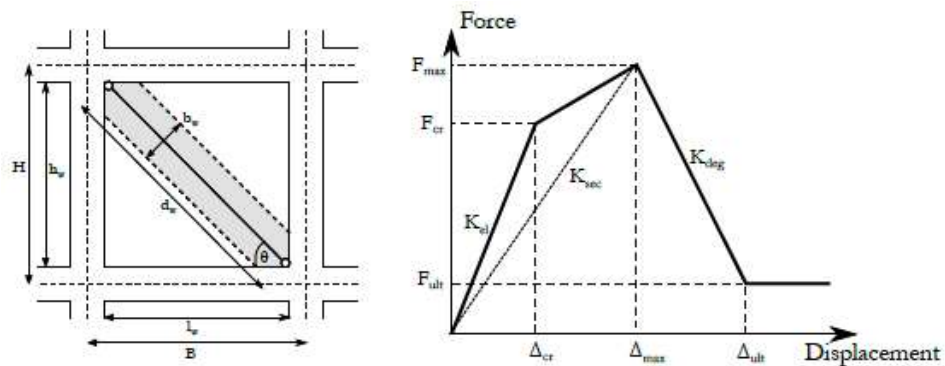


**Figure 2.11.** Trilinear backbone response of the equivalent strut as cited by O'Reilly [2016] (Taken from O'Reilly 2016)

The steps to compute the parameters of the model were given as follows (as in Hak *et al* 2012; Sassun *et al.* 2016; O'Reilly 2016):

**Step 1:** Equivalent strut thickness,  $t_w$ , assumed to be the same to the thickness of the infill.

**Step 2:** Elastic modulus,  $E_{w\theta}$ , of the masonry in the inclined direction, computed as:

$$E_{w\theta} = \left[ \frac{\cos^4 \theta}{E_{wh}} + \frac{\sin^4 \theta}{E_{wv}} + \cos^2 \theta \sin^2 \theta \left( \frac{1}{G} - \frac{2\nu}{E_{wv}} \right) \right]^{-1} \quad 2.7$$

where  $E_{wh}$ ,  $E_{wv}$ ,  $G$  and  $\nu$  were the horizontal and vertical moduli, shear modulus and the axial load to section area ratio of the masonry.

**Step 3:** The parameter  $\lambda$  was computed with the following expression (Stafford Smith 1966):

$$\lambda = \sqrt[4]{\frac{E_{w\theta} t_w \sin 2\theta}{4E_c I_c h_w}} \quad 2.8$$

where  $E_c$ ,  $I_c$ ,  $h_w$  correspond to the elastic modulus of concrete, moment of inertia and the free section height of the boundary column.

**Step 4:** Based on  $\lambda H$ , constants  $K_1$  and  $K_2$  were determined from the Table 2.1(Bertoldi *et al.* 1993), where  $H$  is the storey height calculated as the distance between the centrelines of the storey beams.

**Table 2.1. Coefficients suggested by Bertoldi *et al.* [1993]**

	$\lambda H < 3.14$	$3.14 < \lambda H < 7.85$	$\lambda H > 7.85$
$K_1$	1.300	0.707	0.470
$K_2$	-0.178	0.010	0.040

**Step 5:** The equivalent strut width,  $b_w$ , was computed from (Bertoldi *et al.* 1993):

$$b_w = \left( \frac{K_1}{\lambda H} + K_2 \right) d_w \quad 2.9$$

where  $d_w$  is the free length of the diagonal strut.

**Step 6:** The maximum stress values were computed for each expected failure mode with the following expressions and  $F_{max}$  was taken as the minimum strength times the strut cross sectional area. Failure modes are portrayed at Figure 2.12 (Decanini *et al.*, 2004):

$$F_{max} = \min (\sigma_w) b_w t_w \quad 2.10$$

where:

$$\text{Diagonal tension} \quad \sigma_w = \frac{0.6f_{ws} + 0.3\sigma_v}{\frac{b_w}{d_w}} \quad 2.10a$$

$$\text{Shear sliding} \quad \sigma_w = \frac{(1.2\sin\theta + 0.45\cos\theta)f_{wu} + 0.3\sigma_v}{\frac{b_w}{d_w}} \quad 2.10b$$

$$\text{Corner crushing} \quad \sigma_w = \frac{1.12f_{wv}\sin\theta\cos\theta}{K_1(\lambda H)^{-0.12} + K_2(\lambda H)^{0.88}} \quad 2.10c$$

$$\text{Compressive failure} \quad \sigma_w = \frac{1.16f_{wv}\tan\theta}{K_1 + K_2\lambda H} \quad 2.10d$$

where  $f_{ws}$ ,  $f_{wu}$ ,  $f_{wv}$ ,  $\sigma_v$  are the diagonal shear compression strength, sliding resistance of the mortar, vertical compressive strength of the masonry and vertical stress on the masonry due to gravity loads.

**Step 7:** The secant axial stiffness,  $K_{sec}$ , of the strut is computed as:

$$K_{sec} = \frac{E_w \theta t_w b_w}{d_w} \quad 2.11$$

**Step 8:** Finally, as stated by Sassun *et al.* [2016], the first cracking force,  $F_{cr}$ , residual force,  $F_{ult}$ , and the corresponding initial stiffness,  $K_{el}$  and negative stiffness,  $K_{deg}$  were computed from:

$$F_{cr} = 0.8F_{max} \quad 2.12$$

$$F_{ult} = 0.10F_{max} \quad 2.13$$

$$K_{el} = 4K_{sec} \quad 2.14$$

$$K_{deg} = -0.02K_{sec} \quad 2.15$$

The failure modes of the infill panel that was modelled by the strut analogy, which were given by Decanini *et al.* [2004], are illustrated at Figure 2.12.

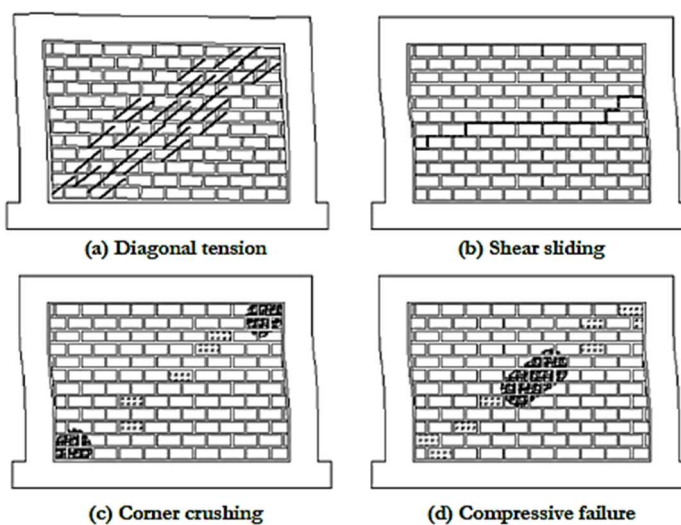


**Figure 2.12. Failure modes of the infill panel given by Decanini *et al.* [2004] (Taken from O'Reilly 2016)**

Based on the experimental data on infilled RC frames, Sassun *et al.* [2016], proposed a modification to the above given strut model. According to Sassun *et al.* [2016], corner drift values of the models that have been introduced by Panagiotakos and Fardis [1994] and Decanini *et al.* [2004] were underestimating the experimental data. Hence, Sassun *et al.* [2016] suggested that once model parameters were obtained through the expressions (2.7 - 2.15) the stiffnesses of the tri-linear parts of the backbone should be modified by adopting the values shown in Table

2.2. Furthermore, Sassun *et al.* [2016] defined four limit states for the infill panel and established a relationship between the system horizontal drift and the attained damage.

**Table 2.2. Experimental median drift and dispersion corresponding to each limit state (Sassun *et al.* 2016)**

Limit State	All Typologies of infills		Solid clay brick infills		Clay brick infills with vertical holes	
	Median (%)	Dispersion	Median (%)	Dispersion	Median (%)	Dispersion
Operational (DS1)	0.18	0.52	0.14	0.36	0.16	0.68
Damage Limitation (DS2)	0.46	0.54	0.33	0.48	0.44	0.70
Life Safety (DS3)	1.05	0.40	0.96	0.21	0.97	0.58
Ultimate (DS4)	1.88	0.38	2.00	0.28	1.33	0.55

Finally, three different typologies of masonry bricks categorized as weak, medium and strong, and their mechanical parameters are given by Hak *et al.* [2012]. Weak typology was defined as a layer of 8.0cm thick hollowed clay brick units laid horizontally with a 1cm plaster on each face while the medium typology was two layers of 12.0cm thick horizontal bricks separated with 5cm in addition to 1cm plaster on both sides. Finally, the strong typology was made of 30cm thick vertically laid bricks. The structure of the infill panels can be seen at Figure 2.13.

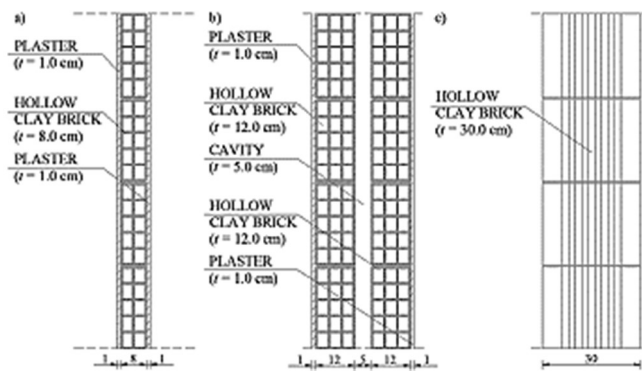


**Figure 2.13. Masonry infill typologies given by Hak *et al.* [2012] (Taken from Hak *et al.* 2012)**

The mechanical properties of the masonry brick with respect to each typology that was given by Hak *et al.* [2012] can be seen in Table 2.3.

**Table 2.3. Mechanical properties of the masonry (Hak *et al.* 2012)**

Typology	$f_{wh}$ [MPa]	$f_{wy}$ [MPa]	$f_{wz}$ [MPa]	$f_{wz}$ [MPa]	$E_{wh}$ [MPa]	$E_{wy}$ [MPa]	G [MPa]	W [kN/m <sup>3</sup> ]
Weak (T1)	1.18	2.02	0.44	0.55	991	1873	1089	6.87
Medium (T2)	1.11	1.50	0.25	0.31	991	1873	1089	6.87
Strong (T3)	1.50	3.51	0.30	0.36	1050	3240	1296	7.36

*This page is intentionally left blank...*

### 3 Methodology

Estimating the horizontal force-deformation capacity or stiffness of a simple one-bay-one-storey frame structure is a routine procedure. If not explicitly stated otherwise, often, the lateral stiffness of a frame is associated only with the flexural deformation of the frame members in the structure, assuming that all the members are rigid in terms of axial and shear deformations. This is a resourceful simplification for bare frames, considering that the contribution of axial and shear stiffness in the induced horizontal displacement of the frame is minimal. However, the same simplification cannot be made when infills are present in the RC system. Infilled frame behaviour is highly dependent on the axial and shear stiffnesses of the system, as well as the flexural stiffness due to the imposed axial deformation introduced by the compression strut formed in the infill panel. The effect of axial and shear stiffness on the horizontal displacement characteristics of the frame is pronounced, especially in low drift ranges (until  $\sim 0.01$  radians). Recognising the significant share of the axial stiffness on the horizontal displacement characteristics of an infilled RC frame, this chapter addresses the theoretical background on the estimation of the infill contribution to the force-displacement behaviour of an infilled RC frame structure. A methodology to estimate the axial stiffness is presented. The reasoning behind the outlined stiffness relationships is examined on hypothetical systems and a generalisation is made at the end. Finally, the possible implications of the discussed theoretical basis on a simplified pushover analysis framework is discussed and an extension of the procedure suggested by Sullivan *et al.* [2018] for the bare frames for infilled RC frame structures is proposed.

#### 3.1 Theoretical Background

As pointed out by Crisafulli [1997], a one-storey-one-bay in-filled frame reasonably behaves analogous to a truss system where the load bearing mechanism is formed through the triangular geometry created by the column in tension, compression zone of the infill and the infinitely rigid ground. Later in the same work by Crisafulli [1997], the same truss analogy was shown to be valid also for multi-bay and multi-storey infilled RC structures. A widely used application of this feature of infilled frames in the literature is the strut analogy for the numerical modelling of infill panels present in the frame openings. Using a strut-type macro model is considered as a practical way of including the axial rigidity introduced to the existing RC frame system by the infill panel through defining an equivalent truss element with an axial stiffness and backbone behaviour. Hence, this study assumes that the horizontal stiffness of an infilled frame is equivalent to a corresponding composite truss-frame structure.

In accordance with the aforementioned assumption, the frame and infill counterparts can be separated as two systems working in parallel (similar to a braced frame). In this case, the lateral stiffness of the dual system can be calculated by breaking down the setup in two sub-structures: a frame (flexural stiffness) and a truss (axial stiffness) system, calculating their individual stiffnesses and then superimposing with the assumption of two springs connected in parallel to a mass, as illustrated in Figure 3.1. As per the parallel spring assumption, the following conditions are imposed:

$$\Delta_{\text{system}} = \Delta_{\text{frame}} = \Delta_{\text{infill}} \quad 3.1$$

$$F_{\text{Total}} = F_{\text{frame}} + F_{\text{infill}} \quad 3.2$$

$$K_{\text{system}} = K_{\text{flexural}} + K_{\text{axial}} \quad 3.3$$

where  $\Delta_{\text{system}}$ ,  $\Delta_{\text{frame}}$  and  $\Delta_{\text{infill}}$  correspond to the lateral displacements,  $F_{\text{total}}$ ,  $F_{\text{frame}}$  and  $F_{\text{infill}}$  are the applied external horizontal forces while  $K_{\text{system}}$ ,  $K_{\text{flexural}}$  and  $K_{\text{axial}}$  indicate the horizontal stiffness of the dual system. Equations 3.1 to 3.3 have three unknowns ( $\Delta_{\text{sys}}$ ,  $F_{\text{frame}}$  and  $F_{\text{infill}}$ ) and three relations in return, which indicates a determinate system. An external force,  $F_{\text{total}}$ , is applied and  $K_{\text{system}}$  is obtained by summing  $K_{\text{flexural}}$  with  $K_{\text{axial}}$  computed through simplified analysis. This work focuses on estimating  $K_{\text{axial}}$  introduced by the infills while relying on the method described by Sullivan *et al.* [2018] for the calculation of  $K_{\text{flexural}}$  associated with the frame behaviour.

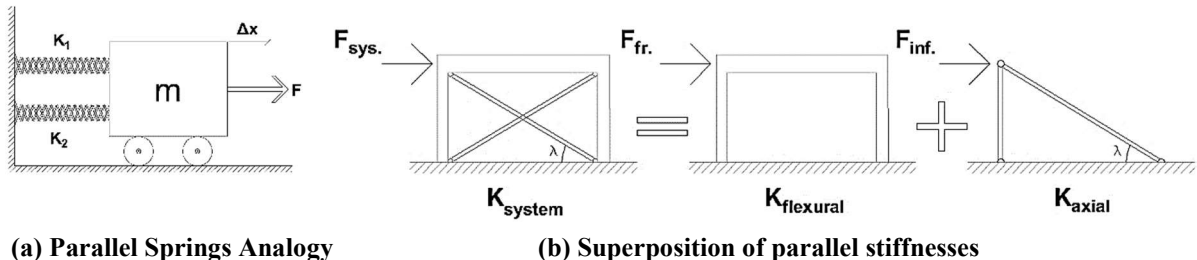


**Figure 3.1. (a) Two springs connected in parallel to a mass (b) Superposition of the flexural and the axial stiffness of the system**

In Figure 3.1(b), considering the truss analogy ( $K_{\text{axial}}$ ), the strut representing the infill is under compression while the leading boundary column is in tension due to the vertical component of the strut force. Members with zero axial force, which are the reverse strut (tension diagonal) beam and the far boundary column, are not shown. Assuming there are no gravity loads acting on the frame in the vertical direction, since the infill struts work only in compression, only a horizontal load applied on the system will activate the diagonal strut. This is not the case when the gravity loads exist on the frame. Any gravity load distribution would introduce a pre-compression on the reverse strut due to the finite beam and column axial stiffnesses, therefore causing an increase in the lateral stiffness of the overall system through unloading behaviour. However, the contribution of the reverse strut fades rapidly due to the increasing elongation as the lateral force increases, usually in the very early stages of an incremental analysis. This phenomenon can be noticed as a short steep initial stiffness portion on the overall force-deformation curve (See Figure 3.2).

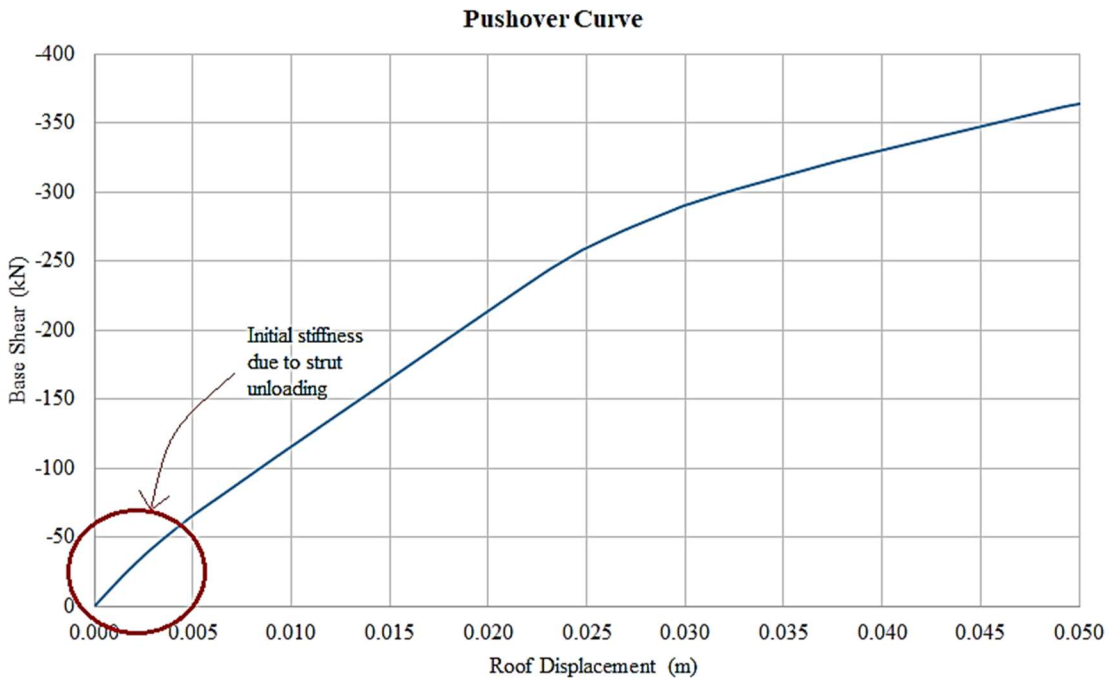


**Figure 3.2. Steep initial stiffness portion due to the contribution of the reverse strut through gravity load unloading (Pushover curve of a 6-storey infilled frame).**

Finally, the difference in the tensile and the compressive axial rigidities for complex composite sections, such as reinforced concrete, should be accounted for during the calculations. For an RC member, the compressive rigidity of the section is obtained by considering the concrete elastic modulus and the concrete area under compression whereas the pure tensile rigidity is only due to the reinforcement area and the steel elastic modulus. Hence, the axial rigidity of the external and internal columns changes throughout the analysis depending on the bending moment and the tension force acting on the column sections. This effect can be considered by introducing an axial backbone curve for the reinforced concrete column sections and through adopting axial-flexure interaction rules during the calculation of the both section axial and flexure capacities. Thus, bearing in mind the aforementioned property of the RC members, regardless of the strut backbone, the axial stiffness of an infilled frame is expected to soften as the applied lateral force increases due to the changing boundary column stiffness.

### 3.1.1 One-Bay-One-Storey Infilled Frame

The axial stiffness of the system can be calculated analytically, after decomposing the system, from the truss structure with well-known analytical procedures. Among various structural analysis methods, the method of virtual work was chosen to be applied since it allows analysts to write member actions in terms of external forces and the structure geometry. A very brief review of the method of virtual work is provided in Appendix B.1. To start with, the axial stiffness of a **one-bay-one-storey** infilled frame, as shown in Figure 3.3, is calculated below.

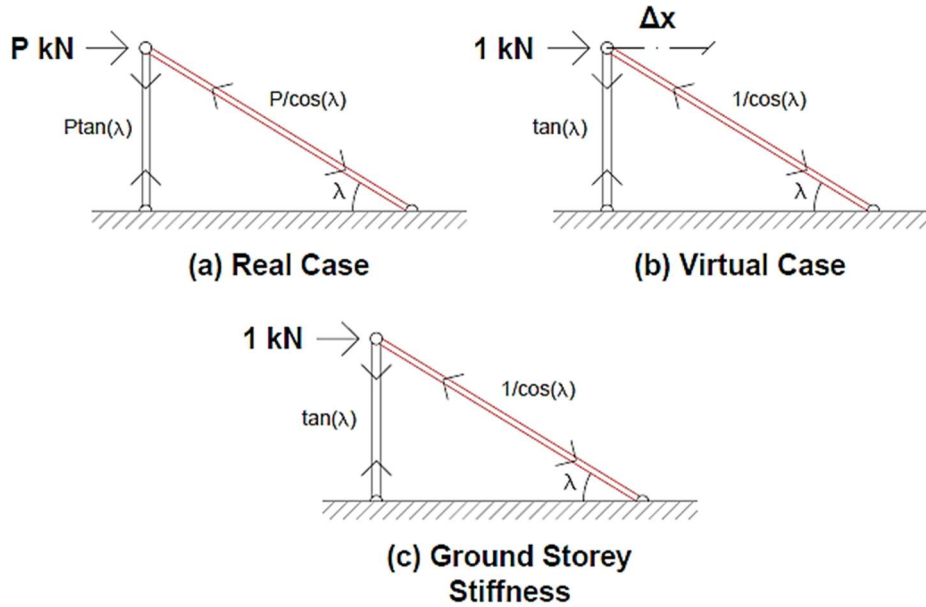


**Figure 3.3. (a) Resultant forces on a one-bay-one-storey truss setup due to applied lateral load P (b) Virtual case set for the horizontal displacement (c) Internal work done in the structure due to 1kN external force**

Regarding the sign convention: (+) corresponds to members in tension and (-) to members in compression. The Young's Modulus E, storey height H, bay width W, diagonal strut length L, column cross section area  $A_{col}$ , strut cross section area  $A_{strt}$ , beam cross section area  $A_{beam}$  and the strut angle  $\lambda$ . With these, the lateral stiffness can be estimated by applying the principle of virtual work. Lateral displacement due to an external force P is obtained by multiplying the internal forces obtained with case (c) with case (a) in Figure 3.3 and then summing the individual member displacements. The horizontal displacement due to load P is found as:

$$\begin{aligned} \Delta_x &= \frac{P(\tan\lambda)(\tan\lambda)L_{col}}{EA_{col}} + \frac{P(\cos^{-1}\lambda)(\cos^{-1}\lambda)L_{strt}}{EA_{strt}} \\ &= \frac{P(\tan^2\lambda)}{K_{col}} + \frac{P}{K_{strt}(\cos^2\lambda)} \\ K_{axial} &= \frac{P}{\Delta_x} = \frac{1}{\frac{\tan^2\lambda}{K_{col}} + \frac{1}{K_{strt}(\cos^2\lambda)}} \end{aligned} \quad 3.4$$

where:

$$L_{strt} = \sqrt{W^2 + H^2} \quad 3.4a \quad \cos\lambda = \frac{W}{L_{st}} \quad 3.4b \quad \sin\lambda = \frac{H}{L_{st}} \quad 3.4c \quad \tan\lambda = \frac{H}{W} \quad 3.4d \quad K_{section} = \frac{EA}{L} \quad 3.4e$$

The displacement (denominator) expression of the one-storey-one-bay frame is composed of a column term and a strut term. The column term handles the elongation due to the strut induced tensile force whereas the strut terms is related with the shortening of the strut due to the external force applied on the joint.

### 3.1.2 Multi-Bay-One-Storey infilled frame

In case of multi-bay frames, the total stiffness of the frame can be estimated by adding the individual stiffnesses of the bays assuming that consecutive bays are connected by axially rigid beams. This is a practical approximation for RC structures, in line with the rigid diaphragm assumption, in which a floor system is constructed by casting a planar RC slab together with the beam elements along with a sufficient shear connection in between. With this assumption, the top node displacement of each bay is assumed to be equal, which implies that bays are working in parallel against the applied external loading, hence allowing the direct addition of individual stiffnesses to obtain the overall stiffness.

For a **two-bay-one-storey** infilled frame as in Figure 3.4, the combined stiffness is calculated below with the given properties: Young's Modulus  $E_{11}$ ,  $E_{12}$ , column section  $A_{col,11}$ ,  $A_{col,12}$ , strut section  $A_{strt,11}$ ,  $A_{strt,12}$ , beam section  $A_{beam,11}$  and the strut angle  $\lambda_{11}$ ,  $\lambda_{12}$  for the first and the second bays, respectively. The lateral stiffness can be estimated by applying the principle of virtual work for bays separately and adding the stiffnesses, which allows the horizontal stiffness of the frame to be derived as follows:

$$K_{axial} = \frac{1}{\frac{\tan^2 \lambda_{11}}{K_{col,11}} + \frac{1}{K_{strt,11}(\cos^2 \lambda_{11})}} + \frac{1}{\frac{\tan^2 \lambda_{12}}{K_{col,12}} + \frac{1}{K_{strt,12}(\cos^2 \lambda_{12})}} \quad 3.5$$

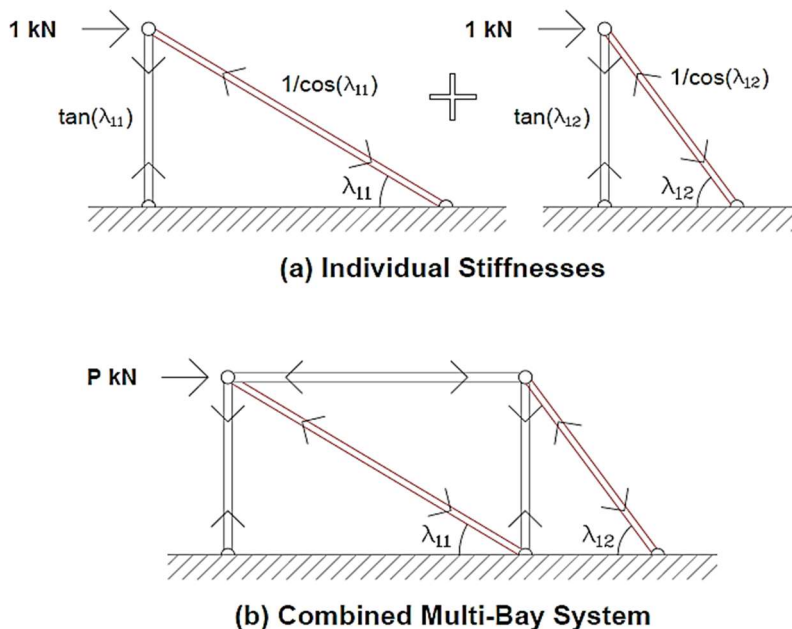


**Figure 3.4.** Summed individual stiffnesses assuming that bays are connected with a rigid beam (a) Individual stiffnesses of bays (b) Total stiffness of the multi-bay frame.

With respect to the above described procedure, the external force  $P$  is shared among consecutive bays in proportion to their stiffnesses. In such a configuration, for a given storey, the wider bay attracts more force than the narrow bay due to the lower strut angle.

### 3.1.3 One-Bay-Multi-Storey Infilled Frame

The preceding case can be taken one step further by adding one more storey, so that the effect of having multiple storeys on the stiffness relationship can be analysed. In case of multi-storey structures, the axial stiffness of the storeys above the ground storey should be calculated also by considering the contribution of the lower storeys. Since the overturning moment due to the lateral force at the bottom of a storey is compensated by the couple moment produced by the tension and the compression columns of the storeys below, the induced displacement due to the storey columns below, as the force is transferred from the storey level towards the rigid supports, should be summed to calculate the total displacement at a storey. Thus, an upper storey is expected to be softer than the bottom storey in terms of lateral axial stiffness. Moreover, it is also possible to observe the effect of this aforementioned stiffness phenomenon in the inter-storey stiffness which is a measure indicating solely the stiffness of a given storey. To isolate the upper storey response, the stiffness should be computed based on inter-storey displacement rather than the storey displacement.

For a **one-bay-two-storey** infilled frame such as the one depicted in Figure 3.5, the second storey stiffness is calculated below, with the given properties; Young's Modulus  $E_1, E_2$ , column section  $A_{\text{col},1}, A_{\text{col},2}$ , strut section  $A_{\text{strut},1}, A_{\text{strut},2}$ , beam section  $A_{\text{beam},1}, A_{\text{beam},2}$ , and the strut angle  $\lambda_1, \lambda_2$  for the first and the second storeys, respectively. The lateral stiffness can be estimated by applying the principle of virtual work and the horizontal displacement due to load  $P$  is computed as follows:

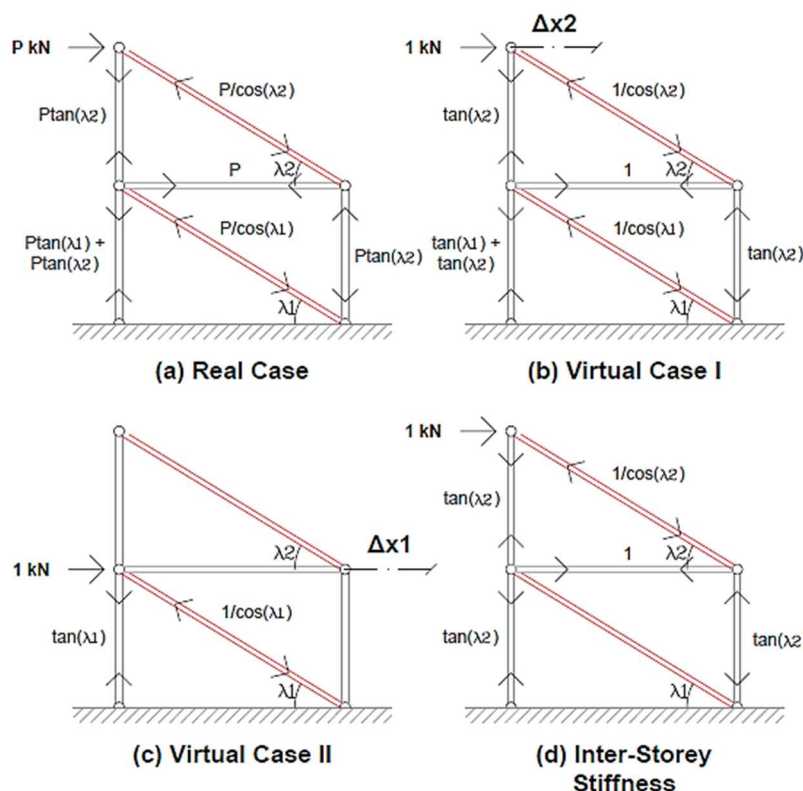


**Figure 3.5. (a) Real Case: One-bay-two-storey representative truss structure (b) Virtual Case I: System set for computing the 2<sup>nd</sup> storey displacement (c) Virtual Case II: System set for estimating 1<sup>st</sup> floor displacement (d) Isolated internal work done by the 2<sup>nd</sup> storey due to 1kN external force**

$$\begin{aligned}
 \Delta_{x,1} &= \frac{P(\tan\lambda_1 + \tan\lambda_2)(\tan\lambda_1)}{K_{col,11}} + \frac{P(\cos^{-2}\lambda_1)}{K_{strt,11}} \\
 \Delta_{x,2} &= \frac{P(\tan^2\lambda_2)}{K_{col,21}} + \frac{P(\cos^{-2}\lambda_2)}{K_{strt,21}} + \frac{P(\tan\lambda_1 + \tan\lambda_2)(\tan\lambda_1 + \tan\lambda_2)}{K_{col,11}} + \frac{P(\cos^{-2}\lambda_1)}{K_{strt,11}} \\
 &\quad + \frac{P(\tan^2\lambda_2)}{K_{col,12}} \\
 \Delta_{x,2} - \Delta_{x,1} &= \frac{P(\tan^2\lambda_2)}{K_{col,21}} + \frac{\cos^{-2}\lambda_2}{K_{strt,21}} + \frac{P(\tan\lambda_1 + \tan\lambda_2)(\tan\lambda_2)}{K_{col,11}} + \frac{P(\tan^2\lambda_2)}{K_{col,12}} \\
 K_{axial} &= \frac{1}{\frac{\tan^2\lambda_2}{K_{col,21}} + \frac{\cos^{-2}\lambda_2}{K_{strt,21}} + \frac{\tan^2\lambda_2 + \tan\lambda_1\tan\lambda_2}{K_{col,11}} + \frac{\tan^2\lambda_2}{K_{col,12}}} \tag{3.6}
 \end{aligned}$$

where  $K_{col,11}, K_{col,12}$  are the first and  $K_{col,21}$  is the second storey column axial rigidity.

Beam member is assumed to be axially rigid in the calculations above. Inter-storey displacement due to external force P is obtained by multiplying the internal forces obtained with case (d) with case (a) in Figure 3.5. Considering Equation 3.6, it is clear that the inter-storey stiffness is composed of the storey strut and the leading boundary column axial rigidities in addition to two more terms that are considering the axial stiffness of the below storey tension (col.,11) and compression (col.,12) columns. The contribution of the column,11 seems to be doubled since it transfers both the action introduced by the upper column and one of the overturning moment couples to the pin support. Considering the term with  $K_{col,11}$  in Equation 3.6,  $\tan^2\lambda_2$  is associated with the transferred force while  $\tan\lambda_1\tan\lambda_2$  is a cross-storey term handling the flow of forces between storeys. Hence the latter term is expected to cumulate as the number of storeys increases. For example, considering the effect of the 2<sup>nd</sup> storey tension column on the 4<sup>th</sup> storey inter-storey stiffness, the cross-storey term would be written as  $\tan\lambda_2\tan\lambda_4 + \tan\lambda_3\tan\lambda_4$  and added to the transferred force  $\tan^2\lambda_4$  the corresponding column term (numerator of the term with  $K_{col,21}$  as the denominator) would be constructed.

### 3.1.4 Multi-Bay-Multi-Storey Infilled Frame

Finally, a second bay can be added to the multi-storey case to better identify the relationship between the upper storey and an underlying multi-bay storey. When multiple bays and storeys exist in the structure, additional to the properties identified in the previous section, there will be some additional cross-bay terms that are governing the force flow (share) between the bays. The main consequence of this fact is that, since the internal column is shared between the ground storey bays, the upper storey stiffness cannot be calculated by simple summation, but a rigorous analytical calculation process is necessary to identify the element force components of the displacement term. Figure 3.6 presents the inter-storey stiffness calculations.

In Figure 3.6, all three cases are indeterminant systems since the vertical reaction at the base consists of three different reactions. To solve these systems, superposition has to be invoked. Figure 3.7 is obtained by releasing the vertical support at node 03 (0<sup>th</sup> floor, 3<sup>rd</sup> bay), solving the system under the lateral load, estimating the vertical settlement at node 03, applying a force

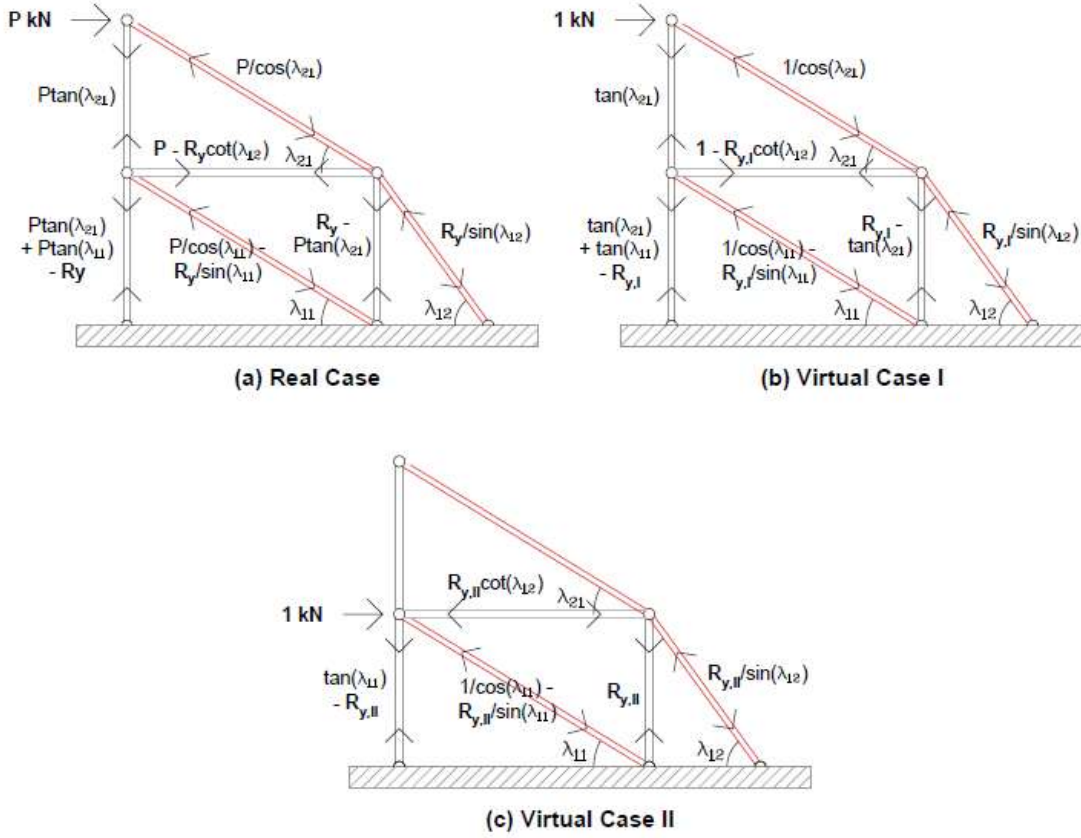


**Figure 3.6. (a) Real multi-bay-multi-storey frame (b) Virtual Case 1 to compute the 2nd floor displacement (c) Virtual case 2 to compute 1st floor displacement**

that will cause the same amount of displacement in the negative direction and superimposing the two cases both for V.C. I and II. Note that the real case superposition setup is the same with V.C. I.

One more equation is needed to connect the horizontal displacement occurred at node 12 with the expected vertical settlement at node 03. This can be done making use of the geometrical relation between the two nodes. Note that if node 03 is free to move vertically, it will translate vertically with node 12, and as node 12 sways horizontally, node 03 will displace vertically. Equation 3.7 indicates the relation between  $\Delta_{x,12}$ ,  $\Delta_{y,12}$  and  $\Delta_{y,03}$ . Note also that, if  $\Delta_{x,12} = 0$ , then  $\Delta_{y,03} = 0$  and, If  $\Delta_{x,12} = W$ , then  $\Delta_{y,03} = L_{strt} - H$ . Hence there are two points  $(0, 0)$  and  $(W, L_{strt} - H)$  on the force displacement curve. Considering a line passing through two points, the slope is given as:

$$slope = \frac{\sqrt{W^2 + H^2} - H}{W} = \frac{1}{\cos(\lambda_{12})} - \tan(\lambda_{12})$$

Thus, using the estimated slope, vertical and horizontal displacement at node 12, the vertical displacement at node 03 becomes:

$$\Delta_{y,03} = \Delta_{y,12} + \frac{\Delta_{x,12}}{\cos(\lambda_{12})} - \Delta_{x,12} \tan(\lambda_{12}) \quad 3.7$$

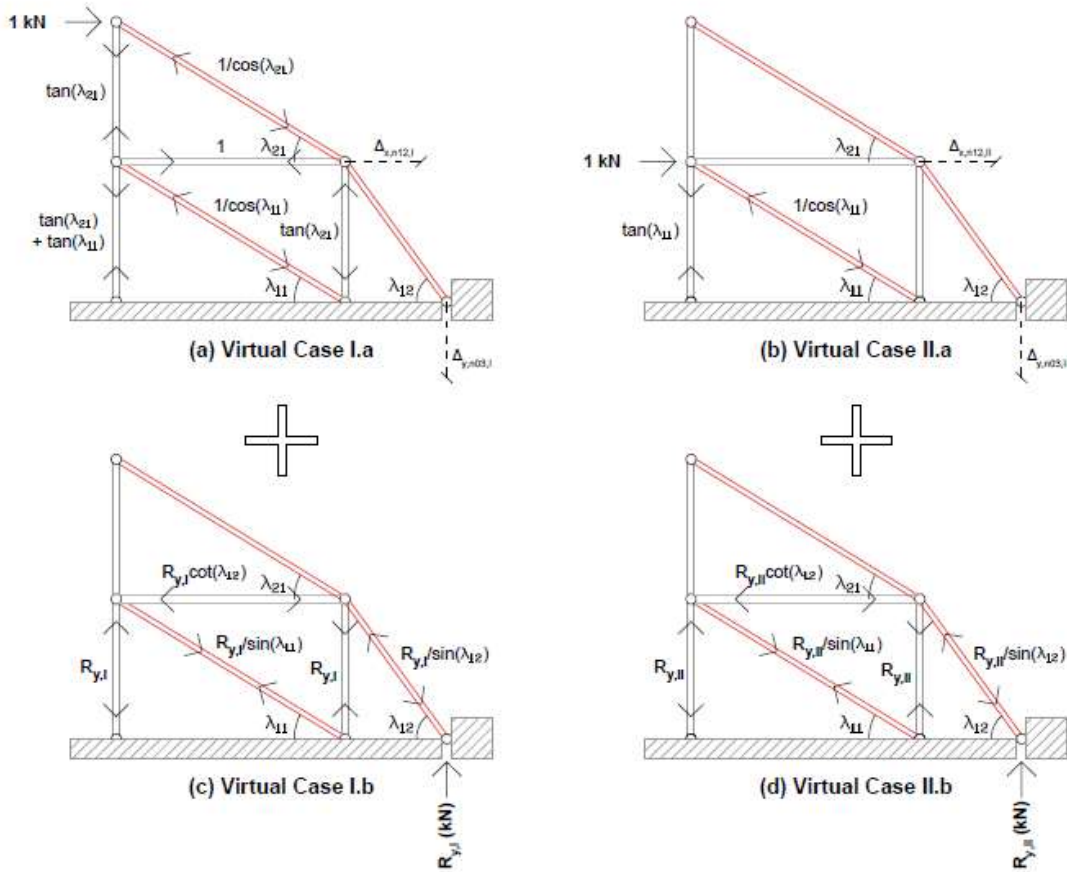


**Figure 3.7.** (a) V.C. I.a: Node 03 is released in the vertical y direction. (b) V.C. II.a: Node 03 is released in the vertical y direction. (c - d) V.C. I-II.b: An external force is applied to node 03 to counter the computed displacement.

From Equation 3.7, the reaction force at node 03 can be computed. To illustrate, for Virtual Case II, first case II.a is solved and the vertical displacement at node 12 is computed and translated to node 03 by using the Equation 3.7. Then, a unit displacement is expected at node 03 due to a unit reaction force (V.C. II.b) and is computed and scaled with the unit reaction force,  $R_{y,II}$ . Therefore, since the displacements coming from II.a and II.b have to be equal, the expression is solved for  $R_{y,II}$  as follows:

$$\Delta_{x,12} = \frac{\tan^2 \lambda_{11}}{K_{col}} + \frac{1}{K_{strt}(\cos^2 \lambda_{11})} \text{ and } \Delta_{y,12} = 0$$

$$\Delta_{y,03,a} = \left[ \frac{1}{\cos(\lambda_{12})} - \tan(\lambda_{12}) \right] \cdot \left[ \frac{\tan^2 \lambda_{11}}{K_{col}} + \frac{1}{K_{strt}(\cos^2 \lambda_{11})} \right] \text{ (due to V.C. II.a)}$$

$$\Delta_{y,03,b} = \frac{R_{y,II}}{K_{strt}(\sin^2 \lambda_{11})} + \frac{2R_{y,II}}{K_{col}} + \frac{R_{y,II}}{K_{strt}(\sin^2 \lambda_{12})} \text{ (due to V.C. II.b)}$$

$$\text{If } \Delta_{y,03,a} = \Delta_{y,03,b}, \text{ then } R_{y,II} = \frac{\left[ \frac{1}{\cos(\lambda_{12})} - \tan(\lambda_{12}) \right] \cdot \left[ \frac{\tan^2 \lambda_{11}}{K_{col}} + \frac{1}{K_{strt}(\cos^2 \lambda_{11})} \right]}{\frac{1}{K_{strt}(\sin^2 \lambda_{11})} + \frac{2}{K_{col}} + \frac{1}{K_{strt}(\sin^2 \lambda_{12})}}$$

A final piece of information can be extracted by focusing on the force flow pattern through node 12. Solving for the node equilibrium, it can be seen that the above storey strut force is shared between the internal column, second bay strut and the beam connecting the first bay. The mentioned complex sharing phenomenon of the upper storey strut force can be solved by plugging  $R_{y,II}$  to V.C. II.b. Note that, even though not shown explicitly here, a similar solution is possible for the V.C. I.a and also for the real case. Hence, the 2<sup>nd</sup> storey axial stiffness can be computed by using Equation 3.8.

$$\begin{aligned}
 \Delta_{x,2} &= \frac{P \tan^2 \lambda_{21}}{K_{col,21}} + \frac{P / \cos^2 \lambda_{21}}{K_{strt,21}} + \frac{[P \tan \lambda_{21} + P \tan \lambda_{11} - R_y][\tan \lambda_{21} + \tan \lambda_{11} - R_{y,I}]}{K_{col,11}} + \\
 &\quad \frac{[P / \cos \lambda_{11} - R_y / \sin \lambda_{11}] [1 / \cos \lambda_{11} - R_{y,I} / \sin \lambda_{11}]}{K_{strt,11}} + \frac{[R_y - P \tan \lambda_{21}] [R_{y,I} - \tan \lambda_{21}]}{K_{col,12}} + \\
 &\quad \frac{[R_y / \sin \lambda_{12}] [R_{y,I} / \sin \lambda_{12}]}{K_{strt,12}} \\
 \Delta_{x,1} &= \frac{[P \tan \lambda_{21} + P \tan \lambda_{11} - R_y][\tan \lambda_{11} - R_{y,II}]}{K_{col,11}} + \frac{[P / \cos \lambda_{11} - R_y / \sin \lambda_{11}] [1 / \cos \lambda_{11} - R_{y,II} / \sin \lambda_{11}]}{K_{strt,11}} + \\
 &\quad \frac{[R_y - P \tan \lambda_{21}] [R_{y,II}]}{K_{col,12}} + \frac{[R_y / \sin \lambda_{12}] [R_{y,II} / \sin \lambda_{12}]}{K_{strt,12}} \\
 \Delta_{x,2} - \Delta_{x,1} &= \frac{P \tan^2 \lambda_{21}}{K_{col,21}} + \frac{P / \cos^2 \lambda_{21}}{K_{strt,21}} + \frac{[P \tan \lambda_{21} + P \tan \lambda_{11} - R_y][\tan \lambda_{21} - R_{y,I} + R_{y,II}]}{K_{col,11}} + \\
 &\quad \frac{[P / \cos \lambda_{11} - R_y / \sin \lambda_{11}] [R_{y,II} - R_{y,I} / \sin \lambda_{11}]}{K_{strt,11}} + \frac{[R_y - P \tan \lambda_{21}] [R_{y,I} - R_{y,II} - \tan \lambda_{21}]}{K_{col,12}} + \\
 &\quad \frac{[R_y / \sin \lambda_{12}] [R_{y,I} - R_{y,II} / \sin \lambda_{12}]}{K_{strt,12}} \\
 K_{axial} &= \frac{1}{\frac{\tan^2 \lambda_{21}}{K_{col,21}} + \frac{1 / \cos^2 \lambda_{21}}{K_{strt,21}}} + \frac{1}{\frac{[\tan \lambda_{21} + \tan \lambda_{11} - R_y][\tan \lambda_{21} - R_{y,I} + R_{y,II}]}{K_{col,11}}} + \\
 &\quad \frac{1}{\frac{[1 / \cos \lambda_{11} - R_y / \sin \lambda_{11}] [R_{y,II} - R_{y,I} / \sin \lambda_{11}]}{K_{strt,11}}} + \frac{1}{\frac{[R_y - \tan \lambda_{21}] [R_{y,I} - R_{y,II} - \tan \lambda_{21}]}{K_{col,12}}} + \\
 &\quad \frac{1}{\frac{[R_y / \sin \lambda_{12}] [R_{y,I} - R_{y,II} / \sin \lambda_{12}]}{K_{strt,12}}} \tag{3.8}
 \end{aligned}$$

### 3.2 Proposed Method to Consider Infill Contribution within a Simplified Pushover Analysis Framework

In this section, the simplified pushover analysis procedure for frame structures introduced by Sullivan *et al.* [2018] is extended in order to capture the infill interaction. Considerations made on the infill-frame behaviour outlined in Section 3.1 are adapted to the iterative displaced shape calculation procedure. By taking advantage of the property of superposition, infills and the bare frame are assumed as parallel structures and their responses are separately constructed, as illustrated previously in Figure 3.1. Then, the decoupled counterparts are superimposed to obtain the system properties. Finally, the system is analysed with an iterative approach to estimate the first mode-based displaced profile of the infilled structure for a given base shear.

As when using a commercial structural analysis software, before starting the analysis, a preparation stage is required. As a first step, the mechanical and geometrical properties of the infilled frame should be defined. Then the force-deformation capacity points for all the frame and infill elements are estimated. Infill characteristics are computed by using a convenient backbone model from the literature, in accordance with the single strut model. The multi-bay structure is then reduced into an equivalent MDOF beam-stick structure by computing a single storey stiffness and capacity. Finally, the individual responses are superposed to obtain the system stiffness and behaviour.

As per the analysis part, for the target base shear, a corresponding displaced shape is assumed with a first mode-based distribution of the base shear along the height of the structure and the displacement profile is iterated until the convergence of the computed storey forces to the target base shear is achieved. After the displaced shape is fixed with an assumed first-mode behaviour, the beam-stick structure is further reduced to a SDOF sub-structure and the force-displacement response for different base shear values is plotted to obtain the capacity curve. The procedure is summarised in Figure 3.8. Since inter-storey displacements are introduced, a lateral force profile is computed at each step until the system converges to a target base shear and this inter-storey displacement profile is updated at each step based on the altering stiffness of the stick structure, meaning that a derivative of the first mode-based displacement-based adaptive pushover (DAP) with incremental update procedure (Antoniou & Pinho, 2004) is being applied.

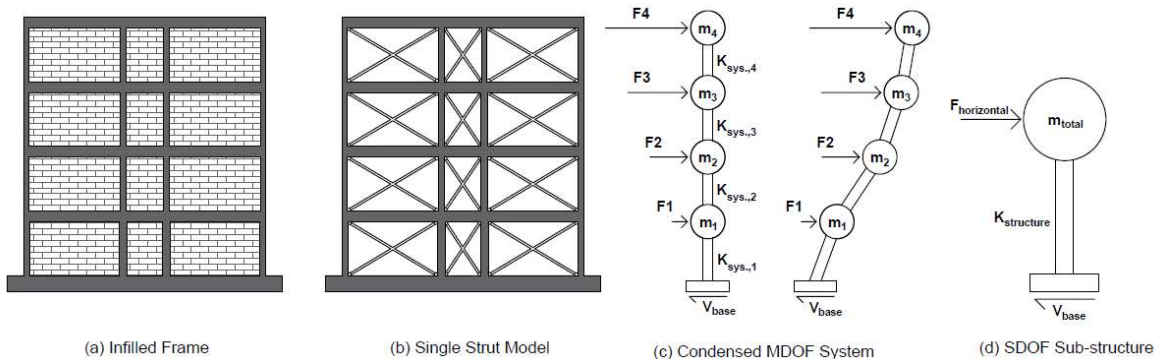


**Figure 3.8. (a) Infilled frame structure (b) Single strut model representation (c) Simplified MDOF structure representation of the strut model with the estimated storey system stiffnesses  $K_{sys,i}$  (d) Final SDOF sub-structure with an applied horizontal force and a resulting displacement**

### 3.2.1 Geometry & Material Definitions

Before starting the simplified analysis procedure, as in the case of any conventional analysis software, several modelling parameters need to be defined. The geometry, member sections, sizes, configuration, material properties, in addition to the gravity loads and masses associated with the structure should be identified. At this step, the infill strut modelling approach that will be adopted for the analysis should also be decided and the necessary mechanical properties of the masonry material and the infill wall should be provided accordingly. Optionally, a structural plan where the members and the components of the structure are named for providing means of effective communication between modelling steps can be attached. Considering a structure in which the struts are modelled according to Bertoldi *et al.* [1993], the list of necessary parameters to complete the simplified analysis is given in Table 3.1.

**Table 3.1. List of Required Mechanical and Geometrical Properties**

Item	Structure	Frame Sections	Infill Panels
1	Number of Storeys, N	Depth of the Section, $D_{sect,i}$	Vertical Young's Modulus of the Masonry, $E_{wv}$
2	Storey Heights, $h_{s,i}$	Width of the Section, $w_{sect,i}$	Horizontal Young's Modulus of the Masonry, $E_{wh}$
3	Number of Bays, B	Cover Thickness, c	Shear Modulus of the Masonry, G
4	Bay Lengths, $W_{i,j}$	Expected Concrete Strength, $\sigma_c$	Thickness of the Infill Wall, t
5	Column Section Distribution	Young's Modulus of the Concrete, $E_c$	Axial Load Ratio of the Boundary Column, v
6	Beam Section Distribution	Expected Rebar Strength, $\sigma_{fy}$	Vertical Stress on the Masonry due to Gravity Loads, $\sigma_v$
7	Infill Panel Distribution	Young's Modulus of the Rebar, $E_s$	The Diagonal Shear Compression Strength, $f_{ws}$
8	Mass Distribution	Longitudinal Reinforcement	Sliding Resistance of the Mortar, $f_{wu}$
9	Gravity Loads	Transverse Reinforcement	Vertical Compressive Strength of the Masonry, $f_{wv}$
10	Infill Typology	Stirrup Spacing, s	Unit Weight of the Masonry
11	-	Frame Section Backbone Model	Strut Backbone Model

This example list of required parameters can be extended with respect to the needs and the level of complexity of the planned analysis. However, considering the structure and frame section parameters, Table 3.1 points out the minimum amount of knowledge required in order to complete the simplified procedure proposed in this work.

### 3.2.2 Flexural Frame System Capacity

This section is focused on quantifying the bare frame flexural stiffness ( $K_{\text{flex.}}$ ) associated with each storey as outlined in Sullivan *et al.* [2018]. In case of infilled frames, on the grounds of the parallel spring assumption made in the Section 3.1, Sullivan *et al.* [2018] approach is also applicable for the analysis of the flexural counterpart of the system.

In accordance with Sullivan *et al.* [2018], the section moment-curvature ( $M-\phi$ ) relationships should be computed by using a dedicated software such as Response-2000 (Bentz & Collins 2001), Cumbia (Montejo & Kowalsky 2007) or OpenSees (McKenna *et al.* 2010), to name a few. The main purpose of the aforementioned step is to define each member's section backbone capacity. To be more specific, for a trilinear response curve, the yield, ultimate and residual moment-curvature ( $M_y$ ,  $\phi_y$ ,  $M_u$ ,  $\phi_u$ ,  $M_r$  and  $\phi_r$ ) values are essential. This way, the existing procedure can be extended to capture also the post-peak response of the members which would allow analyst to incorporate the strength degradation associated with the RC members and the overall system in the structure force-displacement response.

Following the computation of the section capacities, the element force-deformation responses are obtained for each single  $M-\phi$  point (starting from  $M_y - \phi_y$ ) and then, the element responses are condensed into the storey force-drift backbone curve. The maximum joint moment is established and the maximum possible demand in each member framing into that joint is adjusted in order to satisfy the joint equilibrium conditions. With the obtained top and bottom maximum column moments, the storey shear resistance is computed the Equation 3.9 (Sullivan *et al.*, 2018).

$$V_{Ry,frame,i} = \frac{\sum M_{col,b,i} + \sum M_{col,a,i-1}}{(h_i - h_{i-1})} \quad 3.9$$

where  $V_{Ry,frame,i}$  is the frame storey yield shear resistance,  $\sum M_{col,b,i}$  and  $\sum M_{col,a,i-1}$  are the sum of the top and bottom column end moments at yield immediately below joint centrelines. The height terms  $h_i$  and  $h_{i-1}$  should be computed as the height above the foundation level. Note that the difference between  $h$  terms corresponds to the storey height, implying that  $h_{i-1}$  should be taken as zero for the ground floor. On the other hand, the required member yield drifts are computed with the Equations 3.10 – 3.13 as proposed by Sullivan *et al.* [2018] for different expected mechanisms:

$$\text{Beam - sway flexural mechanism:} \quad \theta_{y,i} = 0.5 \frac{\varepsilon_y L_{b,i}}{h_{b,i}} = \theta_{y,bs,i} \quad 3.10$$

$$\text{Column - sway flexural mechanism:} \quad \theta_{y,j} = 0.43 \frac{\varepsilon_y h_{s,i}}{D_{col,i}} = \theta_{y,cs,i} \quad 3.11$$

$$\text{Rectangular ground - storey columns:} \quad \theta_{y,0} = 0.70 \varepsilon_y \frac{h_{cf}}{D_{col}} \quad 3.12a$$

$$\text{Circular ground - storey columns:} \quad \theta_{y,0} = 0.75 \varepsilon_y \frac{h_{cf}}{D_{col}} \quad 3.12b$$

Expected contraflexure height:

$$h_{cf} = \frac{h_1}{\left( \frac{M_{col,b,1}}{M_{col,base}} + 1 \right)} \quad 3.13$$

where  $\varepsilon_y$  is the yield strain of the longitudinal reinforcement,  $L_{b,i}$  is the length of the beam between the column centrelines,  $h_{b,i}$  is the beam section depth,  $h_{s,i}$  is the height of the column,  $D_{col,i}$  is the column section depth,  $h_{cf}$  is the contraflexure height and  $h_1$  is the bottom storey height. The likely storey mechanism is assessed by comparing the storey beam and column moment capacities with the sway potential index  $S_i$ , proposed by Priestley *et al.* [2007]. Considering a possible trilinear backbone for the members (three damage states where yielding is the DS1), the ultimate and the residual drift points can be estimated by the Equation 3.14 and 3.15, which were provided by Paulay and Priestley [1992].

$$\theta_u = \frac{\phi_y L_s}{3} + (\phi_u - \phi_y) L_{pl} \quad 3.14$$

$$L_{pl} = 0.08L_s + 0.022f_y d_{bl} \quad [\text{in mm}] \quad 3.15$$

where  $L_s$  is the member shear span length,  $L_{pl}$  is the plastic hinge length,  $f_y$  is the yield strength of the longitudinal reinforcement [MPa] and  $d_{bl}$  is the rebar diameter [mm]. After the critical drift of each relevant (beam or column) member is defined, the storey critical drift is estimated with Equation 3.16 based on the principle that equals external work and internal work. For the yield drift (Sullivan *et al.*, 2018), Equation 3.16 is used,

$$\theta_{y,frame,i} = \frac{\sum M_{j,i} \theta_{y,i} + \sum M_{j,i-1} \theta_{y,i-1}}{\sum M_{j,i} + \sum M_{j,i-1}} \quad 3.16$$

where  $\theta_{y,frame,i}$  is the storey drift needed to yield the  $i$ -th storey,  $M_{j,i}$  and  $M_{j,i-1}$  are the flexural capacities of each member (with respect to the governing mechanism) and  $\theta_{y,i}$  and  $\theta_{y,i-1}$  are the member yield drifts at the levels  $i$  and the  $i-1$  respectively. Finally, the storey flexural stiffness,  $k_{flex,y,i}$  is computed with Equation 3.17 and the stiffness of the successive branch in the frame backbone is computed according to Equation 3.18, which corresponds to the slope of the line passing through the yield and ultimate storey shear-sway capacity points (Sullivan *et al.*, 2018).

$$K_{y,flexural,i} = \frac{V_{Ry,i}}{\theta_{y,i} h_{s,i}} \quad (\text{in kN/m}) \quad 3.17$$

$$K_{ult,flexural,i} = \frac{V_{Rult,i} - V_{Ry,i}}{(\theta_{ult,i} - \theta_{y,i}) h_{s,i}} \quad (\text{in kN/m}) \quad 3.18$$

where  $h_{s,i}$  is the storey height. The step described in Equation 3.18 can be repeated many times incrementally in order to construct the storey frame shear-displacement backbone which yields the flexural counterpart of the required input for the system capacities step.

### 3.2.3 Truss Infill System Capacity

A procedure to estimate the lateral stiffness ( $K_{\text{axial}}$ ) and capacity of the infill members in the structure is proposed in this section. Similar to the approach taken for calculating the flexural stiffness of the frame, the axial stiffness is calculated by first identifying the section response then passing to the member and storey behaviours consecutively. To do that, concepts and equations discussed in Section 3.1 are utilised in a practical manner. Finally, adopting the proposed methodology, an output horizontal force-displacement response is obtained and is compatible with the frame counterpart for superposition. Similar to a traditional analysis, the infill panel is represented with an appropriate numerical model representation.

Modelling infill behaviour for structural analysis is an extensively studied and a repeatedly addressed issue in the literature. The performance of capturing expected infill failure mechanisms and the applicability of the available various macro-models have been a crucial source of discussion among many investigators and reflected in numerous papers. Hence, it is a matter of the analyst's choice to pick the most suitable modelling methodology for the problem in hand. Recognising this, the method to be used in modelling infill member behaviour for the simplified analysis is left up to the decision of the reader. However, it must be noted that the described methodology in this work is limited to single equivalent diagonal strut models until future research work includes other modelling strategies such as double or triple struts. Some suggested single strut models might include Bertoldi *et al.* [1993], Panagiotakos and Fardis [1996], Crisafulli *et al.* [1997], FEMA 356 [2000], Decanini *et al.* [2004] and Sassun *et al.* [2015]. After the suitable modelling approach has been chosen from the literature, the procedure described in this section is used to estimate the capacity points and the associated stiffnesses of the infill members.

First, the section backbone response is obtained for each infill panel by using the chosen modelling approach. This step of computing strut axial force-deformation capacities and stiffnesses corresponds to the moment-curvature analysis done for the frame sections in Section 3.2.2. The strut yield and ultimate (and also other successive branches) stiffnesses are computed with Equation 3.19 - 3.20.

$$k_{\text{strt},y.} = \frac{F_y}{\varepsilon_y L_{\text{strt}}} \quad (\text{in kN/m}) \quad 3.19$$

$$k_{\text{strt},\text{ult.}} = \frac{F_{\text{ult.}} - F_y}{(\varepsilon_{\text{ult}} - \varepsilon_y)L_{\text{strt}}} \quad (\text{in kN/m}) \quad 3.20$$

where  $k_{\text{strt},y}$  and  $k_{\text{strt},\text{ult.}}$  are the strut axial yield and ultimate stiffnesses,  $F_y$  and  $F_{\text{ult.}}$  are the strut axial yield and ultimate forces,  $\varepsilon_y$  and  $\varepsilon_{\text{ult}}$  are the strut axial yield and ultimate strains, and finally,  $L_{\text{strt}}$  is the length of the strut. Force and strain values should be obtained from one of the strut models listed above. In a similar manner, the boundary column axial stiffness in tension and compression can be calculated with Equations 3.21 - 3.22, respectively.

$$k_{\text{col.t.}} = \frac{E_{\text{rebar}} A_{\text{rebar}}}{h_{s,i}} \quad (\text{in kN/m}) \quad 3.21$$

$$k_{col,c} = \frac{E_{conc} A_{conc}}{h_{s,i}} \text{ (in } kN/m) \quad 3.22$$

where  $k_{col,t}$  and  $k_{col,c}$  are the boundary column tensile and compressive stiffnesses,  $E_{rebar}$  and  $E_{conc}$  are the rebar and concrete elastic moduli,  $A_{rebar}$  and  $A_{conc}$  are the longitudinal reinforcement and concrete area, and finally,  $h_{s,i}$  is the storey height.

At this step, since the member axial stiffnesses are available, the storey stiffnesses can be calculated according to Section 3.1. As per the equivalent truss structure analogy, the infilled structure is represented as two parallel structures, one bare frame and the other truss frame. The storey stiffness of the truss is estimated by summing up the bay stiffnesses in the storey, while the bay stiffness is estimated by computing the unit displacement at the top beam-column joint due to an applied unitary horizontal force and then taking the inverse (unit force divided by the unit displacement). For the ground storey, bay stiffness calculation is shown in Equation 3.24.

$$\Delta_{1j} = \frac{\tan^2 \lambda_{1j}}{k_{col,c,1j}} + \frac{1}{(\cos^2 \lambda_{1j})(k_{strt,y,1j})} \quad 3.23$$

$$K_{axial,1j} = \frac{1}{\Delta_{1j}} \quad 3.24$$

where for the first storey  $j$ -th bay,  $\Delta_{1j}$  is the expected unit displacement,  $\lambda_{1j}$  is the strut angle,  $k_{col,c,1j}$  is the axial rigidity of the boundary column and  $k_{strt,y,1j}$  is the initial strut stiffness. Horizontal component of the bay axial stiffness,  $K_{axial,1j}$ , is recomputed to construct the successive branches of the storey backbone by updating initial column and infill stiffnesses progressively as the members soften.

In case of upper storeys, the expected unit bay displacement should be estimated also by including the contributions coming from the below columns in addition to the boundary column and strut. Considering the effect of the below column to the current storey, there are three different types of actions, as shown in Figure 3.9. The first one is the transferred force which corresponds to the transfer of the axial reactions produced by the storey members due to the applied storey force to the columns below. The second is the cross-storey action produced due to the effect of the storey force to the below storey. Finally, the third, which is only applicable to the internal columns, is the cross-bay term coming through the force transfer pattern of the storey strut to the below storey. If a consecutive bay exists at the below storey, based on the geometrical ratio between two consecutive bays, a component of the storey strut force will be transferred to the internal column whereas the remaining is attracted by the adjacent strut. A similar scenario is applicable if a third bay exists. Then the storey strut force is shared among the internal columns, adjacent struts and the beams connecting the third bay according to their horizontal stiffnesses. Hence, a complex force flow is expected to occur at internal beam-column joints, making the force term in the virtual work displacement expression harder to predict considering the internal columns and the internal bay struts. The flow of these aforementioned forces through a beam column joint are illustrated in Figure 3.9 below.

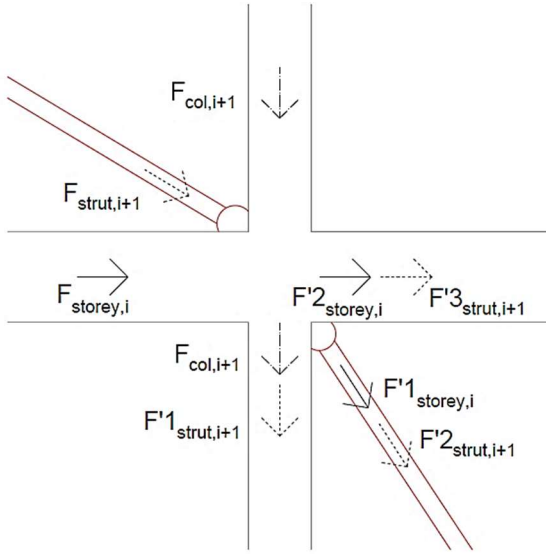


**Figure 3.9. Flow pattern of the external forces through an internal beam-column joint of a multi-bay-multi-storey infilled frame structure. (Observing the joint between 1<sup>st</sup> and 2<sup>nd</sup> bay of the i-th storey. Total number of bays is  $\geq 3$ )**

$F_{\text{col},i+1}$  is the transferred force coming from the upper storey,  $F_{\text{strut},i+1}$ ,  $F'1_{\text{strut},i+1}$ ,  $F'2_{\text{strut},i+1}$ ,  $F'3_{\text{strut},i+1}$  are the upper storey strut and transferred strut forces respectively ( $F_{\text{strut},i+1} = F'1_{\text{strut},i+1} + F'2_{\text{strut},i+1} + F'3_{\text{strut},i+1}$ ), and  $F_{\text{storey},i}$ ,  $F'1_{\text{storey},i}$ ,  $F'2_{\text{storey},i}$  are the storey external force and the transferred storey external forces ( $F_{\text{storey},i} = F'1_{\text{storey},i} + F'2_{\text{storey},i}$ ).

An alternative path to the model multi-bay-multi-storey stiffness might be to assume that instead of a single complex truss, many multi-storey-one-bay truss structures work in parallel against the applied external loading. In this case, the multi bay hinged frame is divided into separate structures as many as the number of bays with the assumption that each separate structure has the same displacement at the top joint of a given storey (similar to a set of parallel springs). This would mean that the stiffness of a storey will be simply the addition of the individual bay stiffnesses at the given storey where each bay is considered as a separate multi-storey structure. However, this methodology somewhat underestimates the storey stiffness since the cross-storey term in Equation 3.6 is expected to be affected of the presence of bays in the frame. A second level of simplification can be made only by taking the transferred force terms and ignoring the cross-storey terms identified in Equation 3.6. This way, the storey stiffness can be estimated with sufficient accuracy. Nonetheless, the validity of this approximation will be checked by rigorous testing on case study structures with different number of bays and storeys.

The upper storey stiffness can be estimated with the aforementioned assumption based on the principle outlined in Section 3.13. Similar with the approach taken with the ground storey, the unit displacement of a bay is computed using the displacement expression given in Equation 3.25 and then inverted for the stiffness as in Equation 3.26. The displacement at the top joint of a bay at the i-th storey should be computed, including the effect of below storeys down to ground floor, as described in Equation 3.25.

$$\Delta_{ij} = \frac{\tan^2 \lambda_{ij}}{k_{col,c,ij}} + \frac{1}{(\cos^2 \lambda_{ij})(k_{strt,y,ij})} + \frac{\tan^2 \lambda_{ij}}{k_{col,c,(i-1)j}} + \frac{\tan^2 \lambda_{ij}}{k_{col,c,(i-1)(j+1)}} + \dots + \frac{\tan^2 \lambda_{ij}}{k_{col,c,1j}} + \frac{\tan^2 \lambda_{ij}}{k_{col,c,1(j+1)}} \quad 3.25$$

$$K_{axial,ij} = \frac{1}{\Delta_{ij}} \quad 3.26$$

where for the i-th storey and j-th bay,  $\Delta_{ij}$  is the expected unit displacement,  $\lambda_{ij}$  is the strut angle,  $k_{col,c,ij}$  is the axial rigidity of the leading boundary column and  $k_{strt,y,ij}$  is the initial strut stiffness. Similar to the ground storey case, the horizontal component of the bay axial stiffness,  $K_{axial,ij}$ , can be adjusted by updating initial column and infill stiffnesses, to obtain the successive branches of the storey backbone. The proposed procedure is illustrated in Figure 3.10.

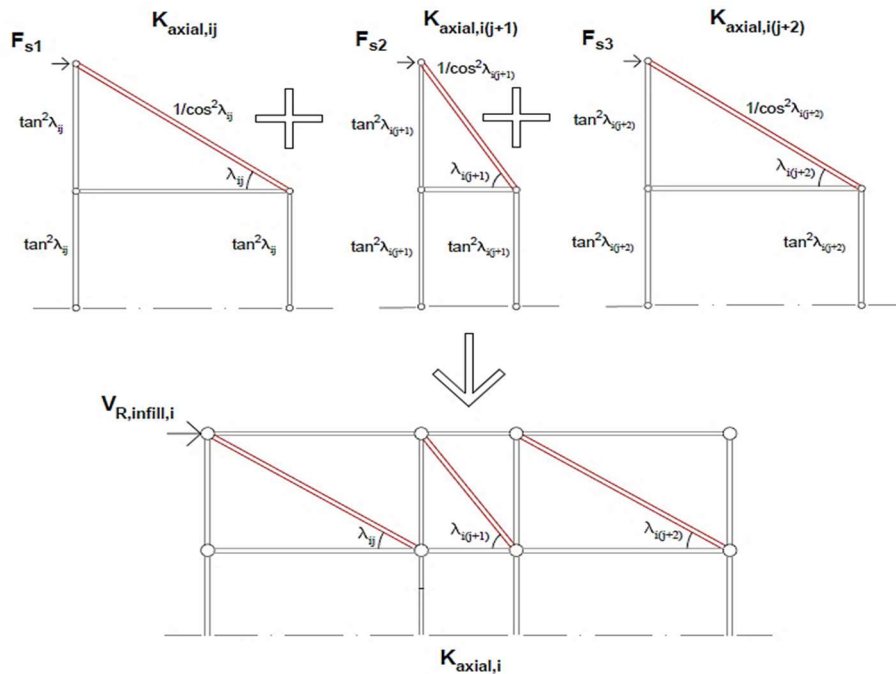


**Figure 3.10. Approximate procedure to estimate the upper storey stiffness (Illustrated for a multi-storey-three-bay infilled frame)**

Finally, having bay stiffnesses and strut axial force capacities at hand, the required properties for the superposition step can be calculated. The storey shear resistance due to infills is computed by summing the horizontal components of the strut forces in a storey as shown in Equation 3.27. Then the bay stiffnesses are summed for each storey to estimate the full storey stiffness as per Equation 3.28. Finally, the strut yield drift is obtained by using the determined storey shear resistance and the initial stiffness. In addition, the ultimate or any post-yield stiffness can be obtained using Equation 3.30.

$$V_{Ry,infill,i} = F_{y,i1} \cos \lambda_{i1} + F_{y,i2} \cos \lambda_{i2} + \dots + F_{y,iN} \cos \lambda_{iN} \quad 3.27$$

$$K_{y,axial,i} = K_{y,axial,i1} + K_{y,axial,i2} + \dots + K_{y,axial,iN} \quad 3.28$$

$$\theta_{y,infill,i} = \frac{V_{Ry,infill,i}}{(K_{y,axial,i})h_{s,i}} \quad 3.29$$

$$\theta_{ult,infill,i} = \theta_{y,infill,i} + \frac{V_{Rult,infill,i} - V_{Ry,infill,i}}{(K_{ult,axial,i})h_{s,i}} \quad 3.30$$

where  $V_{Ry,infill,i}$ ,  $K_{y,axial,i}$ ,  $\theta_{y,infill,i}$  and  $\theta_{ult,infill,i}$  corresponds to the infill yield storey shear, initial storey stiffness, yield storey drift and ultimate storey drift, respectively.  $F_{y,ij}$ ,  $\cos\lambda_{ij}$  and  $K_{DS,axial,ij}$  for the i-th storey and j-th bay, are the axial capacity of the strut, strut angle and the stiffness of the different portions in the backbone.

### 3.2.4 Combined System Capacity

The last step is to combine the estimated horizontal flexural and the axial stiffnesses of the frame and the infill counterparts in order to obtain the combined system stiffness. Recalling once again the parallel springs assumption on the superposition of the flexural and axial stiffnesses, system storey stiffness is evaluated by simply summing for a given level (Equation 3.31). In this context, the primary system critical drift (associated with the infill yield) is taken as the lower drift value while the higher being the secondary critical drift (frame yield) as in Equation 3.32. Finally, the corresponding critical storey shear is computed for the fixed stiffness and drift values as in Equation 3.33.

$$K_{system,i,1} = K_{flexural,i,1} + K_{axial,i,1} \quad 3.31$$

$$\theta_{system,i,1} = \min(\theta_{frame,i,1}, \theta_{infill,i,1}) \quad 3.32$$

$$V_{R,i,k+1} = V_{R,i,j} + K_{sys,i,k+1} \cdot (\theta_{sys,i,k+1} - \theta_{sys,i,k}) \cdot h_{s,i} \quad 3.33$$

where  $K_{system,i,1}$ ,  $K_{flexural,i,1}$  and  $K_{axial,i,1}$  are the initial system, flexural and axial stiffnesses for the i-th storey. The terms  $\theta_{system,i,1}$ ,  $\theta_{frame,i,1}$  and  $\theta_{infill,i,1}$  corresponds to the initial system, frame and infill critical drifts (yield drifts) for the i-th storey. While,  $V_{R,i,k+1}$  and  $V_{R,i,k}$  represent the successive and current system storey shear resistances at level i. Finally, the height of the i-th storey is denoted by the term  $h_{s,i}$ .

Where multiple damage states are considered for both infill and the frame, the storey backbone curve should be constructed by following the strength hierarchy of the storey system. This is done by first comparing and sorting the critical drift values coming from infill and frame subsystems to identify the sequence of each damage state. Then, conforming with the definition of the damage states, individual stiffness values are summed to obtain the system stiffness. For example, for a storey with three damage states that are ordered as yielding of the infill panel, exceeding the ultimate capacity of infill panel and yielding of the frame, the slope of the second branch of the force-drift curve of the system ( $K_{system,i,2}$ ) is the addition of  $K_{flexural,i,1}$  and  $K_{axial,i,2}$ . Additionally, for the sake of having a continuous response curve, the storey shear resistance of the successive damage state ( $V_{R,i,j+1}$ ) should be computed with the equation of a line passing

through a known point ( $V_{R,i,j}, \theta_{sys,i,j}$ ) with the know slope  $K_{system,i,j}$  as shown at Equation 3.31. For this step, the use of a table of storey behaviour hierarchies to record and keep track of the storey response curves is recommended (Table 3.2). Note that  $\theta_{sys,1,1} < \theta_{sys,1,2} < \theta_{sys,1,3} < \theta_{sys,1,4}$ .

**Table 3.2. An example model table of behaviour hierarchy for the first storey**

1 <sup>st</sup> Storey			
L.S. Point	$V_{R,1,j}$ [kN]	$\theta_{sys,1,j}$ [rad]	$K_{sys,1,j}$ [kN/m]
DS1 <sub>infill</sub>	$V_{R,1,1}$	$\theta_{sys,1,1}$	$K_{sys,1,1}$
DS2 <sub>infill</sub>	$V_{R,1,2}$	$\theta_{sys,1,2}$	$K_{sys,1,2}$
DS1 <sub>frame</sub>	$V_{R,1,3}$	$\theta_{sys,1,3}$	$K_{sys,1,3}$
DS2 <sub>frame</sub>	$V_{R,1,4}$	$\theta_{sys,1,4}$	$K_{sys,1,4}$

Finally, before proceeding to the analysis step, a systematic way to update the member stiffnesses as they alter their mechanical properties with the increasing storey inter-displacement values is needed. Having all the members in a given storey lumped into a stick structure, unified storey response will be controlled by the storey backbone which is defined for each storey in Table 3.2. Based on the order of this chart, the properties of the consecutive branch can be chosen when the shear capacity has been exceeded.

### 3.2.5 Proposed Method

Until the analysis step, the main effort was to prepare and identify the necessary structural properties with enough accuracy and in a practical manner. In the previous sections, in order to analytically compute the structural response without creating and dealing with the full stiffness matrix of a structure, an MDOF frame was condensed into a reduced MDOF stick structure where each storey is represented by a single horizontal translational degree of freedom. The current section will discuss the implementation of the simplified analysis procedure employed to yield the full force-displacement response of the equivalent stick structure. The basis of the described procedure here was first defined by Sullivan *et al.* [2018] for bare frames. This work presents additional refinements to the method outlined in such a paper in order to include infill-frame interaction and to better control the pre- and post-yield parts of the structural response and is outlined in Figure 3.11.

In the first step of the procedure, a target base shear (load factor) value is assumed. Target base shear corresponds to the level of excitation that the displaced shape will be computed for. In the following step, the equilibrium of the structure is disturbed by introducing a guessed displacement profile. Then, the storey lateral forces are computed and summed up to compute storey shears. Meanwhile, knowing the storey drifts, the true storey shears are computed. Then, the differences in both storey shears are computed and convergence criteria is checked. If not satisfied, a new sway profile is computed by dividing the storey shears (Equation 3.40) with the storey stiffnesses. This is repeated until convergence is achieved, which is usually after one or two iterations. After the equilibrium state corresponding to the target base shear is identified, the demand indices are checked, and the target base shear is increased until one or more demand indices reaches its capacity. At this point, a capacity point on the force-displacement curve of

the structure has been identified and the displaced shape, roof displacement, inter-storey drifts together with the corresponding true storey drift and base shears are available. After this point has been saved, the stiffness and the capacity properties of the yielded storey are updated, the initial displacement profile guess is changed with the current one if deemed necessary and returning back to step 1, the analysis is repeated for a higher target base shear. By progressively increasing the target base shear and saving the critical true base shear versus engineering demand parameters, the capacity of the structure is obtained and the strength hierarchy between the storeys, frame and infill members is identified.

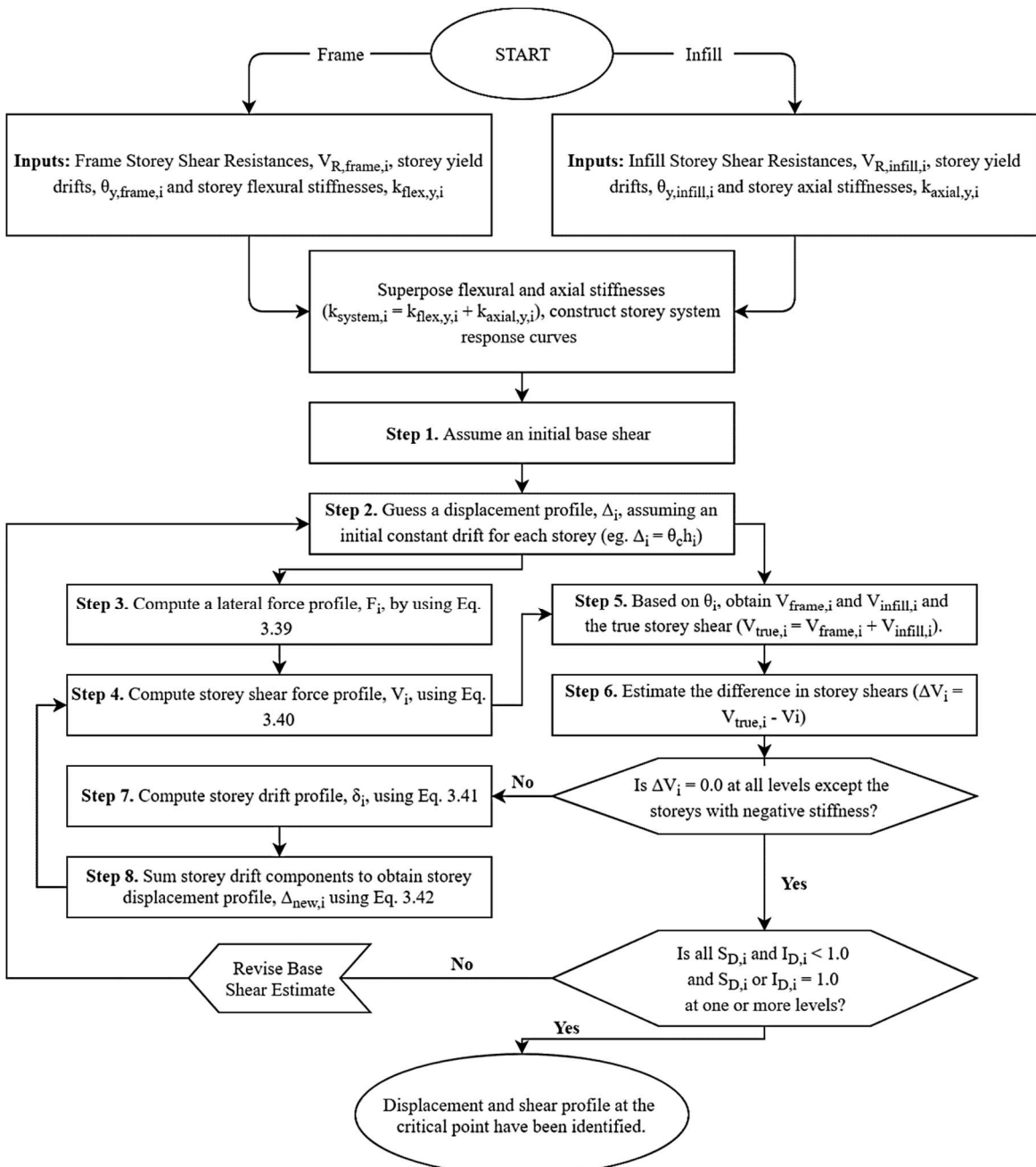


Figure 3.11. Flowchart of the proposed simplified analysis procedure.

The very first matter to discuss is the applicability of the sway potential,  $S_i$ , and sway demand indices,  $S_{Di}$ , in addition to the introduction of a new index concerning the strut member capacities. Excluding a mechanism due to a possible shear yielding in the columns, beam and joint members, the flexural global mechanism of the frame structure is dictated by the frame members, sway potential index,  $S_i$ , and is compatible with the method discussed in this work for identifying the likely storey mechanisms. As the infill and the frame contributions are assumed to be parallel, the frame and infill capacities can be assessed separately. This means that the sway demand index,  $S_{Di}$ , can be used for checking the capacity ratio of the frame whereas a similar check can be done also for the truss infill system. For this reason, a new type of index is introduced as the infill demand index,  $I_{Di}$ , to check the capacity ratio of the infill panel members during the analysis. Similar to sway demand index,  $I_{Di}$ , can be calculated for each storey as follows:

$$I_{Di} = \frac{\text{storey } i \text{ infill shear demand}}{\text{storey } i \text{ infill shear resistance}} = \frac{V_{infill,i}}{V_{R,infill,i}} \quad 3.34$$

Compatible with the introduced infill demand index,  $I_{Di}$ , the sway demand index,  $S_{Di}$ , should be computed as follows:

$$S_{Di} = \frac{\text{storey } i \text{ frame shear demand}}{\text{storey } i \text{ frame shear resistance}} = \frac{V_{frame,i}}{V_{R,frame,i}} \quad 3.35$$

$V_{frame,i}$  and  $V_{infill,i}$  are the shear demand on the frame and infill member in a storey for a displaced shape and a target base shear. Sway and infill demand indices are used in parallel to follow the response stage of each frame and infill members in a structure. As one of these indices hits 1.0, noting that the capacity has been reached, the corresponding member should be switched to the next stage in its previously defined load-rotation/drift backbone. This way, the current status of each element in the structure can be identified and the storey-by-storey softening of the structure is captured. During the analysis,  $V_{frame,i}$  and  $V_{infill,i}$  are computed based on the applied storey drift,  $\Theta_i$ , also the frame and infill storey backbones computed in the preceding sections. In fact, an alternative storey shear value (Equation 3.38) can be computed by adding the individual contributions (Equation 3.36 - 3.37). Since this shear value is obtained through the backbone of the members, it is called as the true base shear.

$$V_{frame,i}(\Theta_i) = \begin{cases} K_{y,flex,i} \cdot (\Theta_i \cdot h_s), & \Theta_i \leq \Theta_{y,fr,i} \\ K_{ult,flex,i} \cdot [(\Theta_i - \Theta_{y,fr,i}) \cdot h_s] + V_{Ry,fr,i}, & \Theta_{y,fr,i} > \Theta_i \leq \Theta_{ult,fr,i} \end{cases} \quad 3.36$$

$$V_{infill,i}(\Theta_i) = \begin{cases} K_{y,ax,i} \cdot (\Theta_i \cdot h_s), & \Theta_i \leq \Theta_{y,in,i} \\ K_{ult,ax,i} \cdot [(\Theta_i - \Theta_{y,in,i}) \cdot h_s] + V_{Ry,in,i}, & \Theta_{y,in,i} > \Theta_i \leq \Theta_{ult,in,i} \end{cases} \quad 3.37$$

$$V_{true,i} = V_{frame,i} + V_{infill,i} \quad 3.38$$

Returning to the presented analysis methodology in Sullivan *et al.* [2018], in order to converge to a target base shear value, a guess displacement profile was introduced to the structure and, based on the storey displacements, the target base shear was distributed to each storey. This was done according to Equation 3.39. Then the storey shear profile was computed and a new

displaced shape was obtained by dividing the storey shear with the storey stiffness (Equation 3.40 - 3.42). The displaced shape was iterated until the difference in the old and the new sway profile was negligible.

$$F_i = \frac{m_i \Delta_i}{\sum m_i \Delta_i} V_{b,target} \quad 3.39$$

$$V_i = \sum_{k=i}^n F_k \quad 3.40$$

$$\delta_i = \frac{V_i}{K_{y,sys,i}} \quad 3.41$$

$$\Delta_{i,new} = \sum_{k=i}^n \delta_i \quad 3.42$$

However, since a monotonically increasing storey shear is considered with this strategy, the aforementioned procedure becomes inefficient when the stiffness becomes negative. In case of negative storey stiffness, the existing method keeps increasing the storey shear with the increasing storey displacement but instead decreases and returns non-realistic values. Therefore, an alternative method for checking the convergence criteria is proposed for the iteration process.

Considering the iterative process described in between Equation 3.39 - 3.42, the storey unbalanced load,  $\Delta V_i$ , can be used as the convergence criteria (Equation 3.43). The unbalanced load is computed as the difference between the storey shear (Equation 3.40) and the true storey shear (Equation 3.38). During the initial stage of the analysis, in which every storey has positive stiffness, the iteration has to be repeated until the unbalanced load becomes zero. When a storey attains negative stiffness, then the iteration is stopped when the  $\Delta V_i$  without the negative stiffness storey converges to zero. Considering the negative stiffness portion, convergence might be improved by updating the guessed displaced shape with the profile obtained from the previous, lower target base shear step.

$$\Delta V_i = V_{true,i} - V_i \quad 3.43$$

Finally, the issue of computing a new storey inter-storey displacement value that is compatible with the changing storey stiffnesses is addressed. If there is more than one branch in the storey backbone, the new storey inter-storey displacement should be calculated with Equation 3.44. In case the storey stiffness is already negative and will be changed to another negative value meaning  $\Delta V_i$  will not be zero, Equation 3.45 should be used instead.

$$\delta_i = \left| \frac{V_i - V_{R,i,(k-1)}}{K_{sys,i,k}} \right| + \theta_{sys,i,(k-1)} \cdot h_s \quad 3.44$$

$$\delta_i = \left| \frac{(V_i - \Delta V_{i,(k-1)}) - V_{R,i,(k-1)}}{K_{sys,i,k}'} \right| + \theta_{sys,i,(k-1)} \cdot h_s \quad 3.45$$

where notation k-1 corresponds to the preceding capacity point of the storey and  $\Delta V_{i,(k-1)}$  corresponds to the last observed  $\Delta V_i$  of a negative stiffness storey just before updating the stiffness and the capacity properties. Finally,  $K_{sys,i,k'}$  is a consecutive negative stiffness value following a negative stiffness branch associated with the i-th storey.

### 3.2.6 Application within Displacement-Based Assessment Framework

The last section discusses the processing of the analysis results for creating the force-displacement history of the structure which is also compatible with the displacement-based assessment procedure described by Priestley *et al.* [2007]. Hence, the stick structure analysed in the previous section will be further reduced to an equivalent SDOF and the displacement versus base shear response found. To do so, the over-turning moment (OTM), effective height  $H_e$ , effective stiffness  $K_e$ , effective mass  $m_e$  and effective period  $T_e$  are computed. The base shear will be estimated by dividing the OTM by the effective height. This procedure and equations can be found in Sullivan *et al.* [2018] although with a minor difference, instead of using  $V_i$  to compute the OTM, the true base shear,  $V_{true,i}$  should be used for all-post processing calculations.

Consistent with the rules of superposition used for frame and infill members, the storey frame and infill ductility can be computed as in Equation 3.46 - 3.47. The instantaneous ductility demand associated with the infill and the frame elements can be utilized in equivalent viscous damping computations which is necessary for the assessment step. Separate ductility values imply that the equivalent viscous damping formulas that are already available in the literature for RC frame structures can be used for the frame part whereas, the infill caused damping contribution can be computed for the infill members with separate formulas. However, there is a need to conduct further study on the damping response of infill panels as well as introducing empirical formulas to compute equivalent viscous damping.

$$\mu_{frame,i} = \theta_i / \theta_{y,frame,i} \quad 3.46$$

$$\mu_{infill,i} = \theta_i / \theta_{y,infill,i} \quad 3.47$$

where  $\Theta_i$  is the current storey drift,  $\Theta_{y,frame,i}$  and  $\Theta_{y,infill,i}$  are the storey yield frame and infill drifts. Sub-structure estimation to calculate the base shear, described by Sullivan *et al.* [2018], can be seen as updated with the true base shear between Equation 3.48 - 3.53.

$$OTM_i = V_{true,i} \cdot h_{s,i} \quad 3.48$$

$$H_{eff.} = \frac{\sum \Delta_i m_i h_{s,i}}{\sum \Delta_i m_i} \quad 3.49$$

$$V_{base} = \frac{OTM_1}{H_{eff.}} \quad 3.50$$

$$K_{eff.} = \frac{V_{base}}{\Delta_{roof}} \quad 3.51$$

$$m_{eff.} = \frac{(\sum \Delta_i m_i)^2}{\sum \Delta_i m_i^2} \quad 3.52$$

$$T_{eff.} = 2\pi \sqrt{\frac{m_{eff.}}{K_{eff.}}} \quad 3.53$$

### 3.3 Summary

A methodology to consider infill contribution to the structure behaviour was addressed in this chapter. First, the theoretical background was outlined, mechanics and the necessary formulation was deduced by starting from a simple problem and incrementally increasing the complexity. A phenomenon related to the overall behaviour of a multi-storey-multi-bay infilled structure was identified at each step. Afterwards, using the knowledge gained in the first part and noting the complexity of the problem, an approximate methodology to take account of the flexural infill-frame interaction was presented. Then, several refinements were proposed considering the simplified analysis procedure introduced by Sullivan et al. [2018] in order to increase the efficiency of the method for the analysis of infilled frames. Overall, the characterisation, compilation and presentation of a full procedure that is applicable for the simplified analysis of an infilled frame was made in this chapter.

*This page is intentionally left blank...*

## 4 Validation of the Simplified Analysis Approach

A novel procedure to include infill interaction in the simplified analysis of RC frame structures was proposed in Chapter 3. Following the steps outlined in the preceding chapter, it is possible to conduct a non-linear static analysis without assembling a detailed numerical model of a given infilled RC frame structure. In this chapter, issues regarding the validity and the application of the proposed approach will be addressed. To do this, a set of case study structures will be first introduced. In order to emulate a realistic assessment study scenario, these structures are selected from the available literature on real existing RC frames in Italy. The details on the numerical modelling of these frames will be given referring to the relevant numerical modelling strategies cited in Chapter 2. Then, using the case study frames, a short investigation into the effect of infills on the global mechanism of the system will be presented and critical issues regarding the range of application of the simplified analysis method will be discussed. Following this, the proposed procedure will be implemented for three 6-storey-3-bay infilled RC structure with different infill typologies and the force-deformation response (pushover) curve will be obtained. The accuracy of the method will be assessed by comparing the resulting pushover curve and the displaced shapes for various points with the non-linear static analysis obtained from a detailed numerical model. Finally, the performance of the proposed approach will be evaluated by comparing the obtained displaced shape with the ones obtained through other simplified methods available in the literature.

### 4.1 Description and Modelling of the Case Study Structures

To validate and test the proposed simplified analysis procedure, a set of existing case study frames are introduced here. Galli [2007] modelled and analysed the behaviour of numerous frames designed between 1950s and 1970s, considering these frames as a sample of the gravity load designed (GLD) frames in Italy and the Mediterranean region in general. Based on the structures described by Galli [2007], a batch of 25 2-D frames consisting of 5 different heights and 4 different infill typologies were prepared and used by O'Reilly [2016], O'Reilly *et al.* [2018] and Sullivan *et al.* [2018] for various studies on infilled and bare frame structures focused on modelling issues, collapse assessment and validation of simplified analysis results. The configuration and the properties of the frames that were adopted from Galli [2007] are portrayed in Figure 4.1.

These frames were slightly modified by O'Reilly [2016], adding different typologies of infills (i.e. weak, medium and strong) using the properties defined by Hak *et al.* [2012]. Finally, two different distribution of infills are considered, namely uniform and pilotis. The set of typologies

can be seen in Figure 4.2. Infills with openings are not considered in the scope of this work hence further attention will be necessary for these typologies in future studies.

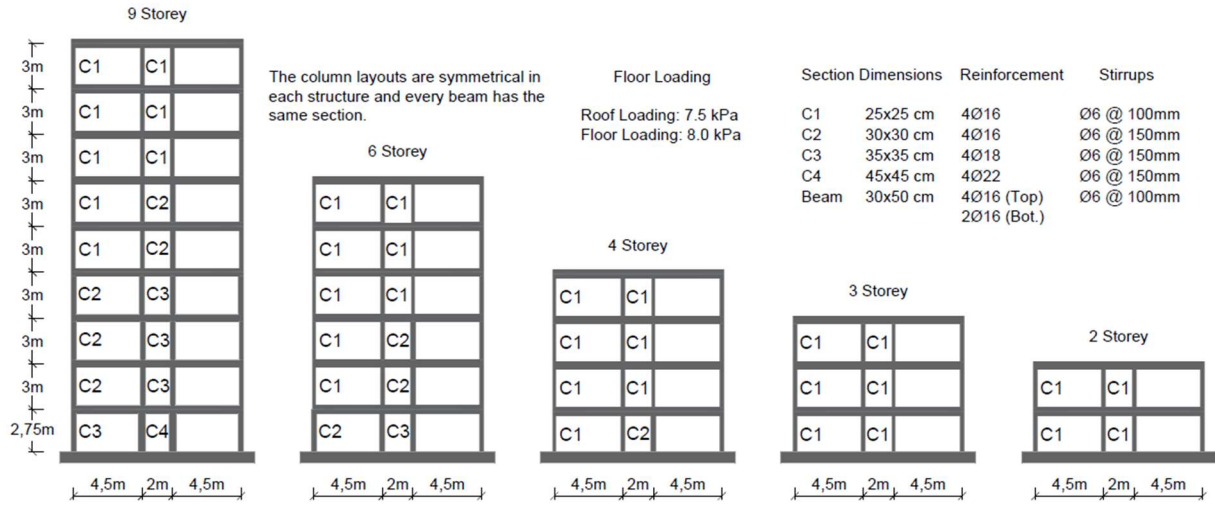


**Figure 4.1. The set of 2D bare frame structures adopted from Galli [2007] by O'Reilly [2016]**

Models of these frames were developed in OpenSees (McKenna *et al.* 2010) environment using the modelling approach outlined in O'Reilly and Sullivan [2017] for the modelling of existing RC frame structures in Italy. Based on the floor loading values, lumped masses at each joint were computed and the gravity forces applied accordingly. A moment-curvature analysis was carried out prior to the analysis for the member cross-section to quantify the strength and deformation response. Infills were modelled as single diagonal struts according to the macromodel introduced by Bertoldi *et al.* [1993] (with the expressions outlined in Chapter 2). The resulting backbone curve of the strut was modified according to the suggestions of Sassun *et al.* [2015] based on the comparison with experimental results. The same strategy and the backbone curves associated with the sections are also adopted in Section 4.3 during the simplified analysis process and the calculation of the proposed displaced shape.

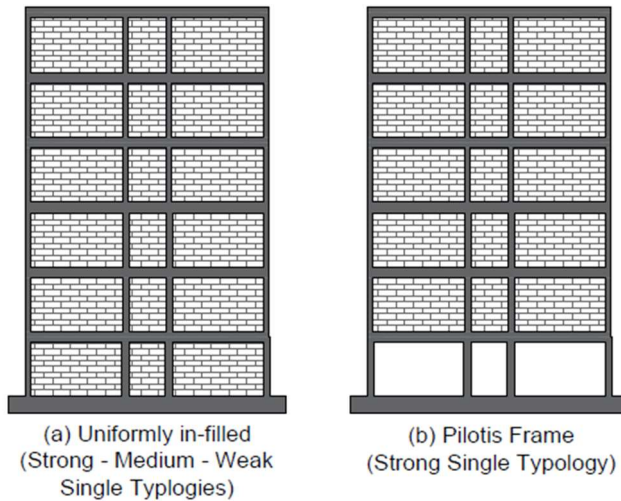


**Figure 4.2. Illustration of the infill typologies and distributions for the 6-storey frame, for example.**

The load-displacement behaviour of these frames was obtained by applying a vector of lateral forces and the structural response was studied in detail. This was to understand the force-displacement capacity, initial stiffness of the structure and individual storeys in addition to the change in the stiffness throughout the analyses, strength hierarchy, progression of the plastic hinges, infill damage states and the global inelastic mechanism. The results were then compared with the proposed simplified analysis methodology to evaluate the capability of the method in capturing these particularities.

## 4.2 Influence of Frame-Infill Interaction on the Global Inelastic Mechanism

This section focuses on understanding the effects of introducing uniformly distributed infill panels along the structure height on the global behaviour of a frame structure. It is a well-studied fact that, unlike irregularly distributed cases, uniformly placed infills stiffen the structure and increases the base-shear capacity. In this case, the infill panels act very much like diagonal braces limiting the absolute lateral deformation of the frame structure through increased strength and stiffness at each storey. Once the infills in a storey begin to fail (i.e. their stiffness reduces significantly) and lose a considerable portion of their resistance suddenly (i.e. in a very narrow range of increasing drift), the shear demand is transferred to the RC frame. This large shear force may cause a brittle failure in the beam-column ends, particularly in existing frames, for which it is highly likely to encounter shear failures with such insufficiently designed frame members. This section aims to outline the expected changes in the structural behaviour in which having a continuous flexural resistance throughout the deformation capacity of the frame is possible.

Once the case study frames have been modelled, several linear and non-linear dynamic analyses can be done to assess the effects of having infill panels with various typologies. For this purpose, assumed to be relatively generic and common, the six-storey frame structure shown in Figure 4.1 is considered first. The frame of interest has a single irregularity level along its height which is the slightly shorter ground storey height (2.75 m) when compared with the rest of the storeys (3 m). This feature is expected to cause a more pronounced contribution of higher modes and possibly a need for superposing several initial modes to exceed 90% mass contribution in case of a response spectrum analysis, for example. For a uniform distribution of relatively stiff infill panels with respect to the flexural stiffness of the frame, a reduction of the aforementioned irregularity in height and a behaviour similar to a more regular structure with an increased first mode contribution is expected. The case with the highest first mode mass participation is expected be observed when there are no infills at the ground storey and uniformly distributed strong infills at the rest of the storeys, typically referred to as a pilotis case. In this configuration, the weak or soft ground storey acts a buffer storey that attracts most of the induced displacement similar to a base isolated building. With these considerations in mind, the modal analysis results conducted in OpenSees for the bare frame and the rest of the typologies can be seen at Table 4.1 and Table 4.2, respectively.

Considering the bare frame, the first mode participation is around 75% which is less than what is required to assume a first mode dominated behaviour. It is worth noting that, for all case study structures, at least the first two modes if not three, must be included in the analysis in order to obtain a realistic representation of the complete response.

**Table 4.1. Modal analysis output of the bare frame**

Typology	Mode	T (sec)	% Mass
<b>Bare Frame</b>	1	2.04	75.48
	2	0.72	12.40
	3	0.44	3.91
	4	0.31	2.21
	5	0.25	2.43
	6	0.19	3.57

As far as the periods of the structures are concerned, the first mode period drastically shortens (more than half) when the infills are present in the structure. Looking at the progression of the first mode mass participation values throughout different typologies, it can be noted that as the relative stiffness of the infill panels increases, the overall structure slightly becomes more controlled by the first mode shape. Finally, comparing the relative change in the first mode period and the percentage of mass participation, one may deduce that despite the substantial differences in the brick laying configuration and the mechanical properties between the medium and the strong typologies, the resulting modal properties (i.e. first mode stiffness) are very close.

**Table 4.2. Percent mass participation of each mode for different infill typologies**

Typology	Mode	T (sec)	% Mass	Typology	Mode	T (sec)	% Mass
<b>Weak Single</b>	1	0.63	76.92	<b>Medium Single</b>	1	0.49	78.03
	2	0.23	13.55		2	0.18	13.40
	3	0.14	3.43		3	0.10	3.52
	4	0.11	1.94		4	0.08	1.72
	5	0.09	1.96		5	0.07	1.74
	6	0.07	2.19		6	0.06	1.59
<b>Strong Single</b>	1	0.42	78.40	<b>Strong Pilotis</b>	1	0.75	82.38
	2	0.15	13.54		2	0.21	11.15
	3	0.09	3.57		3	0.10	2.87
	4	0.07	1.60		4	0.07	1.29
	5	0.06	1.62		5	0.06	1.30
	6	0.05	1.27		6	0.05	1.02

Following the identification of the modal properties, a set of incremental dynamic analyses were performed with the aim of identifying the “true” global inelastic mechanism of the six storey case study structures. Moreover, it was expected that this step would provide a benchmark for the simplified analysis results provided in the upcoming sections in terms of identified global mechanism. It worth mentioning that, this step is only done to have an idea of the expected inelastic mechanism and the analyses conducted in this section are not a prerequisite of the proposed methodology. In fact, the global inelastic mechanism can be identified solely using the proposed analysis procedure, without any dynamic analysis. Ideally,

the proposed first mode based simplified analysis method will capture the global mechanism observed in the incremental dynamic analyses discussed here. To do that, a set of ten records were utilised. These records were taken from the INNOSEIS (Vayas et al. 2017) records database as the high seismicity record set. The record set consist of sixty records corresponding to East-West and North-South directions of thirty different stations. The log-log plot of the response spectra calculated from the record set can be seen at Figure 4.3.

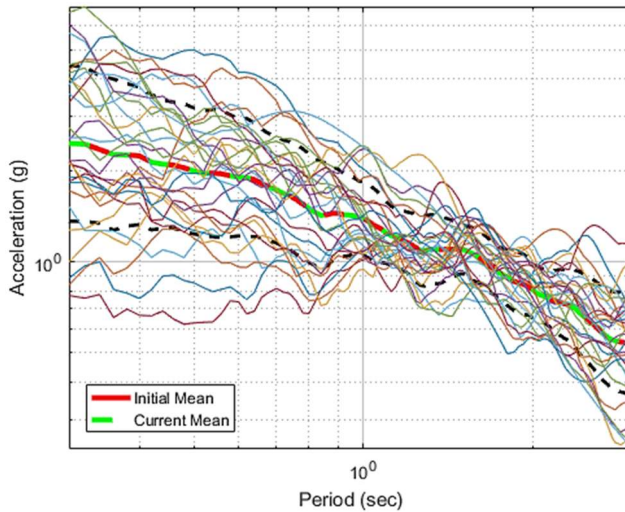


**Figure 4.3. Geo-mean response spectra of the 30 events taken from INNOSEIS high seismicity record set.**

**The geometric mean of each station's two component pairs is plotted.**

For the sake of simplicity, this record set was reduced from 30 to 10 events by carefully selecting the ones which yield a similar mean response spectrum and standard deviation compared with the original dataset. Then, for the analysis, since the case study models are 2D, one of the N-S or E-W components of a given event was selected randomly (Baker and Cornell, 2006). The average spectra and the standard deviation of the reduced record set can be seen in Figure 4.4, where the impact of reducing the set to just ten is seen to be reasonable. It is also worth noting that, even though the history of the records is described, since the main aim of this section is just to identify the global mechanism with a set of incremental dynamic analyses, the record set used are inconsequential in terms of hazard compatibility. The final set of records used for IDA is described in Table 4.3.

Using the above described record set, IDA was conducted in OpenSees by assuming a 5% modal damping (Chopra and McKenna 2015) for the dynamic analysis. According to the suggestions of O'Reilly et al. [2018], the collapse inter-storey drift was set to 10% considering the frame members. The result matrix of the conducted incremental dynamic analyses is shown in Figure 4.5.

Each row of the matrix is associated with a storey of the analysed frame and each column corresponds to a different typology. Typologies are ordered with respect to ascending infill stiffnesses. In each plot, the horizontal axis is given in terms of spectral acceleration at the fundamental period of the structure,  $Sa(T_1)$ , over a domain of 0 to 0.8g with 0.1 intervals and the vertical axis, is given as the inter-storey drift value, in percentage (%). Note that inter-storey drift values were capped at 10% taken as the maximum value corresponding to collapse.

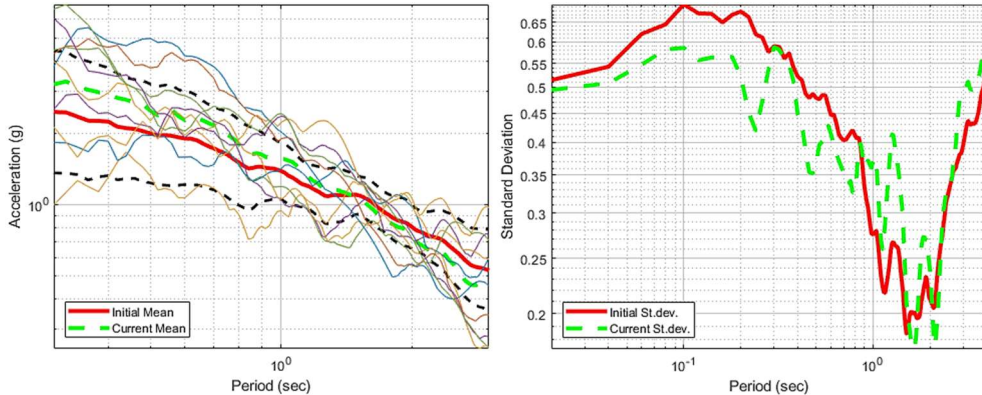


**Figure 4.4. Single component mean spectra of the reduced record set, where 10 selected events are seen to faithful represent the original mean and the standard deviation of the INNOSEIS database.**

**Table 4.3. Final set of selected 10 records for IDA**

No.	Record String	No.	Record String
1	Dinar 180	6	Coyotek G02050
2	Coalinga H-PG5000	7	Coalinga H-CAK360
3	Hector 12026360	8	Northridge MRP180
4	Landers BAK050	9	Northridge SAN180
5	Kocaeli ERG180	10	Loma Prieta SUF180

Considering the bare frame results, it is clear that the soft storey locations are predominantly concentrated at the 4<sup>th</sup> and 2<sup>nd</sup> storeys, with some occurrences at the 1<sup>st</sup> storey. However, by looking at the range of spectral accelerations, it can be seen that the initial soft storey case is found at the 4<sup>th</sup> storey which may also correspond to the result obtained from pushover analysis. Having said that, the occurrence of the soft storey at the 4<sup>th</sup> storey in IDA confirms the results obtained through simplified analysis done on the same structure by Sullivan et al. [2018]. Proceeding with the results of the other typologies, it is worth noting that, in line with the modal analysis results, adding uniformly distributed infills to the structure; results in a more homogenised behaviour along the height of the infilled frame. This is emphasised as the progressive recession of the soft storey at the 4<sup>th</sup> level and further concentration at the 2<sup>nd</sup> storey, as the infill to frame stiffness ratio increases. Hence, contrary to the bare frame characteristics, the likelihood of having a soft storey mechanism at the 2<sup>nd</sup> level increases when the infills are present in the structure.

To summarise, the effect of considering the frame-infill interaction in the flexural response of an infilled frame is essential. Adding uniformly distributed infill panels favours the structure's lateral performance by reducing the effect of irregularities along the height of the structure and increasing the force capacity. In tandem with these improvements, the global mechanism associated with the infilled structure is different from that of the bare frame version of the same structure. These findings are also in line with those of O'Reilly [2016] who noted from pushover analyses that the presence of the masonry infills in such frames tended to modify the expected mechanism location with respect to the corresponding bare frame case, highlighting that the effects of masonry infills on the lateral behaviour of the structure needs to be given explicit consideration and not considered as a secondary addition to the primary bare frame case.

## Validation of the Simplified Analysis Approach

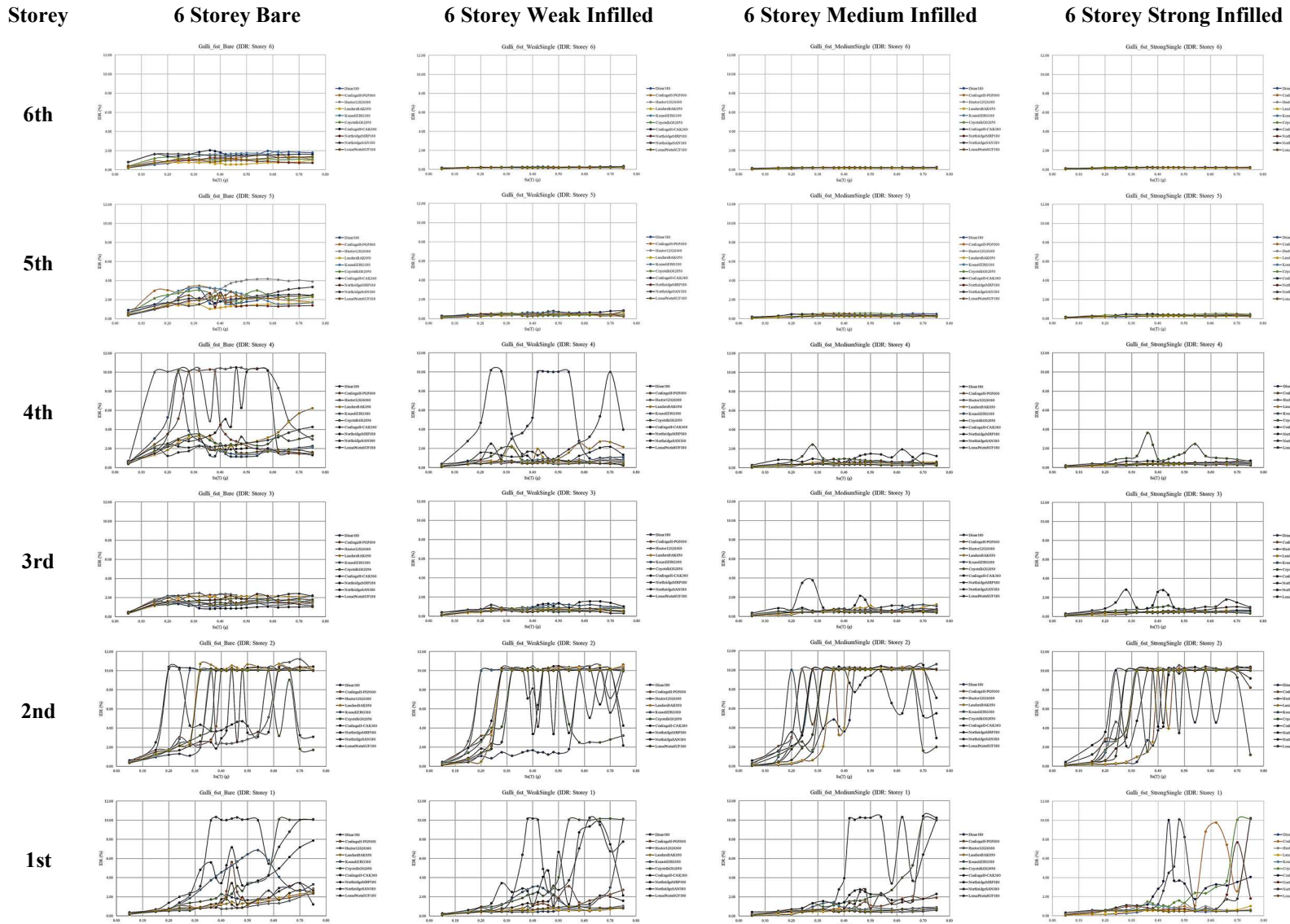


**Figure 4.5. Inter-storey Drift Ratio (IDR) Profile of each structure obtained through incremental dynamic analysis (IDA) [axes: Y - IDR (%) | X -  $Sa(T)$  (g)]**

### 4.3 Application of the Proposed Simplified Assessment Procedure on a 6-Storey Case Study Structure

The current section will address the modelling and the analysis of the six-storey case study infilled RC frame within the proposed simplified assessment procedure, using the concepts and methods developed so far and outlined in Chapter 3. The obtained results will be compared with the results of the pushover analysis outputs.

For the sake of computational ease, the simplified analysis of the infilled structure can be done with a spreadsheet processor such as Microsoft Excel, OpenOffice Calc or Google Sheets etc. but can also be coded into a more specific software tool if needed. Nevertheless, this study adopts Microsoft Excel as the analysis environment since it is one of the most popular spreadsheet processors. One spreadsheet should be utilised for the complete analysis of each frame structure with a given geometry, frame and infill properties. The mentioned document can be divided in to six individual worksheets, which are organised as:

1. Structural information: material properties, structural geometry and mass/gravity load definitions;
2. Frame capacities: frame section sizes and member force-deformation definitions;
3. Infill capacities: infill panel sizes and force-deformation definitions;
4. System capacities: structure/system (frame + infill) definitions;
5. Static analysis;
6. Post-processing.

Three Excel documents that are prepared with the aforementioned strategy for the 6-storey-3-bay weak, medium and strong infilled frames and are provided supplementary to this work. Following the described procedure in Chapter 3, the modelling procedure is demonstrated for the structure Galli\_6st\_MediumSingle in Appendix A. As per the modelling assumptions, masses are calculated through gravity loads, lumped at each joint and summed up for the storey masses. The distribution of mass along the structure height is provided at Table A.1. The frame section and infill/masonry properties used for Galli\_6st\_MediumSingle can be seen in Table A.2 and Table A.3, respectively.

Static pushover (SPO) analyses were carried out on the aforementioned case study frames and four displaced shapes corresponding to various roof displacement values along the pushover curve of each structure were evaluated. These four limit states were picked from the pushover curve with the aim of representing the changing global stiffness of the analysed structure which corresponded to 0.1%, 0.3%, 0.35% and 0.4% roof drift values. Note that, the expected inelastic mechanism forms at around 0.4% roof-drift-ratio and the numerical collapse of the frame (base shear reaches zero) occurs at around 1%. The comparison between the proposed and the numerically computed pushover curves, sway profiles and the lateral force profile obtained at equilibrium can be seen at Figure 4.6, Figure 4.7 and Figure 4.8, respectively. Considering the initial stiffness of each structure, there is an outstanding agreement between the proposed method and the numerical model. This can be seen in the pushover curves and the displaced

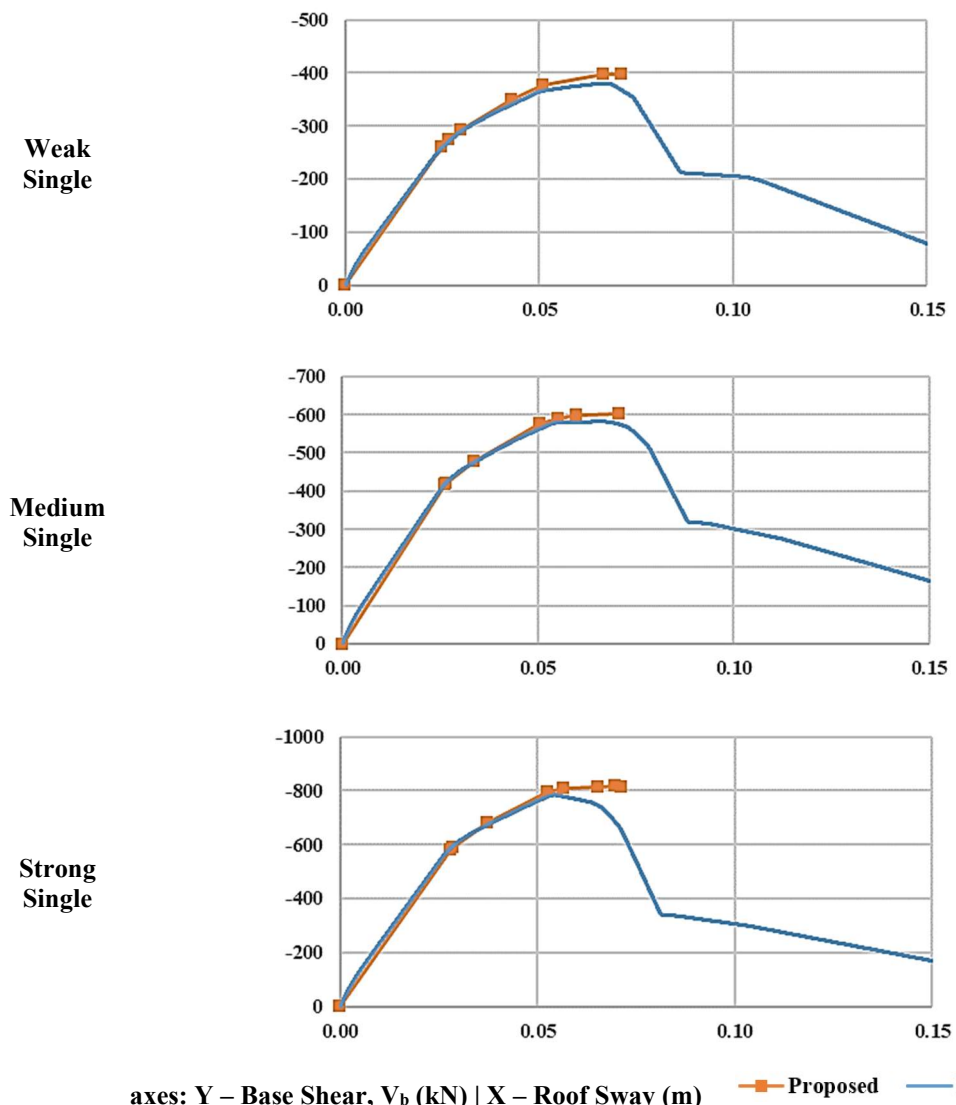


**Figure 4.6. Comparison of the force-displacement response computed via the simplified method with the SPO analyses**

shapes evaluated at limit state 1, corresponding to 0.1% drift when the frame is expected to still remain completely elastic. Increasing the target base shear, the first critical storey identified by the infill demand index was the second storey, which is compatible with Figure 4.5 and the pushover results. At limit state 2, following the yield of the infill panels at the 2<sup>nd</sup>, 1<sup>st</sup>, 3<sup>rd</sup> and 4<sup>th</sup> storeys, respectively, the infill demand index identified the first infill failure to occur at the second storey. At this stage, since the infill panel at the second storey obtained a negative stiffness value, the storey resistance increasingly becomes solely dependent on the remaining available frame stiffness. This causes the sway demand index associated with the second storey to dramatically increase. However, since there is a degree of discrepancy between the predicted and the observed second floor frame stiffness during the pushover analysis (predicted ~14% stiffer), the second storey cannot attract enough inter-storey displacement to reach yielding and the sway demand index instead identifies the soft storey erroneously at the ground level. This difference in the second storey stiffness is attributed to its mixed (beam and column hinging)

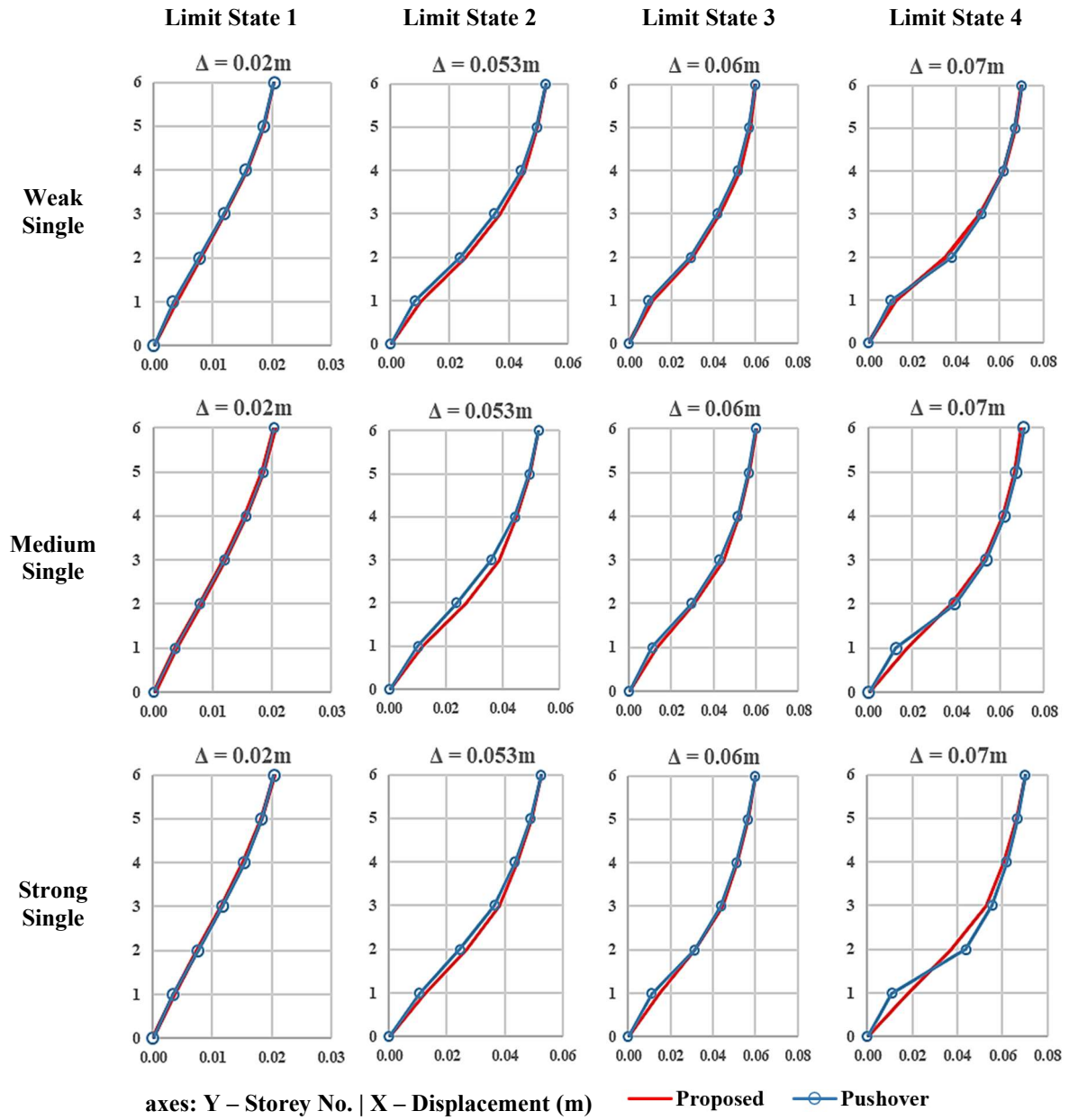


**Figure 4.7. Comparison of the displacement profile obtained through the simplified method with the SPO analyses at various roof displacements.**

type of storey failure mechanism. Since this floor was assumed to be undergoing a column type failure, the simplified method yields a slightly different stiffness. It is suggested that this aspect of the methodology could be further addressed with a refined strategy to obtain better matching results in the future. Since the soft storey is identified at the first floor instead of second, the pushover analyses are stopped at the frame yield point. However, the analysis can be continued to obtain the post-peak part of the pushover curve. In any case, the performance of the proposed method to identify the soft storey should be presented on a different case study structure that does not present a mixed type of failure mode at the expected soft storey location. Despite this minor difference whose cause has been adequately identified, it is shown that the proposed

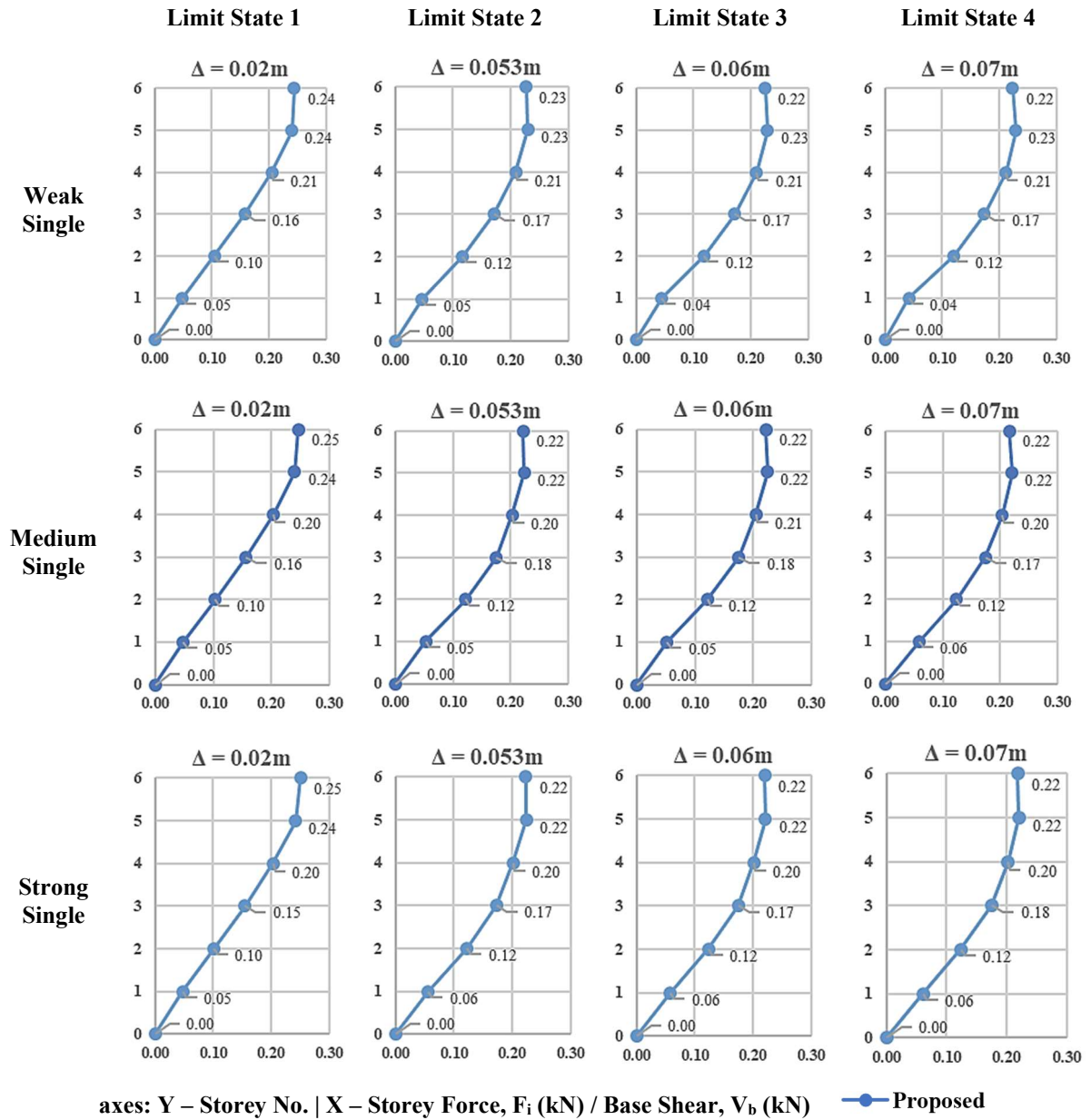


**Figure 4.8. Evolution of the computed lateral storey force profile through subsequent limit states.**

method is able to adapt to the changing inelastic mechanism problem of the infilled frame as identified in Section 4.2.

In Figure 4.7, it is worth noting that the proposed method is very effective in capturing the overall and local softening of the structure as the infill panels yield and eventually fail. There is an excellent match between the displaced shapes obtained through pushover and the simplified method considering the limit states 1, 2 and 3. In terms of limit state 4, where the global inelastic mechanism has been formed, the aforementioned effect of overestimated frame stiffness becomes more present as the infill stiffness increases (i.e. Strong Single). This is because of the increasing stiffness ratio between the first and second storeys. While the second storey was expected to soften because of the overestimation and exhibit increased displacement, the stiffer ground storey governs and following its infill panel failure, the soft storey appears at

the ground floor. After the displaced shape corresponding to the target base shear value converges, the storey force profile computed at the point of equilibrium can be saved as the pushover force vector of that point.

In Figure 4.8, the evolution of the computed force vector that is normalised with the base shear at that step can be observed as the roof displacement increases. At limit state 1, with the exception of the last floor, the force vector can be seen to increase linearly with height, whereas as the structure softens, the force vector gradually becomes more distributed as it adapts to the change in the stiffness distribution along the height of the structure.

#### 4.4 Comparison of the Proposed Methodology with Other Available Approaches

This section provides a comparison of the proposed methodology for estimating the infilled RC frame storey stiffness in Chapter 3 with the existing procedures in the literature. As previously cited in Chapter 2, a novel method based on the additional structural moments due to infill resistance was proposed by Saborio-Romano [2016] (Alternative 1). According to this methodology, the drift attained by the infill panels was rendered as the additional rotational work done by the storey moments and a stiffness value associated with the total work done by the infill panels at a storey was computed (Equation 2.5). On the other hand, at the initial stages of this work, a preliminary method, which only takes into account the strut stiffnesses without considering the effect of boundary and below columns was utilized. Recently, Gentile *et al.* [2019] (Alternative 2) published an alternative simplified framework (SLaMA) to the procedure presented by Sullivan *et al.* [2018], in which the strut stiffness without boundary columns methodology is utilized to estimate the infill contribution of the storey stiffness. has been adequately identified, it is shown that the proposed method is able to adapt to the changing inelastic mechanism problem of the infilled frame as identified in Section 4.2. The force-displacement response at limit state 1 and the associated displaced shape computed with different methodologies are given in Figure 4.9 and Figure 4.10, respectively.

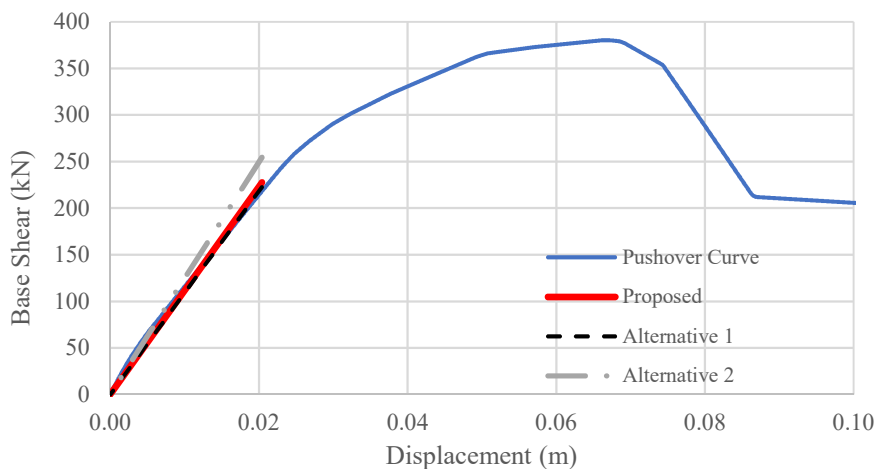


**Figure 4.9. Comparison of the force-displacement behaviour obtained with different approaches at limit state 1 ( $\Delta_{\text{root}} = 0.02\text{m}$ )**

Considering the computed initial stiffnesses, both the herein proposed and the Saborio-Romano [2016] methods yield similar results with the numerical model whereas Gentile *et al.* [2019] overestimates the base shear value. However, in terms of displaced shapes, Saborio-Romano [2016] cannot capture the existing irregularity in height (stiffer first storey) given that the contribution of the consecutive storeys is averaged in Equation 2.5. This results in a displaced shape associated with a softer structure. In the case of the Gentile *et al.* [2019], the characteristics of the infilled frame are more pronounced. Finally, the proposed method presents a much-improved solution that captures both the individual storey stiffnesses and structure stiffness accurately.

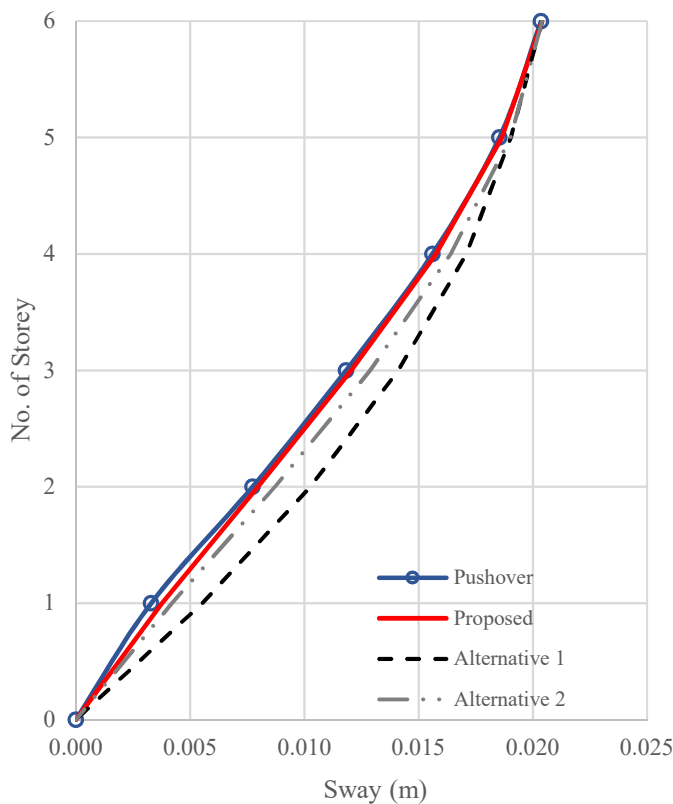


**Figure 4.10. Comparison of the displaced shapes obtained by utilising different approaches at limit state 1 ( $\Delta_{\text{roof}} = 0.02\text{m}$ ).**

## 4.5 Summary

In this chapter, a batch of case study frames were introduced. The method of numerical modelling and the analysis software were described briefly. Then, the case study frames were analysed with dynamic methods in order to study the effect of infill panels on the global inelastic mechanism. It was shown that, uniformly distributed infill panels decrease the effects of existing irregularities in height and alter the expected mechanism when compared to its bare frame counterpart. Then, the 6-storey infilled frame was modelled and analysed with the proposed methodology. The results showed that there is an excellent agreement between the numerical and the simplified model. Considering the weak infilled structure, the initial stiffness values that were obtained with the simplified method and observed in OpenSees are given in

Table 4.4 individually for the frame and the infill counterparts and in Table 4.5 for the combined system stiffnesses. In Table 4.4, the discrepancy between the frame flexural stiffness that is computed by using Sullivan *et al.* [2018] and the stiffness of the bare frame obtained through the numerical model is shown in the first column whereas second column presents the difference between the axial stiffnesses of the infill element that is computed with the proposed methodology and through the numerical model. On the other hand, Table 4.5 compares the system storey stiffnesses that are obtained through adding flexural stiffness with the axial stiffness, versus the numerical model. Examining the error (Equation 4.1) at each storey, it can be seen that it is relatively low. Finally, the proposed method is compared with the other simplified methods that are available in the literature for infilled frames.

$$\text{error} = \left| \frac{K_{t,i,\text{OpenSees}} - K_{t,i,\text{Proposed}}}{K_{t,i,\text{OpenSees}}} \right| \times 100 \quad 4.1$$

where  $K_{t,i,\text{OpenSees}}$  and  $K_{t,i,\text{Proposed}}$  corresponds to the storey stiffness obtained from numerical model and the proposed methodology, respectively. Subscript “i” controls the number of storey whereas “t” is a tag that distinguishes frame, infill and system stiffnesses.

**Table 4.4. Observed vs. proposed storey stiffness for the 6-storey weak infill structure considering limit state 1.**

Storey	Frame Stiffness (kN/m)			Infill Stiffness (kN/m)		
	OpenSees	Sullivan et al. [2018]	error	OpenSees	Proposed	error
6	3705.01	3582.54	3.31%	26773.06	29217.95	-9.13%
5	3861.00	3625.91	6.09%	32198.34	34146.04	-6.05%
4	4018.19	3852.82	4.12%	33822.69	36034.80	-6.54%
3	5304.86	5685.74	-7.18%	37008.20	38290.01	-3.46%
2	5674.14	6510.26	-14.74%	37080.35	40203.83	-8.42%
1	14467.53	13460.64	6.96%	47439.25	43550.33	8.20%

**Table 4.5. Observed vs proposed combined storey stiffness for the 6-storey weak infill structure.**

Storey	Combined Stiffness (kN/m)		
	OpenSees	Proposed	error
6	30478.07	32800.49	-7.62%
5	36059.33	37771.95	-4.75%
4	37840.88	39887.61	-5.41%
3	42313.06	43975.75	-3.93%
2	42754.49	46714.09	-9.26%
1	61906.78	57010.97	7.91%

## 5 Conclusion

This chapter summarises this thesis' work by referring back to the key aspects and conclusions identified in each chapter. Finally, a series of identified topics of future research and interest are presented.

### 5.1 Summary

A simplified method of static analysis for infilled RC frames was presented to allow analysts to compute the force-displacement response of an infilled frame in a spreadsheet file without building the full stiffness matrix via a traditional numerical model. The proposed method was built upon the existing framework described by Sullivan *et al* [2018] on the simplified analysis of bare RC frames susceptible to non-ductile mechanisms typical of older buildings. A novel methodology was proposed to estimate the storey stiffness considering the contribution of the infill panels and several refinements to the iterative analysis procedure that extends the existing framework to capture the highly non-linear behaviour of the infilled frames. First, the flexural horizontal stiffness due to the bare frame and axial stiffness due to the infills were decoupled by assuming that both systems work in parallel against the external forcing action (i.e. the lateral excitation induced during earthquake shaking). Then, after computing individual storey backbone responses, frame and infill counterparts were superposed to obtain the combined storey stiffness. The storey infill stiffness was computed by considering both the effect of the strut elements present in the storey of interest in addition to the effects of the boundary and the storey columns below. In terms of analysis, an unbalanced convergence criterion was introduced that allows analysts to deal with negative stiffnesses and a new index, which the infill demand index,  $I_{Di}$ , was proposed to follow the damage state of the infill elements. Previously, the effect of the infill panels present in the structure was taken into account either by translating their contribution into structural moments or considering solely the horizontal axial stiffness of the struts existing at a storey. However, it was shown that while the former is able to capture the structural stiffness accurately but, underestimates the storey stiffnesses, whereas the latter yields a relatively better displaced shape, overestimating the base shear associated.

Finally, the proposed method was demonstrated on a six storey pre-70s RC structure with different typologies of infill typical of those built in Italy around that time. The results showed that the proposed method was able to capture the initial stiffness and the softening of the structure by displaying a good match when compared with the pushover results. In addition, unlike Saborio-Romano [2016], MIMA (Cardone *et al.* 2017) and Landi *et al.* [2016] (latter

two are computed through scaling the bare frame sway profile), it was also confirmed how methods such as the proposed procedure are sensitive to the changing inelastic global mechanism of the structure for a given typology.

## 5.2 Future Work

The subject of this thesis has been outlining a practical and an efficient simplified non-linear static analysis framework that is capable of capturing fundamental characteristics of infilled RC frame behaviour. It is worth noting that to accomplish the objective, throughout this work, several simplifications and assumptions have been made with the aim of isolating and considering a limited, yet crucial, portion of the overall problem. Evidently, the true infilled frame behaviour is more complicated than the one obtained using the features addressed in this work, which would require the consideration of several other cardinal characteristics to become accurate. These points were highlighted throughout the thesis by referring to them as the future topics of research. As such, this section provides a brief list of further aspects to consider for the future and a few compelling ideas that might be developed as a result of this research.

### 5.2.1 Column and Beam-Column Joint Shear Failure

It is widely known that once an infill element is pushed beyond the peak stiffness (negative stiffness portion), the lateral resistance of the system is solely provided by the boundary frame members. This hints that up to the peak point, all the energy stored by the infill member is transferred to the frame members through the contact surfaces between the infill panels and the surrounding frame, where the forces are carried with a flexural behaviour. This transfer of forces is only possible when there is adequate shear resistance available in the beam-column elements. Otherwise, these frame elements are expected to undergo a brittle shear failure before exhibiting a flexural deformation mode. The likelihood of having a shear type of failure should be checked in parallel with the flexural response of the system. This can be done by using empirical formulas (Priestley 1994) or considering a shear backbone for the frame elements, as outlined in O'Reilly [2016], for example.

Furthermore, joint failure has been shown by several researchers (Pampanin, 2002) to alter the displaced shape of the structure significantly. As previously discussed in Chapter 2 and shown in Calvi et al. [2002b], a joint failure can be distinguished as the localisation of the inelastic displacements at the joints of two consecutive storeys. Bearing these in mind, there is a need for developing a method to first identify a likely joint failure and include its effects into the computed displaced shape.

### 5.2.2 Out-of-Plane and In-Plane Infill Interaction and Infills with Openings

Throughout this thesis, only the in-plane behaviour of the infill wall was considered. This was done by using a strut constitutive law that only takes the in-plane forces and deformations associated with the modelled infill panel into account. However, in reality, since ground motion shaking is expected to excite the structure along two perpendicular axes, the in-plane behaviour of the panel is modified due to the out-of-plane deformations. Consequently, the in-plane force-deformation capacity should be less than that of the wall excited in the pure in-plane direction. This phenomenon can be considered by using strut constitutive laws that account for the interaction between the out-of-plane and in-plane deformations. (Di Trapani et al. 2018).

Likewise, it is common to encounter infill panels with door or window openings, instead of a homogenously laid masonry wall. The force-displacement capacity of such walls with openings is expected to be lower than the fully infilled case mainly due to the complex force transfer paths through the wall introduced with the openings. Previous studies such as Dolsek and Fajfar [2008] reduce the anticipated capacity of the infill panel as a function of the size of the openings.

### **5.2.3 Towards a Probabilistic Displacement-Based Approach**

In a performance-based earthquake engineering framework, accounting for the uncertainties of the problem is a crucial step. Record-to-record and modelling variabilities are two of the major sources of uncertainties considered and attract considerable attention in the engineering community. Hence, a possible extension of the simplified analysis method proposed in this work in order to include these kinds of sources of uncertainty would enhance the strength of this method in terms of assessment purposes and provide a link between static analysis-based modern loss assessment approaches. In this context, two possible topics are suggested for further investigation.

#### **5.2.3.1 Displaced Shape Conditioned on the Infill Wall Yield Drift**

The shear-drift backbone of an infill panel is given by the assumed constitutive model which is calibrated with experimental data obtained through tests. Often, these models are developed in a deterministic way, providing the mean value of the modelling parameters. However, it is possible to find studies in the literature that also provide the observed or expected variation in the model parameters including Sassun *et al.* [2016] and Turgay *et al.* [2014]. The uncertainty in the strut constitutive model parameters such as the yield or the ultimate drift can be introduced in the proposed simplified analysis methodology. This can be done by providing a range of pushover curves and displaced shapes corresponding to the mean and one standard deviation away response. The mean response would be computed using the mean yield drift parameters, which are given with the current procedure describe in this thesis. Then, the procedure would be repeated twice to compute the response with the wall drift values corresponding to one sigma away from the mean. At the end, an envelope of drift profiles would be obtained for a given base shear value. Note that the global mechanism of the structure may change for different assumptions of wall yield drift hence, the effect and the applicability of this approach should be investigated. The results obtained through the simplified procedure should match the sway profiles corresponding to the mean and the standard deviation that are obtained through a set of pushover analyses done with various wall drift assumptions. In this context, the wall drift angle of each infill panel could be considered as a random variable and sampled through Monte Carlo or Latin Hypercube sampling methods before setting up the numerical model.

#### **5.2.3.2 Displaced Shape Considering Record-to-Record Variability**

The simplified analysis of an infilled RC structure can be done considering the hazard associated with its location. This can be done by using the mean response spectra of the selected records for the specified hazard to scale the displacement vector at each step as in the case of a DAP analysis (Antoniou and Pinho, 2004). The same procedure can be repeated to compute the response associated with the plus-minus one sigma response spectra. The main advantage of

this approach would be considering the increase in the period of the infilled structure during the analysis. This way, a range of possible displaced shapes can be obtained compatible with the hazard of the location.

#### ***5.2.4 Displacement-Based Design of Infilled Frames***

Designing for limiting the expected displacements in the structure is considered as an approach to control the performance of the structure for a given design excitation. This is generally done with a force-based approach with several iterations, designing and then assessing the structure for the displacements, refining the design when needed, to obtain the desired behaviour. Direct displacement-based design methodology provides a direct design process for a target displacement value. The core step of this procedure is assuming a displacement profile for the structure (which is a function of the target inter-storey drift) and designing the structural elements in order to provide the structural stiffness that yields the assumed displaced shape. In case of an infilled structure, the stiffness of the structure can be disaggregated by using the proposed methodology in Section 3.2.3. However, there is a need for a study that defines the application of this process and tests the performance of the structures which are designed with the proposed approach.

## 6 REFERENCES

- Antoniou, S., and Pinho, R., [2004] “Development and verification of a displacement-based adaptive pushover procedure”. *Journal of Earthquake Engineering*, 8:5, 643-661, DOI: 10.1080/13632460409350504
- Applied Technology Council (ATC-40) [1996] “Seismic evaluation and retrofit of concrete buildings, volume 1”, California, USA
- Asteris, P.G., Cotsovos, D.M., Chrysostomou, C.Z., Mohebkhah, A., and Al-Chaar, G.K. [2013] “Mathematical micromodeling of infilled frames: state of the art”, *Engineering Structures*, Vol. 56, pp. 1905-1921.
- Baker, J.W., and Cornell, C.A., [2006] “Which spectral acceleration are you using?”. *Earthquake Spectra*: May 2006, Vol. 22, No. 2, pp. 293-312. <https://doi.org/10.1193/1.2191540>
- Baker, J.W., [2011] “Conditional mean spectrum: tool for ground motion selection.” *Journal of Structural Engineering* 2011;137(3):322–31. [http://dx.doi.org/10.1061/\(ASCE\)ST.1943-541X.0000215](http://dx.doi.org/10.1061/(ASCE)ST.1943-541X.0000215).
- Bentz, E., and Collins, M.P. [2001] “Response-2000 User Manual” University of Toronto, Toronto, Ontario, Canada
- Bertoldi, S.H., Decanini, L.D., and Gavarini, C. [1993] “Telaitamponatisoggetti ad azioni sismiche, un modellosemplificato: confronto sperimentale e numerico.” *Atti del 6º Convegno Nazionale L'ingegneria sismica in Italia*, 815-24
- Calvi, G. M., Magenes, G. and Pampanin, S. [2002a] “Relevance of beam-column joint damage and collapse in RC frame assessment,” *Journal of Earthquake Engineering*, 6(Supp 1), 75–100.
- Calvi, G. M., Magenes, G. and Pampanin, S. [2002b] “Experimental test on a three storey RC frame designed for gravity only,” *12th European Conference on Earthquake Engineering*, London, UK.
- Calvi, G.M., Bolognini, D., and Penna, A. [2004] “Seismic performance of masonry-infilled RC frames: benefits of slight reinforcement”, *6º Congresso Nacional de Sismologia e Engenharia Sismica*, pp. 253-276.
- Cardone, D., and Flora, A. [2017] “Multiple inelastic mechanism analysis (MIMA): a simplified method for the estimation of the seismic response of RC frame buildings”, *Engineering Structures*, Vol. 145, pp. 368-380.

- Chopra, A.K., McKenna, F. [2015] “Modelling viscous damping in nonlinear response history analysis of buildings for earthquake excitation”. *Earthquake Engineering & Structural Dynamics*, doi: 10.1002/eqe.2622.
- Cornell, C.A., and Krawinkler, H. [2000] “Progress and challenges in seismic performance assessment”, *PEER Center News*, Vol. 3, No. 2, pp. 1-2.
- Crisafulli, F.J. [1997] “Seismic behaviour of reinforced concrete structures with masonry infills”, *PhD Thesis*, University of Canterbury, Christchurch, New Zealand.
- Crisafulli, F.J., Carr, A.J., and Park, R. [2000] “Analytical modelling of infilled frame structures – a general review”, *Bulletin of the New Zealand Society for Earthquake Engineering*, Vol. 33, No. 1, pp. 30-47.
- Decanini, L., Mollaioli, F., Mura, A., and Saragoni, R. [2004] “Seismic performance of masonry infilled R/C frames”, *Proceedings of 13<sup>th</sup> World Conference on Earthquake Engineering*, Vancouver, Canada.
- Di Ludovico, M., Verderame, G. M., Prota, A., Manfredi, G. and Cosenza, E. [2014] “Cyclic behavior of nonconforming full-scale RC columns,” *Journal of Structural Engineering* 140(5).
- Di Trapani, F., Shing, P.B., and Cavaleri, L. [2018] “Macroelement model for in-plane and out-of-plane responses of masonry infills in frame structures”, *Journal of Structural Engineering*, Vol. 144, No. 2, pp. 1-13.
- Dolšek, M., and Fajfar, P. [2008]. “The effect of masonry infills on the seismic response of a four-storey reinforced concrete frame — a deterministic assessment”. *Engineering Structures*, 30(7), 1991–2001. doi:10.1016/j.engstruct.2008.01.001
- EN 1998-1 [2004] (English): “Eurocode 8: Design of structures for earthquake resistance – Part 1: General rules, seismic actions and rules for buildings”
- Fajfar, P. [2000]. “A nonlinear analysis method for performance based seismic design”. *Earthquake Spectra*, Vol. 16, No. 3, pp. 573-592, August.
- Federal Emergency Management Agency (FEMA 273) [1997] “NEHRP guidelines for the seismic rehabilitation of buildings”, Building Seismic Safety Council, Washington, D.C., USA.
- Federal Emergency Management Agency (FEMA 356) [2000] “Prestandard and commentary for the seismic rehabilitation of buildings”, American Society of Civil Engineers, Reston, Virginia, USA.
- Federal Emergency Management Agency (FEMA P-58-1) [2012] “Seismic performance assessment of buildings”, Applied Technology Council, California, USA.
- Fenerci, A., Binici, B., Pourang, E., Canbay, E., and Özcebe, G. [2016] “The effect of infill walls on the seismic behaviour of boundary columns in RC frames”, *Earthquake and Structures*, Vol. 10, No. 3, pp. 539-562.
- Freeman, S.A. [1978] “Prediction of response of concrete buildings to severe earthquake motion”, *American Concrete Institute*, Vol. 55, pp. 589-606.
- Galli, M. [2006] Evaluation of the Seismic Response of Existing RC Frame Buildings with Masonry Infills. *MSc Thesis*, IUSS Pavia

- Gentile, R., Del Vecchio, C., Pampanin, S., Raffaele, D., and Uva, G. [2019a] “Refinement and validation of the simple lateral mechanism analysis (SLaMA) procedure for RC frames”, *Journal of Earthquake Engineering*.
- Gentile, R., Pampanin, S., Raffaele, D., and Uva, G. [2019b] “Non-linear analysis of RC masonry-infilled frames using the SLaMA method: part 1 – mechanical interpretation of the infill/frame interaction and formulation of the procedure, *Bulletin of Earthquake Engineering*, pp. 1-22.
- Gülkan, P., and Sözen, M.A. [1977] “Inelastic responses of reinforced concrete structures to earthquake motions, *American Concrete Institute*, Vol. 53, pp. 109-116.
- Günay, S., and Mosalam, K.M. [2013] “PEER Performance – Based Earthquake Engineering Methodology, Revisited”, *Journal of Earthquake Engineering*, Vol. 14, No. 6, pp. 829-858.
- Hak, S., Morandi, P., Magenes, G., and Sullivan, T.J. [2012] “Damage control for clay masonry infills in the design of RC frame structures”, *Journal of Earthquake Engineering*, Vol. 16, sup. 1, pp. 1-35.
- Haselton, C. B., Liel, A. B., Taylor Lange, S. and Deierlein, G. G. [2008] “Beam-column element model calibrated for predicting flexural response leading to global collapse of RC frame buildings,” *PEER Report 2007/03*, Berkeley, California.
- Kwan, K.H., Lo, C.Q., and Liauw, T.C., [1990] “Large-scale model tests and plastic analysis of multibay infilled frames”, *Proceedings of the Institution of Civil Engineers*, Part 2, Vol. 89, pp. 261-277.
- Landi, L., Benedetti, A. [2013] "Reinforced Concrete Buildings" Chapter 3 in Developments in the Field of Displacement-Based Assessment, Edited by T.J. Sullivan and G.M. Calvi, *IUSS Press*, Pavia.
- Landi, L., Tardini, A., and Diotallevi, P.P. [2016] “A procedure for the displacement-based seismic assessment of infilled RC frames”, *Journal of Earthquake Engineering*, Vol. 20, No. 7, pp. 1077-1103.
- McKenna, F., Scott, M. H. and Fenves, G. L. [2010] “Nonlinear finite-element analysis software architecture using object composition,” *Journal of Computing in Civil Engineering* 24(1), 95–107. doi: 10.1061/(asce)cp.1943-5487.0000002.
- Melo, J., Varum, H. and Rossetto, T. [2015] “Experimental cyclic behaviour of RC columns with plain bars and proposal for Eurocode 8 formula improvement,” *Engineering Structures* 88, 22–36.
- Moehle, J.P. [1992] “Displacement-based design of RC structures subjected to earthquakes”, *Earthquake Spectra*, Vol. 8, No. 3, pp. 403-428.
- Monteiro, R., Marques, M., Adhikari, G., Casarotti, C., and Pinho, R. [2014] “Spectral reduction factors evaluation for seismic assessment of frame buildings”, *Engineering Structures*, Vol. 77, No. 15, pp. 129-142.
- Montejo, L.A., and Kowalsky, M.J. [2007] “CUMBIA: Set of codes for the analysis of reinforced concrete members”, North Carolina State University, Raleigh, North Carolina, U.S.A.
- NZSEE [2017], “The Seismic Assessment of Existing Buildings – Part C: Moment Resisting Frames with Infill Panels”, New Zealand
- O'Reilly, G.J. [2016] “Performance-based seismic assessment and retrofit of existing RC frame buildings in Italy”, *PhD Thesis*, Scuola Universitaria Superiore IUSS Pavia, Italy.

- O'Reilly, G.J., and Sullivan T.J. [2017] "Modelling techniques for the seismic assessment of the existing Italian RC frame structures", *Journal of Earthquake Engineering*.
- O'Reilly, G.J., Kohrangi, M., Bazzurro P., Monteiro R., [2018] "Intensity measures for the collapse assessment of infilled frames", *16<sup>th</sup> European Conference on Earthquake Engineering*, Thessaloniki, Greece.
- Pampanin, S., Calvi, G. M. and Moratti, M. [2002] "Seismic behaviour of RC beam-column joints designed for gravity loads," *12th European Conference on Earthquake Engineering*, London, UK.
- Panagiotakos, T.B., and Fardis, M.N. [1996] "Seismic response of infilled RC frame structures", *Proceedings of 11<sup>th</sup> World Conference on Earthquake Engineering*, Acapulco, Mexico.
- Paulay, T. and Priestley, M.J.N. [1992] "Seismic design of reinforced concrete and masonry buildings." *John Wiley and Sons*, New York, U.S.A.
- Pettinga, J.D., and Priestley, M.J.N. [2005] "Dynamic behaviour of reinforced concrete frames designed with direct displacement-based design", *Journal of Earthquake Engineering*, Vol. 9, No. 2, pp. 309-330.
- Priestley, M.J.N., and Calvi, G.M. [1991] "Towards a capacity-design assessment procedure for reinforced concrete frames", *Earthquake Spectra*, Vol.7, No.3, pp. 413-437.
- Priestley, M.J.N., Verma, R., and Xiao, Y. [1994] "Seismic shear strength of reinforced concrete columns", *Journal of Structural Engineering*, Vol. 120, No. 8, pp. 2310-2329.
- Priestley, M.J.N. [1997] "Displacement-based seismic assessment of reinforced concrete buildings", *Journal of Earthquake Engineering*, Vol. 1, No. 1, pp. 157-192.
- Priestley, M.J.N. [2003] *Myths and fallacies in earthquake engineering (revisited)*, the ninth Mallet Milne Lecture, European School for Advanced Studies in Reduction of Seismic Risk (ROSE School), University of Pavia, Italy.
- Priestley, M.J.N., Calvi, G.M. and Kowalsky, M.J. [2007] "Displacement-based seismic design of structures." IUSS Pavia, *IUSS Press*, Pavia, Italy.
- Regio Decreto. [1939] "Norme per l'esecuzione Delle Opere Conglomerato Cementizio Semplice Od Armato - 2229/39", Rome, Italy.
- Saborio-Romano, D. [2016] "Performance based and simplified displacement-based assessment of an infilled RC frame building in L'Aquila, Italy", *MSc Thesis*, Scuola Universitaria Superiore IUSS, Pavia, Italy.
- Sassun, K., Sullivan, T.J., Morandi, P., and Cardone, D. [2016] "Characterising the in-plane seismic performance of infill masonry", *Bulletin of the New Zealand Society for Earthquake Engineering*, Vol. 49, No. 1, pp. 100-117.
- SEAOC [1995]. "Vision 2000 – A Framework for Performance Based Design, Volumes I, II, II; Structural Engineers Association of California, Vision 2000 Committee, Sacramento, California.
- Seismosoft [2018] "SeismoStruct 2018 – A computer program for static and dynamic nonlinear analysis of framed structures," available from <http://www.seismosoft.com>.
- Shibata, A., and Sözen, M.A. [1987] "The substitute-structure method for earthquake-resistant design of reinforced concrete frames", University of Illinois, Urbana, Illinois, USA.

- SCEDC [2013], “Significant Earthquakes and Faults – Oak Ridge Fault”. Retrieved from: <http://scedc.caltech.edu/significant/oakridge.html>
- Stafford-Smith, B. [1966] “Behaviour of square infilled frames,” *Journal of the Structural Division ASCE*, 92(1), 381–404.
- Sullivan, T.J., and Calvi, G.M. [2011] “Considerations for the seismic assessment of buildings using the direct displacement-based assessment approach”, *Proceedings of 14<sup>th</sup> Associazione Nazionale Italiana di Ingegneria Sismica*, Bari, Italy.
- Sullivan, T.J., Priestley, M.J.N., Calvi, M.G. [2012] “DDBD12: A model code for the displacement-based seismic design of structures”, *IUSS Press*, Italy
- Sullivan, T.J., Saborio-Romano, D., O'Reilly, G.J., Welch, D.P., and Landi, L. [2018] “Simplified pushover analysis of moment resisting frame structures”, *Journal of Earthquake Engineering*. DOI: 10.1080/13632469.2018.1528911
- Turgay, T., Durmuş, M.C., Binici, B., and Özcebe, G., [2014]. “Evaluation of the predictive models for stiffness, strength, and deformation capacity of RC frames with masonry infill walls”, *Journal of Structural Engineering*, ASCE. DOI: 10.1061/(ASCE)ST.1943-541X.0001069
- USGS [2013] “Response to an Urban Earthquake – Northridge '94”. Retrieved from: <https://pubs.usgs.gov/of/1996/ofr-96-0263/introduc.htm#impacts>
- Vamvatsikos, D., and Cornell, C.A. [2002] “Incremental dynamic analysis”, *Journal of Earthquake Engineering and Structural Dynamics*, Vol. 31, No. 3, pp. 491-514.
- Vayas, I., Vamvatsikos, D. and Thanopoulos, P., [2017]. “Innovative Systems for Seismic Resistance. The INNOSEIS Project”, *EUROSTEEL 2017*, Copenhagen, Denmark.
- Welch, D.P., Sullivan, T.J., and Calvi, G.M. [2012] “Towards a direct displacement-based loss assessment methodology for RC frame buildings”, *Proceedings of 15<sup>th</sup> World Conference on Earthquake Engineering*, Lisbon, Portugal.
- Zimos, D. K., Mergos, P. E. and Kappos, A. J. [2015] “Shear hysteresis model for reinforced concrete elements including the post-peak range,” *COMPDYN 2015-5th ECCOMAS Thematic Conference on Computational Methods in Structural Dynamics and Earthquake Engineering*, Crete Island, Greece

*This page is intentionally left blank...*

## A. APPENDIX A

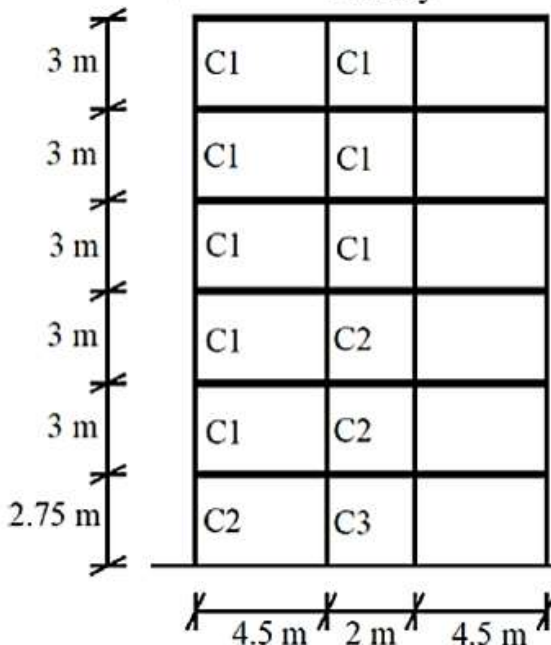
The tables related with the steps of the simplified pushover analysis in Chapter 4 are provided in this appendix. This appendix is divided into subtitles that are concurrent to the headings under Chapter 3.2. Therefore, the corresponding tables that are referred in Chapter 3.2 can be found here, implemented for the 6-storey case study frame under the same titled sub-section.

### A.1. Modelling and the Simplified Analysis of the Case Study Structure: Galli-6-Storey-Medium-Single

#### A.1.1. Geometry & Material Definitions

The column sections layout in each structures is symmetric

6 Storey



Sullivan et al., 2018

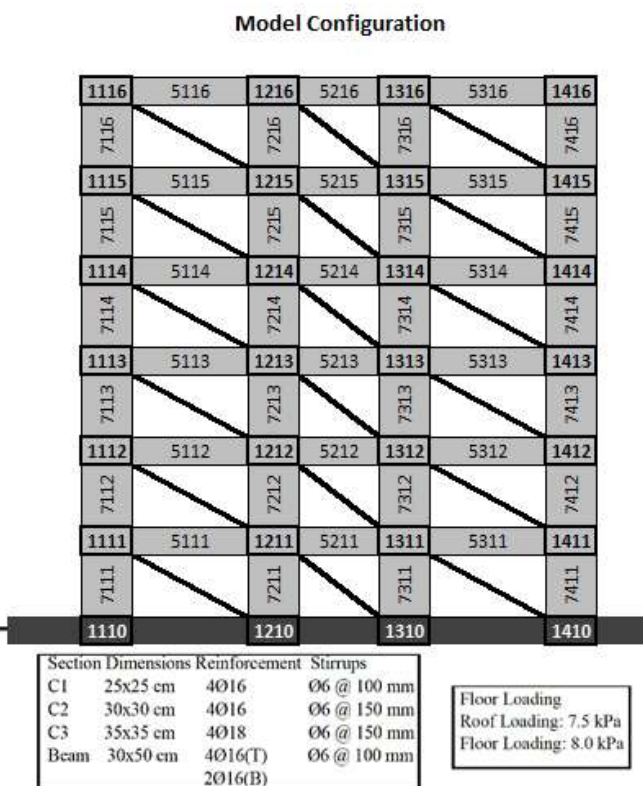


Figure A.1. Section Distribution of Galli\_6st\_WeakSingle vs Assigned Member and Component Numbering

Geometrical properties of the frame are given in Table A.1 together with the lumped masses.

**Table A.1. Distribution of Masses on Galli\_6st\_MediumSingle**

Geometry and Masses									
No. of Storey	Elevation (m)	Storey Height (m)	Distribution of Masses (tonnes)					No. of Bay	Length (m)
			Bay 1	Bay 2	Bay 3	Bay 4	Storey		
6	17.75	3.00	6.31	12.62	12.62	6.31	37.84	3	4.5
5	14.75	3.00	6.73	13.46	13.46	6.73	40.37	2	2
4	11.75	3.00	6.73	13.46	13.46	6.73	40.37	1	4.5
3	8.75	3.00	6.73	13.46	13.46	6.73	40.37		
2	5.75	3.00	6.73	13.46	13.46	6.73	40.37		
1	2.75	2.75	6.73	13.46	13.46	6.73	40.37		
Base	0.00	0.00	0.00	0.00	0.00	0.00	0.00		

The required input parameters (infill mechanical properties), considering the Bertoldi *et al.* [1993] strut model, are given in Table A.2.

**Table A.2. Mechanical Properties of the Weak/Medium/Strong Infill Typologies (Hak *et al.* 2012)**

Weak Infill Typology				
Ewh [MPa]	991.00	fws [MPa]	0.55	tw [mm] 80
Ewv [MPa]	1873.00	fwu [MPa]	0.44	σv 0.00
Gw [MPa]	1089.00	fwv [MPa]	2.02	v 0.20
Ec [MPa]	21696.00	fhw [MPa]	1.80	W [kN/m^3] 6.87
Medium Infill Typology				
Ewh [MPa]	991.00	fws [MPa]	0.31	tw [mm] 240
Ewv [MPa]	1873.00	fwu [MPa]	0.25	σv 0.00
Gw [MPa]	1089.00	fwv [MPa]	1.50	v 0.20
Ec [MPa]	21696.00	fhw [MPa]	1.11	W [kN/m^3] 6.87
Strong Infill Typology				
Ewh [MPa]	1050.00	fws [MPa]	0.36	tw [mm] 300
Ewv [MPa]	3240.00	fwu [MPa]	0.30	σv 0.00
Gw [MPa]	1296.00	fwv [MPa]	3.51	v 0.20
Ec [MPa]	21696.00	fhw [MPa]	1.50	W [kN/m^3] 7.36

## Appendix A

---

Frame section detailing properties are given in Table A.3.

**Table A.3. Frame Section Properties of Galli\_6st\_MediumSingle**

Beam									
Dimensions (mm)		Long. Reinforcement			Trans. Reinforcement			Concrete Rebar	
Height	500	Pos.	Qty.	Dia. (mm)	Area	Pos.	Dia. (mm)	Spacing (mm)	F <sub>c</sub> (Mpa) F <sub>y</sub> (Mpa)
Width	350	Top	4	16	804.25	Along H.	6	100	19.6 372
Cover	20	Bottom	2	16	402.12				$\varepsilon_{co}$ 0.0018 $\varepsilon_y$ 0.0019
									$\varepsilon_{cu}$ 0.0038 $\varepsilon_u$
Column 1									
Dimensions (mm)		Long. Reinforcement			Trans. Reinforcement			Concrete Rebar	
Height	250	Pos.	Qty.	Dia. (mm)	Area	Pos.	Dia. (mm)	Spacing (mm)	F <sub>c</sub> (Mpa) F <sub>y</sub> (Mpa)
Width	250	Section	4	16	804.25	Along H.	6	100	19.6 372
Cover	20				0.00				$\varepsilon_{co}$ 0.0018 $\varepsilon_y$ 0.0019
									$\varepsilon_{cu}$ 0.0038 $\varepsilon_u$
Column 2									
Dimensions (mm)		Long. Reinforcement			Trans. Reinforcement			Concrete Rebar	
Height	300	Pos.	Qty.	Dia. (mm)	Area	Pos.	Dia. (mm)	Spacing (mm)	F <sub>c</sub> (Mpa) F <sub>y</sub> (Mpa)
Width	300	Section	4	16	804.25	Along H.	6	150	19.6 372
Cover	20				0.00				$\varepsilon_{co}$ 0.0018 $\varepsilon_y$ 0.0019
									$\varepsilon_{cu}$ 0.0038 $\varepsilon_u$
Column 3									
Dimensions (mm)		Long. Reinforcement			Trans. Reinforcement			Concrete Rebar	
Height	500	Pos.	Qty.	Dia. (mm)	Area	Pos.	Dia. (mm)	Spacing (mm)	F <sub>c</sub> (Mpa) F <sub>y</sub> (Mpa)
Width	350	Section	4	18	1017.88	Along H.	6	150	19.6 372
Cover	20				0.00				$\varepsilon_{co}$ 0.0018 $\varepsilon_y$ 0.0019
									$\varepsilon_{cu}$ 0.0038 $\varepsilon_u$

### A.1.2. Flexural Frame System Capacity

After conducting moment curvature analysis for all the frame sections in the structure, in Figure A.2., member capacities were computed through joint equilibrium. Figure A.2. shows the joint equilibrium done for the yield moment and rotation. This step is repeated for other limit states such as ultimate moment-rotation or residual moment-rotation.

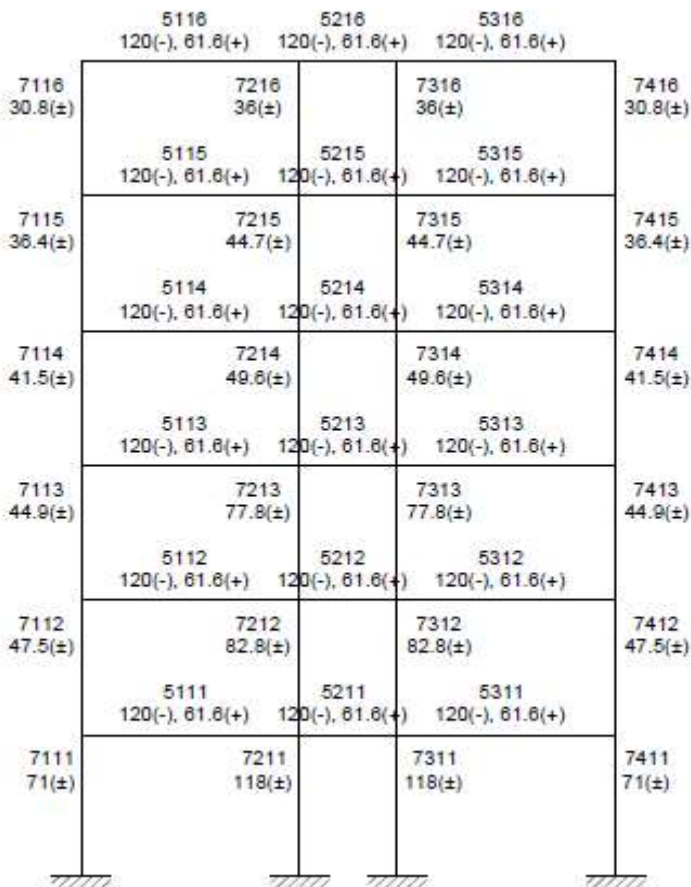


**Figure A.2. Element flexural strengths (kNm) (at joint centrelines)**

Appendix A

Moment-curvature analysis results done for each beam section are shown in Table A.4.-A.5.

**Table A.4. Beam section moment-curvature results done in OpenSees**

Beam Moment Capacities (O'Reilly & Sullivan, 2017)										
Bay	ID	Section	My+ (kNm)	My- (kNm)	Mc+ (kNm)	Mc- (kNm)	Mu+ (kNm)	Mu- (kNm)	Muu+ (kNm)	Muu- (kNm)
1	5111	Beam	61.6	120.0	66.3	129.2	53.1	103.4	6.6	12.9
	5112	Beam	61.6	120.0	66.3	129.2	53.1	103.4	6.6	12.9
	5113	Beam	61.6	120.0	66.3	129.2	53.1	103.4	6.6	12.9
	5114	Beam	61.6	120.0	66.3	129.2	53.1	103.4	6.6	12.9
	5115	Beam	61.6	120.0	66.3	129.2	53.1	103.4	6.6	12.9
	5116	Beam	61.6	120.0	66.3	129.2	53.1	103.4	6.6	12.9
2	5211	Beam	61.6	120.0	66.3	129.2	53.1	103.4	6.6	12.9
	5212	Beam	61.6	120.0	66.3	129.2	53.1	103.4	6.6	12.9
	5213	Beam	61.6	120.0	66.3	129.2	53.1	103.4	6.6	12.9
	5214	Beam	61.6	120.0	66.3	129.2	53.1	103.4	6.6	12.9
	5215	Beam	61.6	120.0	66.3	129.2	53.1	103.4	6.6	12.9
	5216	Beam	61.6	120.0	66.3	129.2	53.1	103.4	6.6	12.9
3	5311	Beam	61.6	120.0	66.3	129.2	53.1	103.4	6.6	12.9
	5312	Beam	61.6	120.0	66.3	129.2	53.1	103.4	6.6	12.9
	5313	Beam	61.6	120.0	66.3	129.2	53.1	103.4	6.6	12.9
	5314	Beam	61.6	120.0	66.3	129.2	53.1	103.4	6.6	12.9
	5315	Beam	61.6	120.0	66.3	129.2	53.1	103.4	6.6	12.9
	5316	Beam	61.6	120.0	66.3	129.2	53.1	103.4	6.6	12.9

**Table A.5. Beam section moment-curvature results done in OpenSees (cont.)**

Beam Deformation Capacities (O'Reilly & Sullivan, 2017)													
Bay	ID	Section	$\phi y^+$ (1/m)	$\phi y^-$ (1/m)	$\phi c^+$ (1/m)	$\phi c^-$ (1/m)	$\phi u^+$ (1/m)	$\phi u^-$ (1/m)	$\phi uu^+$ (1/m)	$\phi uu^-$ (1/m)	v (axial load ratio)	$\mu \phi c$	$\mu \phi u$
1	5111	Beam	0.008	0.008	0.045	0.045	0.140	0.140	0.472	0.472	0.0000	5.8077	17.9744
	5112	Beam	0.008	0.008	0.045	0.045	0.140	0.140	0.472	0.472	0.0000	5.8077	17.9744
	5113	Beam	0.008	0.008	0.045	0.045	0.140	0.140	0.472	0.472	0.0000	5.8077	17.9744
	5114	Beam	0.008	0.008	0.045	0.045	0.140	0.140	0.472	0.472	0.0000	5.8077	17.9744
	5115	Beam	0.008	0.008	0.045	0.045	0.140	0.140	0.472	0.472	0.0000	5.8077	17.9744
	5116	Beam	0.008	0.008	0.045	0.045	0.140	0.140	0.472	0.472	0.0000	5.8077	17.9744
2	5211	Beam	0.008	0.008	0.045	0.045	0.140	0.140	0.472	0.472	0.0000	5.8077	17.9744
	5212	Beam	0.008	0.008	0.045	0.045	0.140	0.140	0.472	0.472	0.0000	5.8077	17.9744
	5213	Beam	0.008	0.008	0.045	0.045	0.140	0.140	0.472	0.472	0.0000	5.8077	17.9744
	5214	Beam	0.008	0.008	0.045	0.045	0.140	0.140	0.472	0.472	0.0000	5.8077	17.9744
	5215	Beam	0.008	0.008	0.045	0.045	0.140	0.140	0.472	0.472	0.0000	5.8077	17.9744
	5216	Beam	0.008	0.008	0.045	0.045	0.140	0.140	0.472	0.472	0.0000	5.8077	17.9744
3	5311	Beam	0.008	0.008	0.045	0.045	0.140	0.140	0.472	0.472	0.0000	5.8077	17.9744
	5312	Beam	0.008	0.008	0.045	0.045	0.140	0.140	0.472	0.472	0.0000	5.8077	17.9744
	5313	Beam	0.008	0.008	0.045	0.045	0.140	0.140	0.472	0.472	0.0000	5.8077	17.9744
	5314	Beam	0.008	0.008	0.045	0.045	0.140	0.140	0.472	0.472	0.0000	5.8077	17.9744
	5315	Beam	0.008	0.008	0.045	0.045	0.140	0.140	0.472	0.472	0.0000	5.8077	17.9744
	5316	Beam	0.008	0.008	0.045	0.045	0.140	0.140	0.472	0.472	0.0000	5.8077	17.9744

Moment-curvature analysis results done for each column section are shown in Table A.6.-A.7.

**Table A.6. Column section moment-curvature results done in OpenSees**

Column Moment Capacities (O'Reilly & Sullivan, 2017)									
Set	ID	Section	My+ (kNm)	My- (kNm)	Mc+ (kNm)	Mc- (kNm)	Mu+ (kNm)	Mu- (kNm)	Muu+ (kNm)
1	7111	Column 2	71.3	71.3	76.8	76.8	61.4	61.4	7.7
	7112	Column 1	47.5	47.5	51.1	51.1	40.9	40.9	5.1
	7113	Column 1	44.9	44.9	48.4	48.4	38.7	38.7	4.8
	7114	Column 1	41.5	41.5	44.7	44.7	35.8	35.8	4.5
	7115	Column 1	36.4	36.4	39.2	39.2	31.3	31.3	3.9
	7116	Column 1	30.8	30.8	33.1	33.1	26.5	26.5	3.3
2	7211	Column 3	118.8	118.8	128.0	128.0	102.4	102.4	12.8
	7212	Column 2	82.8	82.8	89.2	89.2	71.4	71.4	8.9
	7213	Column 2	77.8	77.8	83.8	83.8	67.0	67.0	8.4
	7214	Column 1	49.6	49.6	53.4	53.4	42.7	42.7	5.3
	7215	Column 1	44.7	44.7	48.1	48.1	38.5	38.5	4.8
	7216	Column 1	36.0	36.0	38.8	38.8	31.0	31.0	3.9
3	7311	Column 3	118.8	118.8	128.0	128.0	102.4	102.4	12.8
	7312	Column 2	82.8	82.8	89.2	89.2	71.4	71.4	8.9
	7313	Column 2	77.8	77.8	83.8	83.8	67.0	67.0	8.4
	7314	Column 1	49.6	49.6	53.4	53.4	42.7	42.7	5.3
	7315	Column 1	44.7	44.7	48.1	48.1	38.5	38.5	4.8
	7316	Column 1	36.0	36.0	38.8	38.8	31.0	31.0	3.9
4	7411	Column 2	71.3	71.3	76.8	76.8	61.4	61.4	7.7
	7412	Column 1	47.5	47.5	51.1	51.1	40.9	40.9	5.1
	7413	Column 1	44.9	44.9	48.4	48.4	38.7	38.7	4.8
	7414	Column 1	41.5	41.5	44.7	44.7	35.8	35.8	4.5
	7415	Column 1	36.4	36.4	39.2	39.2	31.3	31.3	3.9
	7416	Column 1	30.8	30.8	33.1	33.1	26.5	26.5	3.3

**Table A.7. Column section moment-curvature results done in OpenSees (cont.)**

Column Deformation Capacities (O'Reilly & Sullivan, 2017)													
Set	ID	Section	$\phi y^+$ (1/m)	$\phi y^-$ (1/m)	$\phi c^+$ (1/m)	$\phi c^-$ (1/m)	$\phi u^+$ (1/m)	$\phi u^-$ (1/m)	$\phi uu^+$ (1/m)	$\phi uu^-$ (1/m)	v (axial load ratio)	$\mu \phi c$	$\mu \phi u$
1	7111	Column 2	0.013	0.013	0.079	0.079	0.158	0.158	0.437	0.437	0.2220	6.0538	12.1692
	7112	Column 1	0.016	0.016	0.088	0.088	0.169	0.169	0.453	0.453	0.2660	5.6242	10.7834
	7113	Column 1	0.016	0.016	0.098	0.098	0.197	0.197	0.546	0.546	0.2120	6.2293	12.5669
	7114	Column 1	0.016	0.016	0.108	0.108	0.237	0.237	0.689	0.689	0.1580	6.8981	15.1083
	7115	Column 1	0.016	0.016	0.094	0.094	0.277	0.277	0.918	0.918	0.1040	5.9809	17.6561
	7116	Column 1	0.016	0.016	0.091	0.091	0.280	0.280	0.944	0.944	0.0510	5.7771	17.8599
2	7211	Column 3	0.011	0.011	0.073	0.073	0.121	0.121	0.288	0.288	0.3260	6.5179	10.7946
	7212	Column 2	0.013	0.013	0.091	0.091	0.141	0.141	0.315	0.315	0.3690	7.0231	10.8462
	7213	Column 2	0.013	0.013	0.080	0.080	0.141	0.141	0.356	0.356	0.2950	6.1231	10.8462
	7214	Column 1	0.016	0.016	0.100	0.100	0.169	0.169	0.411	0.411	0.3170	6.3885	10.7834
	7215	Column 1	0.016	0.016	0.099	0.099	0.200	0.200	0.553	0.553	0.2090	6.2994	12.7261
	7216	Column 1	0.016	0.016	0.092	0.092	0.280	0.280	0.938	0.938	0.1010	5.8280	17.8153
3	7311	Column 3	0.011	0.011	0.073	0.073	0.121	0.121	0.288	0.288	0.3260	6.5179	10.7946
	7312	Column 2	0.013	0.013	0.091	0.091	0.141	0.141	0.315	0.315	0.3690	7.0231	10.8462
	7313	Column 2	0.013	0.013	0.080	0.080	0.141	0.141	0.356	0.356	0.2950	6.1231	10.8462
	7314	Column 1	0.016	0.016	0.100	0.100	0.169	0.169	0.411	0.411	0.3170	6.3885	10.7834
	7315	Column 1	0.016	0.016	0.099	0.099	0.200	0.200	0.553	0.553	0.2090	6.2994	12.7261
	7316	Column 1	0.016	0.016	0.092	0.092	0.280	0.280	0.938	0.938	0.1010	5.8280	17.8153
4	7411	Column 2	0.013	0.013	0.079	0.079	0.158	0.158	0.437	0.437	0.2220	6.0538	12.1692
	7412	Column 1	0.016	0.016	0.088	0.088	0.169	0.169	0.453	0.453	0.2660	5.6242	10.7834
	7413	Column 1	0.016	0.016	0.098	0.098	0.197	0.197	0.546	0.546	0.2120	6.2293	12.5669
	7414	Column 1	0.016	0.016	0.108	0.108	0.237	0.237	0.689	0.689	0.1580	6.8981	15.1083
	7415	Column 1	0.016	0.016	0.094	0.094	0.277	0.277	0.918	0.918	0.1040	5.9809	17.6561
	7416	Column 1	0.016	0.016	0.091	0.091	0.280	0.280	0.944	0.944	0.0510	5.7771	17.8599

## Appendix A

---

Table A.8.-A.11, presents the resulting maximum moment values from the joint equilibrium analysis done with respect to Figure A.2 for a four branched element moment-rotation backbone behaviour.

**Table A.8. Yield moment capacities obtained through joint equilibrium**

Yield Moments at the end of Column Sections															
Storey	1					2					3				
Column	1-1	1-2	1-3	1-4	Sum	2-1	2-2	2-3	2-4	Sum	3-1	3-2	3-3	3-4	Sum
M <sub>col,i</sub> [kNm]	30.80	98.80	98.80	60.00	288.40	30.80	82.80	82.80	47.50	243.90	30.80	77.80	77.80	44.90	231.30
M <sub>col,i-1</sub> [kNm]	71.30	118.80	118.80	71.30	380.20	30.80	82.80	82.80	60.00	256.40	30.80	77.80	77.80	44.90	231.30
Cont.'															
Storey	4					5					6				
Column	4-1	4-2	4-3	4-4	Sum	5-1	5-2	5-3	5-4	Sum	6-1	6-2	6-3	6-4	Sum
M <sub>col,i</sub> [kNm]	30.80	49.60	49.60	36.40	166.40	30.80	44.70	44.70	36.40	156.60	30.80	36.00	36.00	30.80	133.60
M <sub>col,i-1</sub> [kNm]	30.80	49.60	49.60	36.40	166.40	30.80	44.70	44.70	36.40	156.60	30.80	36.00	36.00	30.80	133.60

**Table A.9. Capping moment capacities obtained through joint equilibrium**

Capping Moments at the end of Column Sections															
Storey	1					2					3				
Column	1-1	1-2	1-3	1-4	Sum	2-1	2-2	2-3	2-4	Sum	3-1	3-2	3-3	3-4	Sum
M <sub>col,i</sub> [kNm]	33.15	106.30	106.30	64.60	310.35	33.15	89.20	89.20	51.10	262.65	33.15	83.80	83.80	48.40	249.15
M <sub>col,i-1</sub> [kNm]	76.80	128.00	128.00	76.80	409.60	33.15	89.20	89.20	64.60	276.15	33.15	83.80	83.80	48.40	249.15
Cont.'															
Storey	4					5					6				
Column	4-1	4-2	4-3	4-4	Sum	5-1	5-2	5-3	5-4	Sum	6-1	6-2	6-3	6-4	Sum
M <sub>col,i</sub> [kNm]	33.15	53.40	53.40	44.70	184.65	33.15	48.10	48.10	39.20	168.55	33.10	38.80	38.80	33.10	143.80
M <sub>col,i-1</sub> [kNm]	33.15	53.40	53.40	44.70	184.65	33.15	48.10	48.10	39.20	168.55	33.10	38.80	38.80	33.10	143.80

**Table A.10. Ultimate moment capacities obtained through joint equilibrium**

Ultimate Moments at the end of Column Sections															
Storey	1					2					3				
Column	1-1	1-2	1-3	1-4	Sum	2-1	2-2	2-3	2-4	Sum	3-1	3-2	3-3	3-4	Sum
M <sub>col,i</sub> [kNm]	26.55	85.10	85.10	51.70	248.45	26.55	71.40	71.40	40.90	210.25	26.55	67.00	67.00	38.70	199.25
M <sub>col,i-1</sub> [kNm]	61.40	102.40	102.40	61.40	327.60	26.55	71.40	71.40	51.70	221.05	26.55	67.00	67.00	38.70	199.25
Cont.'															
Storey	4					5					6				
Column	4-1	4-2	4-3	4-4	Sum	5-1	5-2	5-3	5-4	Sum	6-1	6-2	6-3	6-4	Sum
M <sub>col,i</sub> [kNm]	26.55	42.70	42.70	35.80	147.75	26.55	38.50	38.50	31.30	134.85	26.50	31.00	31.00	26.50	115.00
M <sub>col,i-1</sub> [kNm]	26.55	42.70	42.70	35.80	147.75	26.55	38.50	38.50	31.30	134.85	26.50	31.00	31.00	26.50	115.00

**Table A.11. Residual moment capacities obtained through joint equilibrium**

Residual Moments at the end of Column Sections															
Storey	1					2					3				
Column	1-1	1-2	1-3	1-4	Sum	2-1	2-2	2-3	2-4	Sum	3-1	3-2	3-3	3-4	Sum
M <sub>col,i</sub> [kNm]	3.30	10.60	10.60	6.45	30.95	3.30	8.90	8.90	5.10	26.20	3.30	8.40	8.40	4.80	24.90
M <sub>col,i-1</sub> [kNm]	7.70	12.80	12.80	7.70	41.00	3.30	8.90	8.90	6.45	27.55	3.30	8.40	8.40	4.80	24.90
Cont.'															
Storey	4					5					6				
Column	4-1	4-2	4-3	4-4	Sum	5-1	5-2	5-3	5-4	Sum	6-1	6-2	6-3	6-4	Sum
M <sub>col,i</sub> [kNm]	3.30	5.30	5.30	4.50	18.40	3.30	4.80	4.80	3.90	16.80	3.30	3.90	3.90	3.30	14.40
M <sub>col,i-1</sub> [kNm]	3.30	5.30	5.30	4.50	18.40	3.30	4.80	4.80	3.90	16.80	3.30	3.90	3.90	3.30	14.40

## Appendix A

---

Expected yield, ultimate, capping and residual rotation capacities that were computed with respect to Equation 3.10-3.15. and the moment curvature analysis results are given in Table A.12.

**Table A.12. Frame element moment-rotation capacities**

Element Drift and Flexural Capacities														
Stry.	Mech.	Node	Element	hcf [m]	Lp (m)	$\theta_{y,i}$ [rad]	$M_{col,i}$ [kNm]	$M_{j,i\theta_y,I}$ [kNmrad]	$\theta_{c,i}$ [rad]	$M_{col,i}$ [kNm]	$M_{j,i\theta_c,I}$ [kNmrad]	$\theta_{u,i}$ [rad]	$M_{col,i}$ [kNm]	$M_{j,i\theta_u,I}$ [kNmrad]
<b>6</b>	Col.	1116	7116	1.29	0.2341	0.0068	30.80	0.2079	0.0243	33.10	0.8047	0.0687	26.50	1.8213
		1216	7216	1.29	0.2341	0.0068	36.00	0.2430	0.0245	38.80	0.9506	0.0686	31.00	2.1255
		1316	7316	1.29	0.2341	0.0068	36.00	0.2430	0.0245	38.80	0.9506	0.0686	31.00	2.1255
		1416	7416	1.29	0.2341	0.0068	30.80	0.2079	0.0243	33.10	0.8047	0.0687	26.50	1.8213
<b>5</b>	Col.	1115	7116	1.29	0.2341	0.0096	30.80	0.2956	0.0356	33.15	1.1811	0.0966	26.55	2.5659
		1215	7216	1.29	0.2341	0.0096	44.70	0.4290	0.0373	48.10	1.7938	0.0709	38.50	2.7289
		1315	7316	1.29	0.2341	0.0096	44.70	0.4290	0.0373	48.10	1.7938	0.0709	38.50	2.7289
		1415	7416	1.29	0.2341	0.0096	36.40	0.3494	0.0356	39.20	1.3966	0.0966	31.30	3.0249
<b>4</b>	Col.	1114	7115	1.29	0.2341	0.0096	30.80	0.2956	0.0404	33.15	1.3400	0.0833	26.55	2.2124
		1214	7215	1.29	0.2341	0.0096	49.60	0.4760	0.0378	53.40	2.0163	0.0607	42.70	2.5930
		1314	7315	1.29	0.2341	0.0096	49.60	0.4760	0.0378	53.40	2.0163	0.0607	42.70	2.5930
		1414	7415	1.29	0.2341	0.0096	36.40	0.3494	0.0404	44.70	1.8068	0.0833	35.80	2.9832
<b>3</b>	Col.	1113	7114	1.29	0.2341	0.0096	44.90	0.4309	0.0369	33.15	1.2241	0.0700	26.55	1.8598
		1213	7214	1.29	0.2341	0.0096	77.80	0.7467	0.0364	83.80	3.0479	0.0611	67.00	4.0907
		1313	7314	1.29	0.2341	0.0096	77.80	0.7467	0.0364	83.80	3.0479	0.0611	67.00	4.0907
		1413	7414	1.29	0.2341	0.0096	30.80	0.2956	0.0369	48.40	1.7872	0.0700	38.70	2.7108
<b>2</b>	Col.	1112	7113	1.29	0.2341	0.0096	30.80	0.2956	0.0338	33.15	1.1193	0.0607	26.55	1.6123
		1212	7213	1.29	0.2341	0.0080	82.80	0.6622	0.0342	89.20	3.0532	0.0509	71.40	3.6327
		1312	7313	1.29	0.2341	0.0080	82.80	0.6622	0.0342	89.20	3.0532	0.0509	71.40	3.6327
		1412	7413	1.29	0.2341	0.0096	47.50	0.4559	0.0338	51.10	1.7253	0.0607	40.90	2.4837
<b>1</b>	Col.	1111	7112	1.29	0.2341	0.0096	30.80	0.2956	0.0338	33.15	1.1193	0.0607	26.55	1.6123

## Appendix A

---

		1211	7212	1.29	0.2341	0.0080	82.80	0.6622	0.0342	89.20	3.0532	0.0509	71.40	3.6327
		1311	7312	1.29	0.2341	0.0080	82.80	0.6622	0.0342	89.20	3.0532	0.0509	71.40	3.6327
		1411	7412	1.29	0.2341	0.0096	60.00	0.5759	0.0338	64.60	2.1812	0.0607	51.70	3.1396
<b>0</b>	Col.	1110	7111	1.92	0.2846	0.0083	71.30	0.5943	0.0271	76.80	2.0782	0.0497	61.40	3.0527
		1210	7211	1.50	0.2511	0.0039	118.80	0.4645	0.0147	128.00	1.8856	0.0231	102.40	2.3674
		1310	7311	1.50	0.2511	0.0039	118.80	0.4645	0.0147	128.00	1.8856	0.0231	102.40	2.3674
		1410	7411	1.49	0.2504	0.0065	71.30	0.4621	0.0230	76.80	1.7632	0.0429	61.40	2.6339

Finally, the output storey shear-rotation capacities that were calculated according to Equation 3.16.-3.18. are given in Table A.13.

Table A.13. Storey Flexural Backbone Curves

Mean Horizontal Shear Resistance					Mean Flexural Stiffness				Mean Damage State Drift Limit					
Force	DS1	DS2	DS3	DS4	Stiffness	DS1	DS2	DS3	DS4	Drift	DS1	DS2	DS3	DS4
<b>VR,6 [kN]</b>	89.07	95.87	76.67	9.60	<b>K, 6 [kN/m]</b>	3582.54	99.90	-142.74	0.00	<b>0,6</b>	0.0083	0.0310	0.0758	0.2166
<b>VR,5 [kN]</b>	104.40	112.37	89.90	11.20	<b>K, 5 [kN/m]</b>	3625.91	94.22	-196.82	0.00	<b>0,5</b>	0.0096	0.0378	0.0758	0.1956
<b>VR,4 [kN]</b>	110.93	123.10	98.50	12.27	<b>K, 4 [kN/m]</b>	3852.82	145.12	-281.56	0.00	<b>0,4</b>	0.0096	0.0375	0.0667	0.1544
<b>VR,3 [kN]</b>	154.20	166.10	132.83	16.60	<b>K, 3 [kN/m]</b>	5685.74	151.15	-469.84	0.00	<b>0,3</b>	0.0090	0.0353	0.0589	0.1329
<b>VR,2 [kN]</b>	166.77	179.60	143.77	17.92	<b>K, 2 [kN/m]</b>	6510.26	167.54	-593.26	0.00	<b>0,2</b>	0.0085	0.0341	0.0542	0.1177
<b>VR,1 [kN]</b>	243.13	261.80	209.47	26.16	<b>K, 1 [kN/m]</b>	13460.64	372.04	-1183.39	0.00	<b>0,1</b>	0.0066	0.0248	0.0409	0.0915

### A.1.3. Truss Infill System Capacity

According to Bertoldi *et al.* [1993], the strut model parameters are computed through Table A.14-A.15.

**Table A.14. Infill-strut geometry computations.**

Infill Strut Geometry												
Storey	Bay	ID	H (m)	B (m)	hb (m)	hc (m)	bc (m)	Ic (m <sup>4</sup> )	lw (m)	hw (m)	dw (m)	Θ (rad.)
6	1	116	3.00	4.50	0.50	0.20	0.30	0.00020	4.30	2.50	4.97	0.53
	2	216	3.00	2.00	0.50	0.20	0.30	0.00020	1.80	2.50	3.08	0.95
	3	316	3.00	4.50	0.50	0.20	0.30	0.00020	4.30	2.50	4.97	0.53
5	1	115	3.00	4.50	0.50	0.20	0.30	0.00020	4.30	2.50	4.97	0.53
	2	215	3.00	2.00	0.50	0.20	0.30	0.00020	1.80	2.50	3.08	0.95
	3	315	3.00	4.50	0.50	0.20	0.30	0.00020	4.30	2.50	4.97	0.53
4	1	114	3.00	4.50	0.50	0.20	0.30	0.00020	4.30	2.50	4.97	0.53
	2	214	3.00	2.00	0.50	0.20	0.30	0.00020	1.80	2.50	3.08	0.95
	3	314	3.00	4.50	0.50	0.20	0.30	0.00020	4.30	2.50	4.97	0.53
3	1	113	3.00	4.50	0.50	0.30	0.30	0.00068	4.20	2.50	4.89	0.54
	2	213	3.00	2.00	0.50	0.30	0.30	0.00068	1.70	2.50	3.02	0.97
	3	313	3.00	4.50	0.50	0.30	0.30	0.00068	4.20	2.50	4.89	0.54
2	1	112	3.00	4.50	0.50	0.30	0.30	0.00068	4.20	2.50	4.89	0.54
	2	212	3.00	2.00	0.50	0.30	0.30	0.00068	1.70	2.50	3.02	0.97
	3	312	3.00	4.50	0.50	0.30	0.30	0.00068	4.20	2.50	4.89	0.54
1	1	111	2.75	4.50	0.50	0.35	0.35	0.00125	4.15	2.25	4.72	0.50
	2	211	2.75	2.00	0.50	0.35	0.35	0.00125	1.65	2.25	2.79	0.94
	3	311	2.75	4.50	0.50	0.35	0.35	0.00125	4.15	2.25	4.72	0.50

**Table A. 15. Strut model calculations for the medium infill typology**

Infill Strut Capacities (Medium) (Bertoldi et al., 1993)																	
Stry.	Bay	ID	Ewθ [MPa]	λ	λH	K1	K2	bw [m]	σw1 [MPa]	σw2 [MPa]	σw3 [MPa]	σw4 [MPa]	σmax [MPa]	Fmax [kN]	Fer [kN]	Fult [kN]	
6	1	116	1368.42	1.60	4.80	0.707	0.010	0.78	1.18	1.58	1.17	3.14	1.17	218.97	175.18	21.90	
	2	216	1969.86	1.79	5.38	0.707	0.010	0.44	1.31	2.19	1.28	7.43	1.28	134.00	107.20	13.40	
	3	316	1368.42	1.60	4.80	0.707	0.010	0.78	1.18	1.58	1.17	3.14	1.17	218.97	175.18	21.90	
5	1	115	1368.42	1.60	4.80	0.707	0.010	0.78	1.18	1.58	1.17	3.14	1.17	218.97	175.18	21.90	
	2	215	1969.86	1.79	5.38	0.707	0.010	0.44	1.31	2.19	1.28	7.43	1.28	134.00	107.20	13.40	
	3	315	1368.42	1.60	4.80	0.707	0.010	0.78	1.18	1.58	1.17	3.14	1.17	218.97	175.18	21.90	
4	1	114	1368.42	1.60	4.80	0.707	0.010	0.78	1.18	1.58	1.17	3.14	1.17	218.97	175.18	21.90	
	2	214	1969.86	1.79	5.38	0.707	0.010	0.44	1.31	2.19	1.28	7.43	1.28	134.00	107.20	13.40	
	3	314	1368.42	1.60	4.80	0.707	0.010	0.78	1.18	1.58	1.17	3.14	1.17	218.97	175.18	21.90	
3	1	113	1383.44	1.19	3.56	0.707	0.010	1.02	0.89	1.20	1.16	3.26	0.89	218.19	174.55	21.82	
	2	213	1988.45	1.32	3.96	0.707	0.010	0.57	0.99	1.65	1.23	8.02	0.99	134.96	107.97	13.50	
	3	313	1383.44	1.19	3.56	0.707	0.010	1.02	0.89	1.20	1.16	3.26	0.89	218.19	174.55	21.82	
2	1	112	1383.44	1.19	3.56	0.707	0.010	1.02	0.89	1.20	1.16	3.26	0.89	218.19	174.55	21.82	
	2	212	1988.45	1.32	3.96	0.707	0.010	0.57	0.99	1.65	1.23	8.02	0.99	134.96	107.97	13.50	
	3	312	1383.44	1.19	3.56	0.707	0.010	1.02	0.89	1.20	1.16	3.26	0.89	218.19	174.55	21.82	
1	1	111	1326.32	1.02	2.81	1.300	-	0.178	1.34	0.65	0.85	1.00	2.76	0.65	210.73	168.59	21.07
	2	211	1962.92	1.16	3.20	0.707	0.010	0.64	0.81	1.34	1.25	7.51	0.81	124.55	99.64	12.46	
	3	311	1326.32	1.02	2.81	1.300	-	0.178	1.34	0.65	0.85	1.00	2.76	0.65	210.73	168.59	21.07

By using the critical force values that were taken from Table A.14-A.15 and strut strain values from Sassun *et al.* [2016], the strut axial and then strut horizontal axial stiffness were computed in Table A.16 and Table A.17 for different branches of the strut backbone.

**Table A.16. Strut element force-drift values for different critical points**

Horizontal Yield Drift and Shear Capacities (Medium)												
Storey	Bay	ID	hs,i [m]	Fcr [kN]	$\varepsilon_{DS1}$	Kel* [kN/m]	Kelh. * [kN/m]	Fmax [kN]	$\varepsilon_{DS2}$	Ksec* [kN/m]	Ktrue* [kN/m]	Ktrueh.* [kN/m]
6	1	116	3.00	175.18	0.0008	40487.97	30259.60	218.97	0.0022	18403.62	5784.00	4322.80
	2	216	3.00	107.20	0.0008	37165.03	12688.59	134.00	0.0022	16893.19	5309.29	1812.66
	3	316	3.00	175.18	0.0008	40487.97	30259.60	218.97	0.0022	18403.62	5784.00	4322.80
5	1	115	3.00	175.18	0.0008	40487.97	30259.60	218.97	0.0022	18403.62	5784.00	4322.80
	2	215	3.00	107.20	0.0008	37165.03	12688.59	134.00	0.0022	16893.19	5309.29	1812.66
	3	315	3.00	175.18	0.0008	40487.97	30259.60	218.97	0.0022	18403.62	5784.00	4322.80
4	1	114	3.00	175.18	0.0008	40487.97	30259.60	218.97	0.0022	18403.62	5784.00	4322.80
	2	214	3.00	107.20	0.0008	37165.03	12688.59	134.00	0.0022	16893.19	5309.29	1812.66
	3	314	3.00	175.18	0.0008	40487.97	30259.60	218.97	0.0022	18403.62	5784.00	4322.80
3	1	113	3.00	174.55	0.0008	40343.11	29788.71	218.19	0.0022	18337.78	5763.30	4255.53
	2	213	3.00	107.97	0.0008	37430.50	11835.25	134.96	0.0022	17013.86	5347.21	1690.75
	3	313	3.00	174.55	0.0008	40343.11	29788.71	218.19	0.0022	18337.78	5763.30	4255.53
2	1	112	3.00	174.55	0.0008	40343.11	29788.71	218.19	0.0022	18337.78	5763.30	4255.53
	2	212	3.00	107.97	0.0008	37430.50	11835.25	134.96	0.0022	17013.86	5347.21	1690.75
	3	312	3.00	174.55	0.0008	40343.11	29788.71	218.19	0.0022	18337.78	5763.30	4255.53
1	1	111	2.75	168.59	0.0008	39958.62	30881.19	210.73	0.0022	18163.01	5708.37	4411.60
	2	211	2.75	99.64	0.0008	36629.22	12809.64	124.55	0.0022	16649.64	5232.75	1829.95
	3	311	2.75	168.59	0.0008	39958.62	30881.19	210.73	0.0022	18163.01	5708.37	4411.60

**Table A. 17. Strut element force-drift values for different critical points (cont.)**

Horizontal Yield Drift and Flexural Capacities (Medium) (contd)							
Storey	Bay	ID	hs,i [m]	Fult [kN]	εDS3	Kdeg* [kN/m]	Kdegh.* [kN/m]
6	1	116	3.00	21.90	0.0089	-11341.40	-8476.25
	2	216	3.00	13.40	0.0089	-10268.65	-3505.84
	3	316	3.00	21.90	0.0089	-11341.40	-8476.25
5	1	115	3.00	21.90	0.0089	-11341.40	-8476.25
	2	215	3.00	13.40	0.0089	-10268.65	-3505.84
	3	315	3.00	21.90	0.0089	-11341.40	-8476.25
4	1	114	3.00	21.90	0.0089	-11341.40	-8476.25
	2	214	3.00	13.40	0.0089	-10268.65	-3505.84
	3	314	3.00	21.90	0.0089	-11341.40	-8476.25
3	1	113	3.00	21.82	0.0089	-11369.40	-8394.99
	2	213	3.00	13.50	0.0089	-10746.52	-3397.97
	3	313	3.00	21.82	0.0089	-11369.40	-8394.99
2	1	112	3.00	21.82	0.0089	-11369.40	-8394.99
	2	212	3.00	13.50	0.0089	-10746.52	-3397.97
	3	312	3.00	21.82	0.0089	-11369.40	-8394.99
1	1	111	2.75	21.07	0.0089	-11709.11	-9049.14
	2	211	2.75	12.46	0.0089	-10288.07	-3597.85
	3	311	2.75	21.07	0.0089	-11709.11	-9049.14

Then in Table A.18, the strut and column components of the unit horizontal displacements in Equation 3.23. and 3.25 were computed.

**Table A. 18. Unit horizontal displacements due to the axial stiffness of each member**

Unit Horizontal Displacements due to axial stiffness (m)							
No. of Bay	Storey	6	5	4	3	2	1
1	Column 1	1.62E-06	1.62E-06	1.62E-06	1.62E-06	1.62E-06	8.68E-07
	Strut 1	3.30E-05	3.30E-05	3.30E-05	3.36E-05	3.36E-05	3.24E-05
	Strut 1	2.31E-04	2.31E-04	2.31E-04	2.35E-04	2.35E-04	2.27E-04
	Strut 1	-1.18E-04	-1.18E-04	-1.18E-04	-1.19E-04	-1.19E-04	-1.11E-04
	Column 2a	1.62E-06	1.62E-06	1.62E-06	1.13E-06	1.13E-06	4.46E-07
2	Column 2b	8.21E-06	8.21E-06	8.21E-06	5.70E-06	5.70E-06	2.26E-06
	Strut 2	7.88E-05	7.88E-05	7.88E-05	8.45E-05	8.45E-05	7.81E-05
	Strut 2	5.52E-04	5.52E-04	5.52E-04	5.91E-04	5.91E-04	5.46E-04
	Strut 2	-2.85E-04	-2.85E-04	-2.85E-04	-2.94E-04	-2.94E-04	-2.78E-04
	Column 3a	8.21E-06	8.21E-06	8.21E-06	5.70E-06	5.70E-06	2.26E-06
3	Column 3b	1.62E-06	1.62E-06	1.62E-06	1.13E-06	1.13E-06	4.46E-07
	Strut 3	3.30E-05	3.30E-05	3.30E-05	3.36E-05	3.36E-05	3.24E-05
	Strut 3	2.31E-04	2.31E-04	2.31E-04	2.35E-04	2.35E-04	2.27E-04

	<b>Strut 3</b>	-1.18E-04	-1.18E-04	-1.18E-04	-1.19E-04	-1.19E-04	-1.11E-04
	<b>Column 4</b>	1.62E-06	1.62E-06	1.62E-06	1.62E-06	1.62E-06	8.68E-07

Following, in Table A.19, the storey strut stiffnesses were computed for the ground storey and the upper storeys with Equation 3.24. and 3.26.

**Table A.19. Computed horizontal axial storey stiffnesses**

Horizontal Axial Storey Stiffnesses				
Storey	Bay	DS1 (m)	DS2	DS3
<b>6</b>	1			
	2	41511.95	9427.25	-26040.51
	3			
<b>5</b>	1			
	2	52361.13	9886.63	-23102.34
	3			
<b>4</b>	1			
	2	56957.34	10044.36	-22262.91
	3			
<b>3</b>	1			
	2	60696.71	9949.66	-21260.77
	3			
<b>2</b>	1			
	2	65719.73	10076.81	-20698.05
	3			
<b>1</b>	1			
	2	72985.78	10620.11	-21833.95
	3			

Finally, the storey infill backbone curves are given in Table A.20 - A.21.

**Table A.20. Infill storey backbone. Shear resistance vs drift values.**

Mean Horz. Shear Resist. (Infill-Strut System)					Mean Damage State Drift Limit (Inf.-Str. Sys.)				
Force	DS1	DS2	DS3	DS4	Drift	DS1	DS2	DS3	DS4
<b>VRin,6 [kN]</b>	365.52	456.90	45.69	45.69	<b>0in,6</b>	0.0029	0.0062	0.0114	0.0800
<b>VRin,5 [kN]</b>	365.52	456.90	45.69	45.69	<b>0in,5</b>	0.0023	0.0054	0.0113	0.0800
<b>VRin,4 [kN]</b>	365.52	456.90	45.69	45.69	<b>0in,4</b>	0.0021	0.0052	0.0113	0.0800
<b>VRin,3 [kN]</b>	360.69	450.86	45.09	45.09	<b>0in,3</b>	0.0020	0.0050	0.0114	0.0800

<b>VRin,2</b> [kN]	360.69	450.86	45.09	45.09	<b>θin,2</b>	0.0018	0.0048	0.0113	0.0800
<b>VRin,1</b> [kN]	355.33	444.17	44.42	44.42	<b>θin,1</b>	0.0018	0.0048	0.0115	0.0800

**Table A. 21. Infill storey stiffness values.**

Mean Horizontal Stiffness (Infill-Strut System)				
Stiffness	DS1	DS2	DS3	DS4
<b>Kin,6 [kN/m]</b>	41511.95	9427.25	-26040.51	0.00
<b>Kin,5 [kN/m]</b>	52361.13	9886.63	-23102.34	0.00
<b>Kin,4 [kN/m]</b>	56957.34	10044.36	-22262.91	0.00
<b>Kin,3 [kN/m]</b>	60696.71	9949.66	-21260.77	0.00
<b>Kin,2 [kN/m]</b>	65719.73	10076.81	-20698.05	0.00
<b>Kin,1 [kN/m]</b>	72985.78	10620.11	-21833.95	0.00

#### A.1.4. Combined System Capacities

In Table A.22., the behaviour hierarchy (superposed infill and frame storey backbone curve) are given for each storey. Note that, because of the superposition, the rotation values are in increasing order and the storey shears are computed with Equation 3.33.

**Table A.22. Table of behaviour hierarchy for all storeys**

Table of Behaviour Hierarchy											
Storey 6				Storey 5				Storey 4			
L.S. Point	Vi [kN]	θi [rad]	Ki [kN/m]	L.S. Point	Vi [kN]	θi [rad]	Ki [kN/m]	L.S. Point	Vi [kN]	θi [rad]	Ki [kN/m]
DSi 1	397.07	0.0029	45094.50	DSi 1	390.83	0.0023	55987.04	DSi 1	390.25	0.0021	60810.16
DSi 2	523.17	0.0062	13009.79	DSi 2	515.73	0.0054	13512.54	DSi 2	516.68	0.0052	13897.18
DSf 1	380.28	0.0083	-22457.97	DSf 1	270.93	0.0096	-19476.44	DSf 1	272.24	0.0096	-18410.10
DSi 3	135.70	0.0114	-25940.61	DSi 3	150.58	0.0113	-23008.12	DSi 3	157.38	0.0113	-22117.79
DSf 2	141.56	0.0310	99.90	DSf 2	158.06	0.0378	94.22	DSf 2	168.79	0.0375	145.12
DSf 3	122.36	0.0758	-142.74	DSf 3	135.59	0.0758	-196.82	DSf 3	144.19	0.0667	-281.56
DSi 4	122.36	0.0800	0.00	DSi 4	135.59	0.0800	0.00	DSi 4	144.19	0.0800	0.00
Table of Behaviour Hierarchy (cont.)											
Storey 3				Storey 2				Storey 1			
L.S. Point	Vi [kN]	θi [rad]	Ki [kN/m]	L.S. Point	Vi [kN]	θi [rad]	Ki [kN/m]	L.S. Point	Vi [kN]	θi [rad]	Ki [kN/m]
DSi 1	394.48	0.0020	66382.44	DSi 1	396.42	0.0018	72229.99	DSi 1	420.87	0.0018	86446.42
DSi 2	536.18	0.0050	15635.40	DSi 2	544.85	0.0048	16587.07	DSi 2	622.30	0.0048	24080.75
DSf 1	347.49	0.0090	-15575.03	DSf 1	386.24	0.0085	-14187.79	DSf 1	581.86	0.0066	-8373.31
DSi 3	200.34	0.0114	-21109.62	DSi 3	213.26	0.0113	-20530.52	DSi 3	292.56	0.0115	-21461.90
DSf 2	211.19	0.0353	151.15	DSf 2	224.69	0.0341	167.54	DSf 2	306.22	0.0248	372.04
DSf 3	177.92	0.0589	-469.84	DSf 3	188.85	0.0542	-593.26	DSf 3	253.89	0.0409	-1183.39
DSi 4	177.92	0.0800	0.00	DSi 4	188.85	0.0800	0.00	DSi 4	253.89	0.0800	0.00

*This page is intentionally left blank...*

## B. APPENDIX B

This appendix provides a brief review of the analytical methods employed in this thesis.

### B.1. Method of Virtual Work

Concepts and formulas shown in this section are taken from:

- Hibbeler, R.C. [2012] “Chapter 9: Deflections Using Energy Methods” (pp. 341-354). *Structural Analysis (8<sup>th</sup> Ed.)* Upper Saddle River, New Jersey. Pearson Prentice Hall

Proposed by John Bernoulli in 1717, the method of virtual work is based on the theory that work done by the external loads must be equal to the work done by internal forces for a given system. By using this principle, real global displacements of the system can be computed. Considering a system that is under the influence of a real load  $P$ , this can be done by explicitly writing the external work done in the direction of the desired displacement due to a unit load of “1” acting towards the concurrent direction and by comparing this with the internal work done by the members due to the real loading case. The aforementioned approach can be demonstrated as Equation B.1.

$$1. \Delta = \sum u \cdot dL \quad \text{B.1}$$

where

$P' = 1$  = external virtual unit load acting in the direction of  $\Delta$

$u$  = internal virtual load acting on the element in the direction of  $dL$

$\Delta$  = external displacement caused by the real loads

$dL$  = internal deformation of the element caused by the real loads

Equation A.1. can be written both for translational and rotational degrees of freedom by interchanging between point load and moment load also, between axial/shear and flexural rigidity of the element. Hence, the system should be analysed at least two times for the internal member actions, once considering the real external loading case and then a second time considering the virtual case consisting of a unit load (preferably on the order of 1) acting on the

interested node/component/level of the system in the direction of the desired displacement direction.

For trusses, the virtual work method can be reduced to the translational global degrees of freedom and the internal axial actions of the truss members. Hence Equation A.1 can be explicitly written as Equation B.2.

$$1.\Delta = \sum \frac{nNL}{EA} \quad \text{B.2}$$

where

$P' = 1$  = external virtual unit load acting on the truss joint in the direction of  $\Delta$

$n$  = internal virtual force in a truss member due to the external virtual load

$\Delta$  = external joint displacement caused by the real loads

$N$  = internal force in a truss member due to the real load case

$L$  = Length of a member

$A$  = Cross – sectional area of a member

$E$  = Young's Modulus of a member